Synaptic signal transduction and transcriptional control

Thesis by

Holly C. Beale

In Partial Fulfillment of the Requirements

for the Degree of

Doctor of Philosophy

California Institute of Technology

Pasadena, California

2010

(Submitted Friday 21st May, 2010)

This thesis is dedicated to Gwen Murdock Pollard, to the many people whose friendship and support exceeded anything I could have anticipated, and to Julia Scheinmann.

Acknowledgments

First I would like to thank my advisor, Mary Kennedy, for the the insights she provided over the past seven years and for the freedom she gave me. The breadth of her scientific interest is inspiring. I would also like to thank the other members of my thesis committee, Paul Patterson, Paul Sternberg and the chair, Henry Lester, for their time and feedback over the years. In particular, I thank Paul Patterson for his writing suggestions, which have transformed how I think about my writing, and Henry Lester for his advice and teaching example.

As a body, members of the Kennedy lab have been exemplars of insight, collaboration and persistence. Holly Carlisle, Tinh Luong and Tami Ursem were invaluable in the completion of this thesis. Andrew Medina-Marino provided a critical opportunity and example of kindness. Dado Marcora has been terrific geek company, a walking encyclopedia of methods and an asker of fundamental questions. Leslie Schenker has been the silent engine of the lab and is a delight every day. It has been an honor to work with these lab members and others past and present, including Mee Choi, Cheryl Gause, Irene Knuesel, Pat Manzerra, Ward Walkup, and Lori Washburn.

I would also like to thank Caltech professional staff, postdocs and other graduates students too numerous to name for creating such a dynamic, supportive, and inspiring context. The professional staff at Caltech are as extraordinary as the science.

Finally, this would not have been possible without the love and perspective of my family and friends, near and far.

Abstract

Synaptic signal transduction regulates synaptic plasticity, and, on a larger scale, memory itself. The aim of this dissertation is to elucidate some of the mechanisms that control synaptic plasticity in the short term by modulating synaptic morphology and in the long term by controlling gene expression.

One modification associated with synaptic plasticity is the change in the size of the spine, the micron-scale structure on the dendrite which supports the synapse. The size and shape of the spine are controlled by the actin cytoskeleton. I studied how stimulation of synaptic receptors drives changes in activation of proteins that regulate actin polymerization. We identified neuron-specific aspects of a canonical actin regulation pathway and characterized activity-regulated phosphatase activity.

Changes in spine size and other events associated with synaptic plasticity can begin within seconds of synaptic stimuli, but persistent changes require gene expression. For example, Arc, an immediate early gene required for changes in synaptic strength to persist, is the only transcript known to be both transcribed in response to synaptic stimulation and translocated specifically to the site of the stimulation. However, the role of Arc in promoting the plasticity of the synapse is still under inves-

tigation. We studied its binding partners and found that an interaction demonstrated in non-neuronal cells was not evident in neurons.

We also studied changes in transcription over longer time periods. In order to identify pathways involving the postsynaptic protein densin, we assessed global changes in transcription with RNA-Seq, which uses ultra-high-throughput, short-read sequencing to measure transcript abundance. Compared to wild-type mice, densin knockout mice exhibit increased abundance of CaMKIIα (a densin binding partner), increased abundance of immediate early gene expression including Arc, and downregulated $GABA_AR$ subunits.

In summary, we investigated posttranslational modifications that take place within seconds of stimulation, binding interactions occurring in steady-state conditions in wild-type mice, and homeostatic adaptations to the chronic absence of a gene. These investigations into synaptic signaling illustrate not only the complexity of synapse-related regulatory networks but also the range of time scales they span.

Contents

List of Figures

List of Tables

Acronyms

ABA Allen Mouse Brain Atlas

AMPA α-amino-3-hydroxyl-5-methyl-4-isoxazole-propionate

CaMKII Calcium/Calmodulin-Dependent Protein Kinase II

CaMKIIα CaMKIIα

CaMKIIβ CaMKIIβ

CsA Cyclosporin A

DE differentially expressed

DIV days *in vitro*

DOC deoxycholate

EM electron microscopy

F-actin filamentous actin

Fmr1 fragile X mental retardation 1

FRET fluorescence resonance energy transfer

G-actin globular actin

GABA$_A$R γ-aminobutyric acid$_A$ receptor

GSH glutathione

GST glutathione-S-transferase

HSP heat shock protein

IEG immediate early gene

kDa kilodaltons

LAP LRR And PDZ domain-containing

LRR leucine rich repeat

LTD long term depression

LTP long term potentiation

NMDA N-methyl-D-aspartate

PAK p21-activated kinase

PBS phosphate-buffered saline

PMSF phenylmethylsulphonyl fluoride

PP1 protein phosphatase 1

PP2A protein phosphatase 2A

PSD postsynaptic density

qPCR quantitative polymerase chain reaction

RNAi RNA interference

RPKM reads per kilobase per million

Chapter 1

Introduction

Synaptic plasticity, the ability of synapses to adjust their capacity for transmitting information, is a prominent cellular mechanism by which the brain stores information. In the postsynaptic cell, these adjustments involve receptor insertion, cytoskeletal remodeling, and changes in gene expression. The signal transduction that underlies some of these processes is initiated in the postsynaptic density (PSD), a tightly bound group of receptors, scaffolds, and signaling molecules. This thesis describes studies of these signal transduction cascades and the responses they trigger.

My doctoral work involved three main projects, covered in chapters 2 through 4. Chapter 2 describes changes in transcript abundance in a mouse line in which a prominent postsynaptic protein, densin-180, has been genetically knocked out. Chapter 3 discusses the regulation of the cytoskeleton by N-methyl-D-aspartate (NMDA) receptor-dependent signaling cascades. Chapter 4 describes the protein-protein interactions of Arc, the product of an immediate early gene that is transcribed in response to memory-generating events and whose transcript is targeted to activated regions of the dendrite. These studies add to our body of knowledge of the cellular processes that support learning and memory.

1.1 Densin and its effect on transcription

Densin is an abundant PSD protein whose function has been less studied than many other PSD proteins. It is the focus of Chapter 2, in which I describe our study of transcription in the densin knockout mouse. To provide context for that chapter, I survey results of previous densin experiments and introduce RNA-Seq, a new RNA-sequencing method we used to measure transcription.

1.1.1 Densin, a postsynaptic protein

The PSD is central to synaptic structure and function, and many PSD components have been extensively investigated. These include the α-amino-3-hydroxyl-5-methyl-4-isoxazole-propionate (AMPA) and NMDA-type glutamate receptors, the scaffold protein PSD-95, and signaling molecules Calcium/Calmodulin-Dependent Protein Kinase II (CaMKII) and SynGAP. These core PSD proteins are tightly associated and are not solubilized by the relatively harsh detergent N-lauroyl sarcosinate (sarcosyl).

Another core PSD protein is densin-180, the product of the *lrrc7* gene (Apperson et al., 1996; Wang et al., 2003). Much of the predicted function of densin is inferred from its structural motifs and binding partners. Densin is a large protein (180 kiloDaltons) and the founding protein in the LAP (leucine rich repeat and PDZ-containing) family of proteins (PDZ domains are binding domains, often found in multi-domain scaffold proteins, named for the proteins PSD-95, discs large, and zona occludens 1.). Densin has 16 leucine rich repeats (LRRs) and a C-terminal PDZ domain. It also contains a mucin-like domain that is glycosylated with large sialic acid residues, which

are only found on extracellular protein domains (Apperson et al., 1996). Like other PSD proteins, densin is not solubilized by sarcosyl. However, a solution containing 1 M NaCl and 2 percent of either of the detergents Triton or CHAP solubilizes approximately half the densin in the PSD fraction, suggesting that it is bound by a combination of lipid and hydrophilic interactions (Apperson et al., 1996).

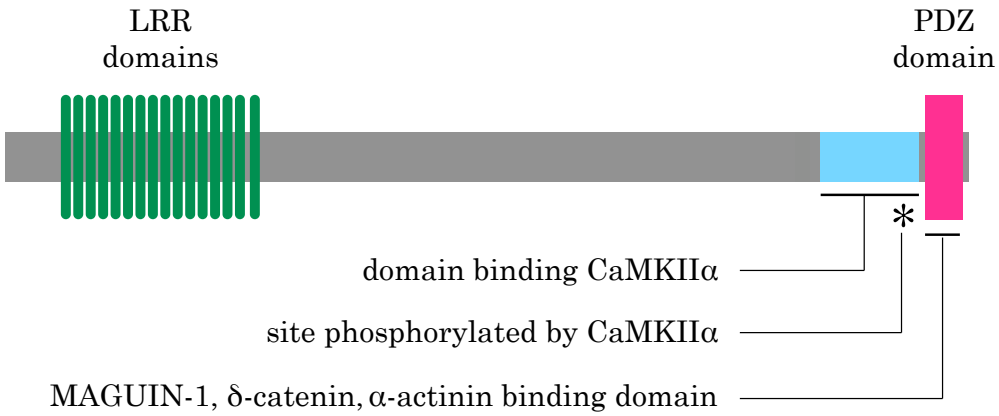

Figure 1.1: Densin contains 16 leucine rich repeat (LRR) domains and a C-terminal PDZ domain.

Densin binds PSD proteins such as CaMKII (a major regulator of synaptic plasticity), MAGUIN-1 (a direct binding partner of PSD-95), α-actinin (a calcium-regulated, actin-binding protein that also binds the NMDA receptor) and shank (a postsynaptic scaffold) (Nakagawa et al., 2004; Ohtakara et al., 2002; Quitsch et al., 2005; Walikonis et al., 2001; Wyszynski et al., 1997). A yeast two-hybrid approach (Izawa et al., 2002) revealed that densin binds δ-catenin/NPRAP (neural plakophilin-related armadillo repeat protein). This association was also seen in Triton extracts from synaptoso-

mal fractions where δ-catenin and N-cadherin were immunoprecipitated with densin (Izawa et al., 2002).

Densin may anchor CaMKII to the PSD, acting as a link between α-actinin and CaMKII. α-actinin is a calcium-regulated, actin-binding protein that regulates spine density and has been implicated in anchoring NMDA receptors in the PSD (Wyszynski et al., 1997, Nakagawa et al., 2004 but see also Wyszynski et al., 1998). Distinct regions of densin (the PDZ domain and the membrane proximal region respectively) mediate the direct binary interactions between densin and α-actinin or CaMKII. Current experimental evidence indicates that densin can bind to α-actinin and CaMKII at the same time, thus supporting our hypothesis that densin can act as a link between these two proteins. In particular, CaMKII is unable to out-compete the α-actinin–densin interaction and, conversely, α-actinin is unable to out-compete the CaMKII–densin interaction (Walikonis et al., 2001)

Densin may also have a role in synaptic plasticity. CaMKII is central to synaptic plasticity. For example, it triggers signal cascades that regulate numerous aspects of synaptic potentiation, including receptor insertion, changes in spine shape and gene expression. The affinity of densin for CaMKIIα increases dramatically when CaMKII is autophosphorylated (Strack et al., 2000; Walikonis et al., 2001). This observation suggests that densin may be important for normal synaptic plasticity because autophosphorylation of CaMKII increases dramatically after LTP. The increased affinity under these conditions may be a mechanism by which activated CaMKII is localized to the PSD.

Densin may play different roles in developing and mature neurons. Developmentally-regulated splice variants of densin have been identified (Jiao et al., 2008; Strack et al., 2000). In rat, 3 major variants are expressed at embryonic day 15 (E15, the earliest time point measured), and these are no longer expressed by postnatal day 14 (P14). The canonical adult densin transcript, densin-180, is not detectable at E15 or E18, is weakly expressed at P1 and is strongly expressed at P7 and later (Strack et al., 2000). Additionally, proteins produced from splice variants are differentially distributed by centrifugal fractionation, suggesting that these variants are targeted to different cellular locations. Protein products of the densin-180 transcript and the two splice variants are enriched in the cytoskeletal, detergent-insoluble fraction. The product of another variant is enriched in the cytoskeletal, detergent-soluble fraction. Products of three other splice variants are found in the cytosolic fraction (Jiao et al., 2008).

Because the potential roles described above are inferred from binding-study data, a densin knockout mouse was created (Medina-Marino, 2009). These mice are viable and breed normally, but display clasping and runting phenotypes. Clasping behavior is characterized by suspending the mouse from its tail and observing whether the limbs splay apart (which is normal wild-type behavior) or are tucked into its body (which is common in many different types of neuropathy). Runted densin knockout mice achieve normal weight by adulthood (Medina-Marino, 2009). The cause of the runt period is unknown, but deficiencies seen in adults could be, in part, the result of these developmental defects. It was also observed that approximately fifty percent of densin

knockout mice injected with the general anesthetic Nembutal (a γ-aminobutyric acid receptor agonist), display tonic clonic seizures before development of full anesthesia; the other half display an abnormal jittery behavior (personal communication, T. Luong). Under the same regimen, no wild-type animals display seizures.

The densin knockout mice have altered steady-state levels of phosphorylated CaMKII (H. Carlisle, T. Luong, personal communication) as measured in cultured hippocampal neurons from these knockout mice. The proportion of CaMKII that is autophosphorylated in knockout neurons is approximately 25 percent lower than that found in wild-type neurons. Autophosphorylated CaMKII was also measured in glutamate receptor-stimulating conditions (treatment with bicuculline and glycine). In wild-type neurons, these conditions cause an increase in CaMKII autophosphorylation. In densin knockout neurons, the increase in CaMKII autophosphorylation was twice that in the wild-type neurons. If densin is a docking site for CaMKII in the PSD, this dysregulation could be due to the absence of densin and a perturbation of CaMKII localization and exposure to ionic currents through receptor channels in the PSD. The difference in activation of CaMKII is unlikely to be due to changes in AMPA or NMDA receptor function; the currents mediated by these receptors in hippocampal slices from the knockout mice do not differ from wild-type (H. Carlisle, T. Luong, personal communication).

Immunoblot results from the knockout mice suggest a small decrease in numerous postsynaptic proteins. The expression levels of many synaptic proteins measured

in forebrain homogenate are consistently lower in the densin knockout samples (H. Carlisle, T. Luong, personal communication).

Densin is implicated in regulation of the cytoskeleton, not only by its association with actin-regulating binding partners, but also by two studies of neuronal morphology. Overexpression of densin induces extensive neuronal branching in cultured hippocampal rat neurons (Quitsch et al., 2005). In sections from hippocampi of densin knockout mice, the necks of dendritic spines are elongated. Quantification of spine morphology shows that spines on the neurons of knockout mice are longer than than those from wild-type mice. Probably as a consequence of the greater length, more of the spines are classified as mushroom spines (H. Carlisle, personal communication).

Taken together, these studies show that densin is a core protein in the PSD that is very likely a docking site for CaMKII and that is required for normal neuronal morphology. Its binding partners are prominently involved in synaptic plasticity, membrane adhesion, PSD scaffolding, and cytoskeletal regulation. To learn more about these relationships, and to identify others in an unbiased manner, we looked for changes in transcription resulting from the loss of densin, using RNA-Seq, an ultra-high-throughput technique.

1.1.2 Measuring transcription by sequencing

We sought a global, precise measurement of transcription in the densin knockout mouse to identify any extra-synaptic roles for densin and to determine whether the overall expression of synaptic proteins is caused by a decrease in their transcription

in the knockout mouse. First, since synaptic function can regulate gene expression, we reasoned that impaired synaptic function resulting from the loss of densin might perturb gene expression. Analysis of a pattern of changes in gene expression could illuminate the function of densin. Second, perturbations in pathways not known to be regulated by densin could indicate a role for densin outside the synapse. This possibility is supported by the presence of extrasynaptic densin, as well as its expression in kidney and pancreas (Rinta-Valkama et al., 2007). Finally, immunoblot results suggest decrease in numerous synaptic proteins in the densin knockout mice. Knowing the abundance of transcripts corresponding to depleted proteins would allow us to test whether such depletion might be the result of decreased transcription.

We measured transcript abundance by sequencing millions of transcripts on an ultra-high-throughput sequencer, a technique called RNA-Seq (for RNA-Sequencing). In Chapter 2, we discuss our results. Because RNA-Seq is a new technology, the remainder of this section describes the RNA-Seq technique, compares it with microarrays, and evaluates its advantages and limitations.

The RNA-Seq method

RNA-Seq is a technique for measuring transcript abundance by sequencing a sample, and then inferring the number of transcripts from the number of matching sequences. The most comparable method is the microarray, but RNA-Seq represents a paradigm shift: whereas microarrays measure a continuous fluorescent signal that is dependent on probe hybridization, RNA-Seq produces digital data from the count of sequences.

For RNA-Seq, a cDNA library is prepared by purifying RNA followed by reverse transcription. The resulting cDNA is fragmented and ligated to adapters (Ansorge, 2009; Harismendy et al., 2009; Simon et al., 2009). Fragments are hybridized to a surface coated with complementary adapters, and are locally amplified, generating dense clusters of identical sequences. The next steps depend on the technology of the sequencer. Both the Gene Analyzer from Illumina (Bennett et al., 2005) and the Genome Sequencer from Roche (Margulies et al., 2005) sequence the fragments by synthesis: a newly added base is identified either by its fluorescence signature (Illumina) or by the light emitted by a luciferase reaction triggered by polymerase activity (pyrosequencing, Roche; one type of base is added at a time). The SOLiD (Supported Oligonucleotide Ligation and Detection) system from Applied Biosystems sequences by repeatedly ligating labelled oligos to the fragment (Shendure et al., 2005). The different systems are further compared in Table 1.1.

Table 1.1: Comparison of currently available sequencers in side-by-side experiments (Harismendy et al., 2009; Wall et al., 2009).

Device	Illumina Genome Analyzer	Roche Genome Sequencer	Applied Biosystems SOLiD
Developed by	Solexa	454 Life Sciences	Agencourt
Sequencing method	synthesis	synthesis	ligation
Detection method	fluorescence	emitted light (pyrosequencing)	fluorescence
Sequencing accuracy (percent)	99.99	99.99	99.99
Length of each sequence	36	245	30
Reads per sample	5,900,000	50,000	20,000,000
Usable reads per sample (percent)	43	95	34
Usable bases per sample	91,332,000	11,637,500	204,000,000
Cost per plate ($)	4000	6000	9000

Evaluation of RNA-Seq

Until recently, microarrays have been the only way to measure transcript abundance on a large scale. Microarrays use oligonucleotide probes that are designed to hybridize with the transcripts to be measured. This strategy requires advance knowledge of the sequence. The probes are systematically arrayed on a solid support. The experimenter fluorescently labels the cDNA to be measured and incubates them on the microarray. Transcripts that are complementary to probe sequences hybridize, and the resulting fluorescent signal is imaged. The position of the signal on the array is used to determine the oligo sequence, and the intensity of the signal is used to determine the amount of corresponding transcript present.

Because they depend on probe hybridization, microarrays require advance knowledge of the sequence to be measured. RNA-Seq does not; it can identify unexpected transcripts, transcript lengths, splice variants, or the presence of viral transcripts.

RNA-Seq also has greater sensitivity than microarrays. The linear dynamic range of expression measured by microarrays is less than 4 orders of magnitude (Wilhelm and Landry, 2009). The demonstrated linear dynamic range for RNA-Seq is greater than five orders of magnitude (Mortazavi et al., 2008).

The abundance of different transcripts cannot be directly compared within a sample using microarrays, because different probes have different hybridization properties; a higher value could indicate either greater abundance of transcript or a more favorable hybridization. This is not a limitation of RNA-Seq.

In spite of extensive improvements, microarrays remain subject to background hybridization, further limiting the linear dynamic range and reducing the signal to noise ratio. Microarrays are a mature technology with many major improvements already implemented. Compared to microarrays, RNA-Seq is highly accurate and eliminates target bias. Many improvements in RNA-Seq are in progress.

Direct comparison of RNA-Seq and microarrays

The relative accuracy of RNA-Seq and microarrays has been directly tested by applying the two techniques to the same samples. These few head-to-head comparisons find that RNA-Seq is at least as accurate as microarrays, probably more so.

One study compared measurements of human liver and kidney samples using RNA-Seq and microarrays. The transcript abundance measurements made by the two methods were positively correlated, but RNA-Seq identified more differentially expressed genes with higher accuracy (Marioni et al., 2008). In the liver samples, the fluorescence signal from the microarray and the read count from the RNA-Seq experiment had a Spearman correlation (a rank-based measure) of 0.73. In the kidney sample, the Spearman correlation was 0.75. When the sets of differentially expressed genes were compared, these sets overlap, but many genes were only identified by one of the methods. RNA-Seq identified 11,493 genes that were differentially expressed between human liver and kidney, while microarray analysis of the same samples identified 8,113 differentially expressed genes, with 6,534 genes identified by both methods.

A similar study compared RNA-Seq and microarray measurements of transcript abundance from HEK and B cell lines (Sultan et al., 2008). The measurements were

highly correlated, with a Pearson (linear) correlation coefficient of 0.88. As in the Marioni study, the sets of differentially expressed genes overlapped, but many genes were only identified by one of the methods. RNA-Seq identified 4,376 genes and the microarray identified 3,421. Of those, 2,685 genes were identified by both methods.

Both Sultan et al. (2008) and Marioni et al. (2008) identify similar proportions of differentially expressed genes on each platform. For example, in Marioni's data, of all the genes identified as differentially expressed by either platform, 12 percent were only identified by microarray, 50 percent were identified by both, and 38 percent were only identified by sequencing. The equivalent numbers for Sultan are 14, 53 and 33. The congruence in the two experiments increases the strength of the results. If this trend is persistent, it is reasonable to expect to be able to identify the underlying cause and thus better understand the relationship of the data to the underlying biology.

RNA-Seq and microarrays have different underlying mechanisms, and thus some disparity may be inevitable. Specifically, many parameters cannot be entirely standardized between the two. These include probe design, handling of intragenic regions, signal quality thresholds, data processing methods, and methods of identifying differentially expressed genes.

Quantitative polymerase chain reaction (qPCR) can be used as a third measure of transcript abundance. Marioni et al. (2008) used qPCR to measure transcripts that were identified as differentially expressed by either RNA-Seq or microarray, but not both. Five genes identified by RNA-Seq were measured by qPCR; four (80 percent) were confirmed to be differentially expressed. Six genes identified by microarray were

measured by qPCR; two (33 percent) were confirmed to be differentially expressed. These qPCR results indicate that, while RNA-Seq generates some false positives and false negatives, it may be more accurate than microarray. The results are, however, limited in scope: very few discrepancies were tested. Thousands of transcripts were identified as differentially expressed by either RNA-Seq or microarray, but only eleven of these were subsequently measured by PCR. More testing is required for a conclusive assessment of the relative accuracy of the microarray method and RNA-Seq.

Precision of RNA-Seq

Like every measurement technique, RNA-Seq requires repetition for precision. Repetition in sequencing-based experiments is measured by depth of sequencing: the number of bases produced by the sequencer. In RNA-Seq experiments, deeper sequencing results in more precise measurements of transcript abundance. However, no commonly-accepted standard exists for determining whether a sample has been sequenced sufficiently.

A method used to compare the depth of sequencing in DNA sequencing experiments is fold-coverage: the amount of sequence generated divided by the length of the target. For example, recent sequencing of the cucumber genome achieved 68-fold coverage using short read sequencing to obtain 25 billion bases of sequence information for a 350 million base genome (Huang et al., 2009). Fold-coverage has been used to communicate the depth of sequencing of RNA-Seq experiments (Wilhelm et al., 2008), but is of value only in comparing experiments on the same tissue and species in similar conditions.

Precision can be assessed by calculating the fraction of transcripts that have been precisely measured. This approach to assessing the precision of RNA-Seq measurements was carried out by Mortazavi et al. (2008). Transcript abundance measurements (in reads per kilobase per million (RPKM)) are repeatedly calculated, using more of the total sequencing results with each iteration. Ongoing changes in the values suggest insufficient depth of sequencing. If the abundance of a transcript is constant as it is repeatedly calculated with increasing numbers of reads, the depth of sequencing is adequate for that transcript. A percentage of allowed variability is chosen; Mortazavi et al. (2008) calculated the fraction of transcript measurements that were within 5 percent of the value resulting from using all available reads.

This method can only be used with a transcript abundance measurement unit that includes normalization by the total number of mapped reads available, like RPKM, which divides the number of reads for a specific transcript by the total number of reads for all transcripts. As more sequencing results are included in the calculations, the number of reads corresponding to the transcript in question increases, but the total number of mapped reads does as well.

This approach is illustrated in Figure 1.2. Transcript abundance is measured for each transcript using increasing numbers of total mapped reads: 0.82 million, 2 million, etc., to the maximum total number of mapped reads generated: 41 million. The transcript abundance measurement for each transcript is compared to the final value measured for the transcript (for those transcripts with a final value above 3 RPKM). The fraction of transcripts within 5 percent of their final value is calculated.

Fifty percent of the values calculated with 8.2 million reads are within 5 percent of the same value they have after all 41 million reads are analyzed. As additional reads are included in the calculation, more and more transcripts reach a value within 5 percent of their final value.

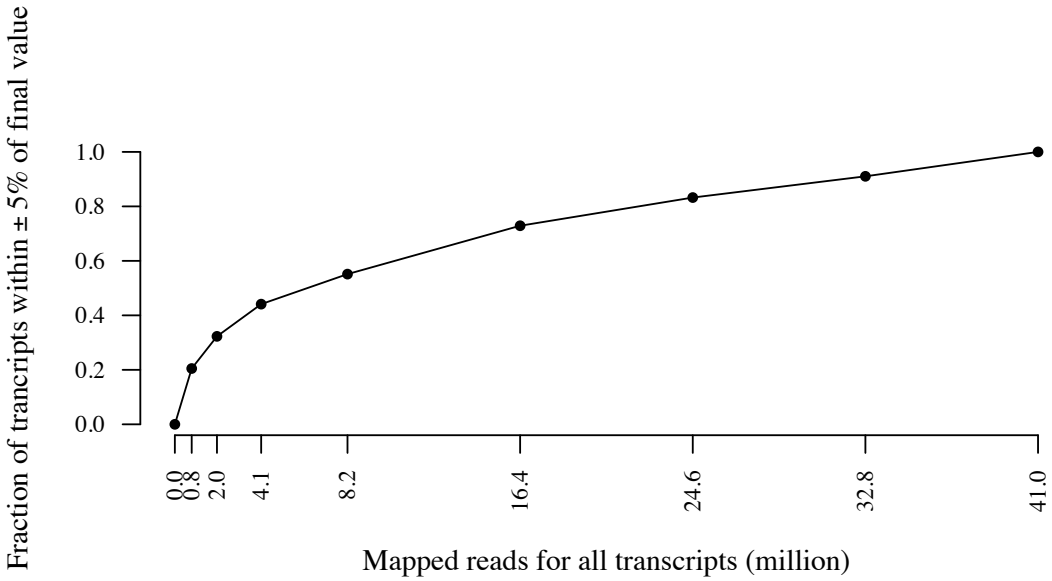

Figure 1.2: Deeper sequencing improves the precision of measurements of transcript abundance. Precision (on the y-axis) is represented by the fraction of genes with transcript abundance measurements within 5 percent of the final measured value, where the final measured value is the value calculated with the maximum available reads, in this case, 41 million. Precision is calculated at various sequencing depths, shown on the x-axis as mapped reads for all transcripts. Only transcripts with a final value above 3 RPKM are shown here. The abundance of each transcript was calculated for the first 0.82 million reads, and then for the first 2.05 million reads, and so on. Over half of the transcripts are within 5 percent of their final value at a sequencing depth of 8.2 million reads, above which precision increases more slowly. Graph after Mortazavi et al. (2008).

The relationship between deeper sequencing and increased precision is true for transcripts of any abundance. However, precision increases much faster for highly-abundant transcripts than for rarer ones, as shown in Figure 1.3. As in Figure 1.2,

precision (shown on the y-axis) is represented by the fraction of genes with transcript abundance measurements within 5 percent of the final measured value; the total number of mapped reads for all transcripts is shown on the x-axis; and all data is from Mortazavi et al. (2008). Transcripts were divided into four groups based on their final abundance measurement. Transcripts with abundance values greater than 3,000 RPKM reached 99 percent precision with less than a million reads, while transcripts with abundance values between 300 and 2,999 RPKM reached 99 percent precision only after 16.4 million reads are considered. Transcripts with abundance values between 30 and 299 RPKM reached a maximum of 94 percent precision.

Precision increases faster for highly-abundant transcripts because they comprise the majority of a transcript library and are thus favored by random sampling. The predominance of highly expressed transcripts is illustrated in the RNA-Seq results reported in Chapter 2, in which 50 percent of the transcript library is comprised of products from only seven percent of genes (Figure 2.2 on page 48).

This method of assessing the precision of RNA-Seq measurements is superior to fold-coverage assessments and will probably undergo improvements as RNA-Seq is more widely implemented. It only measures precision, not accuracy, but the increasing stability of abundance measurements further validate the quality of RNA-Seq measurements and provides quantitative information about imprecision in different categories of transcripts.

In summary, RNA-Seq is a sequencing-based technique that measures transcript abundance, identifies novel transcripts and provides linear measurements over a range

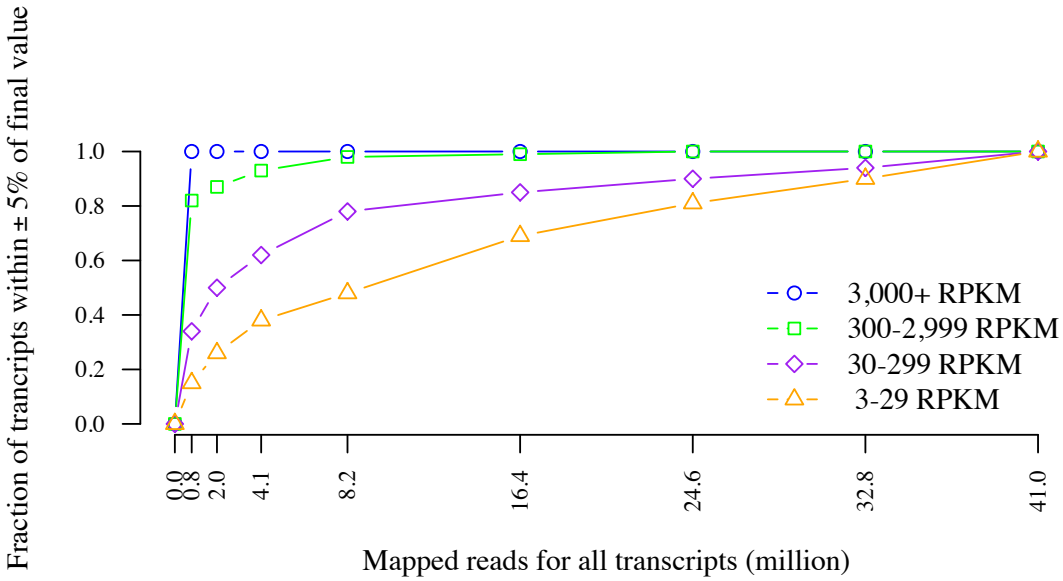

Figure 1.3: Less abundant transcripts require deeper sequencing for precise measurement. As in Figure 1.2, the fraction of transcripts with a measured abundance within 5 percent of their final value is shown on the Y axis, and the number of mapped reads for all transcripts is on the x-axis. Transcripts are grouped by final RPKM value. Transcripts of greater than 3,000 RPKM require fewer than a million reads for high precision: more than 99 percent of the transcripts are within 5 percent of their final value. However, of transcripts with final abundance measurements between 3 and 29 RPKM, 10 percent of them change more than 5 percent between 33 million and 41 million reads, adding uncertainty to the interpretation of the data. Graph after Mortazavi et al. (2008).

of five orders of magnitude. Although imperfect, the best information available suggests that RNA-Seq is more accurate than microarrays. Consequently, we chose to use RNA-Seq to identify differential expression in the densin knockout mouse.

1.2 Cofilin and the regulation of the dendritic spine cytoskeleton in synaptic potentiation

Dendritic spines exist in a variety of different shapes and sizes, corresponding to different functional characteristics. Spines on mature neurons fall into three morphological classes: mushroom-shaped, stubby, and thin. Shape impacts spine function: Mushroom-shaped spines have large heads and very thin necks that restrict Ca^{2+} transients from spreading to the dendritic shaft, and stubby spines have heads that lie close to the dendritic shaft and as such are less chemically isolated from the rest of the dendrite (Harris and Stevens, 1989; Hayashi and Majewska, 2005).

The strength of the synapse is proportional to the volume of the spine head, as demonstrated by electron microscopic (EM) reconstruction of dendrites from rat hippocampi. Head volume correlates with both the area of the PSD and the number of vesicles in the presynaptic compartment (Harris and Stevens, 1989).

Like synapses, spines are plastic. Spines emerge, retract, and change shape even in the adult brain. In long-term imaging of the cortex of adult mice *in vivo*, only about 50 percent of the spine population remains stable over the period of a month, while the rest grow and retract on the order of minutes to days (Trachtenberg et al., 2002). Changes in spine size can be elicited by synaptic stimulation, such as repeatedly uncaging glutamate in a way similar to high-frequency stimulation. This stimulation also causes an increase in synaptic strength as measured by AMPA current elicited by uncaging glutamate. This increase in AMPA current is proportional to the increase

in spine size (Matsuzaki et al., 2004), suggesting coordinated regulation of spine size and synaptic strength.

Together, these data show that spine size is variable, that it is proportional to the strength of the synapse, and that the two change in parallel in response to synaptic activity. We next consider mechanisms by which synaptic stimulation can regulate spine morphology.

Spine morphology is dictated by the underlying actin cytoskeleton (Carlisle and Kennedy, 2005). Like the well-studied leading edge of migrating cells, spines are actin-rich structures, and the changes to the cytoskeleton require changes in actin polymerization. Induced synaptic plasticity leads to increased spine size and an increased ratio of filamentous actin (F-actin) to globular actin (G-actin), demonstrated using fluorescence resonance energy transfer (FRET) between actin monomers (Okamoto et al., 2004). F-actin is a polar, continually treadmilling polymer, with one end favoring addition of monomers and the other removal. The rates of addition and removal of subunits are highly regulated by a number of actin-binding proteins, which are themselves highly regulated. For example, ADF/cofilin binds F-actin and promotes severing of filaments and dissociation of subunits at the dissociation-favoring end (Rosenblatt et al., 1997). ADF/cofilin activity is regulated by LIM kinase; when ADF/cofilin is phosphorylated, it becomes less active (Arber et al., 1998). This phosphorylation thus reduces depolymerization and supports stability or growth of the actin filaments and cytoskeleton (Carlisle and Kennedy, 2005).

Many actin-binding proteins are regulated by the Rho family of GTPases in an NMDA receptor-dependent manner (Carlisle and Kennedy, 2005). p21-activated kinase (PAK) is an important mediator for this signaling. PAK in turn activates LIMK. LIMK reduces actin depolymerization by phosphorylating cofilin and reducing its activity (Edwards et al., 1999). However, NMDA treatment leads to dephosphorylation of cofilin, indicating the involvement of an activity-regulated phosphatase (Carlisle et al., 2008). Chapter 3 discusses work on identifying the NMDA-regulated phosphatase that regulates activity-dependent changes in the spine and cytoskeleton.

1.3 Arc protein binding

Changes in synaptic strength can occur within minutes of stimulation. For these changes to represent memory, they must persist for days and months. A unique combination of properties suggests that Arc, an immediate early gene (IEG) named for its *A*ctivity *R*egulated and *C*ytoskeleton-associating properties, serves an important role in the transition to long-lasting forms of potentiation, which require transcription and protein synthesis. Arc can be linked to a synaptic event in two ways: temporally (it is transcribed in response to synaptic stimulation) and spatially (unique among IEG transcripts, Arc transcripts are localized to the activated portion of the dendrite) (Lyford et al., 1995; Steward et al., 1998). Arc is required for maintenance of synaptic plasticity and memory; both are impaired in the absence of Arc (Guzowski et al., 2000; Messaoudi et al., 2007; Plath et al., 2006). These compelling characteristics

have led several groups to investigate the mechanism by which Arc supports memory and synaptic plasticity.

A survey of the deficits that result from the absence of Arc indicates that it is involved in both hippocampal- and amygdala-dependent learning. Arc knockout mice have impaired memory, long term potentiation (LTP) and long term depression (LTD) (Plath et al., 2006). In the Morris water maze, the mice are deficient in both acquisition and reversal. Their performance in conditioned and cued fear tests is significantly poorer than that of the wild-type mice. The same is true for conditioned taste-aversion trials (Plath et al., 2006).

To identify the underlying cause of these memory deficits, LTP and LTD were studied in Arc knockout mice. *In vivo* induction of LTP at perforant path/granule cell synapses in anesthetized knockout mice results in enhanced early LTP and an early return to baseline compared to wild-type mice (Plath et al., 2006). The same trend is found when LTP is induced at the Schaffer collateral/CA1 pyramidal cell synapses in slice preparations. The results of LTD induction at the Schaffer collateral/CA1 pyramidal cell synapses are complementary to the LTP findings: initial depression is reduced in the knockout, and responses return to baseline earlier than in the wild-type mice (Plath et al., 2006). These changes in synaptic potentiation were not limited to mice: Rats that have decreased levels of Arc protein due to hippocampal infusions of Arc antisense oligodeoxynucleotides have impaired maintenance of LTP beyond 4 hours (Guzowski et al., 2000).

These data demonstrate the requirement for Arc in memory and synaptic potentiation, but do not indicate the mechanism by which it supports them. Two possible mechanisms are suggested by the nature of the proteins that bind Arc: regulation of AMPA receptor endocytosis through dynamin and endophilin and cytoskeletal regulation through actin-binding partners.

Arc's ability to promote AMPA receptor endocytosis through dynamin and endophilin has been demonstrated (Chowdhury et al., 2006). Furthermore, loss of Arc results in increased surface AMPA receptors and decreased endocytosis rates. This phenotype can be rescued by Arc overexpression, but not by expression of a mutant version of Arc lacking the endophilin-binding domain (Chowdhury et al., 2006).

Arc-induced endocytosis of AMPA receptors is undisputed, and no other synaptic role for Arc is supported by as much data. However, LTP studies in Arc knockout mice indicate that Arc is involved in maintaining increases in synaptic strength, and it is unclear how AMPA receptor endocytosis, which decreases synaptic strength, could underlie Arc's role in LTP. A homeostatic role has been hypothesized. Alternately, Arc's role in LTP may be due to a different activity.

Arc may support maintenance of memory and changes in synaptic strength via actin regulation. Maintenance of LTP requires remodeling of the actin cytoskeleton, and several lines of evidence indicate an association between Arc and actin: (1) Arc co-sediments with purified filamentous actin in cell extracts, but not with purified filamentous actin, suggesting that an intermediate protein binds Arc to actin (Lyford et al., 1995); (2) Arc binds MAP2, which also binds F-actin (Fujimoto et al., 2004;

Roger et al., 2004); (3) Arc binds dynamin, which co-localizes with actin and directly binds several actin-binding proteins (Chowdhury et al., 2006; Schafer, 2004); (4) Arc binds CaMKII (Donai et al., 2003), the β subunit of which binds actin (Sanabria et al., 2009). A role for Arc in cytoskeletal regulation is further suggested by the similarities between electrophysiological studies of Arc knockout mice and mice in which cytoskeletal reorganization has been prevented. Compounds that block reorganization specifically affect the maintenance but not the induction of LTP (Krucker et al., 2000).

To clarify the mechanism by which Arc regulates synaptic strength, we further investigated Arc binding proteins. Chapter 4 focuses on identifying Arc binding proteins in the forebrains of mice and identifying the Arc binding domains involved. These studies were inconclusive, but negative results are presented.

1.4 Conclusion

Synaptic potentiation is supported by signaling machinery in the postsynaptic density, activity-dependent regulation of the size of dendritic spines and synaptically-regulated gene expression. I will describe studies into each in the following chapters.

References

Ansorge WJ (2009) Next-generation DNA sequencing techniques. New biotechnology 25:195–203.

Apperson ML, Moon IS, Kennedy MB (1996) Characterization of Densin-180, a New Brain-Specific Synaptic Protein of the O-Sialoglycoprotein Family. Journal of Neuroscience 16:6839–6852.

Arber S, Barbayannis F, Hanser H, Schneider C, Stanyon C, Bernard O, Caroni P (1998) Regulation of actin dynamics through phosphorylation of cofilin by LIM-kinase. Nature 393:805–809.

Bennett S, Barnes C, Cox A, Davies L, Brown C (2005) Toward the thousand dollar human genome. Pharmacogenomics 6:373–382.

Carlisle H, Kennedy M (2005) Spine architecture and synaptic plasticity. Trends in Neurosciences 28:182–187.

Carlisle HJ, Manzerra P, Marcora E, Kennedy MB (2008) SynGAP regulates steady-state and activity-dependent phosphorylation of cofilin. Journal of Neuroscience 28:13673–83.

Chowdhury S, Shepherd J, Okuno H, Lyford G, Petralia R, Plath N, Kuhl D, Huganir R, Worley P (2006) Arc/Arg3.1 interacts with the endocytic machinery to regulate AMPA receptor trafficking. Neuron 52:445–459.

Donai H, Sugiura H, Ara D, Yoshimura Y, Yamagata K, Yamauchi T (2003) Interaction of Arc with CaM kinase II and stimulation of neurite extension by Arc in neuroblastoma cells expressing CaM kinase II. Neuroscience Research 47:399–408.

Edwards D, Sanders L, Bokoch G, Gill G (1999) Activation of LIM-kinase by Pak1 couples Rac/Cdc42 GTPase signalling to actin cytoskeletal dynamics. Nature Cell Biology 1:253–259.

Fujimoto T, Tanaka H, Kumamaru E, Okamura K, Miki N (2004) Arc interacts with microtubules/microtubule-associated protein 2 and attenuates microtubule-associated protein 2 immunoreactivity in the dendrites. Journal of Neuroscience Research 76:51–63.

Guzowski JF, Lyford GL, Stevenson GD, Houston FP, McGaugh JL, Worley PF, Barnes CA (2000) Inhibition of activity-dependent arc protein expression in the rat hippocampus impairs the maintenance of long-term potentiation and the consolidation of long-term memory. Journal of Neuroscience 20:3993–4001.

Harismendy O, Ng PC, Strausberg RL, Wang X, Stockwell TB, Beeson KY, Schork NJ, Murray SS, Topol EJ, Levy S, Frazer KA (2009) Evaluation of next generation sequencing platforms for population targeted sequencing studies. Genome Biology 10:R32.

Harris KM, Stevens JK (1989) Dendritic spines of CA 1 pyramidal cells in the rat hippocampus: serial electron microscopy with reference to their biophysical characteristics. Journal of Neuroscience 9:2982–2997.

Hayashi Y, Majewska AK (2005) Dendritic spine geometry: functional implication and regulation. Neuron 46:529–32.

Huang S, Li R, Zhang Z, Li L, Gu X, Fan W, Lucas WJ, Wang X, Xie B, Ni P, Ren Y, Zhu H, Li J, Lin K, Jin W, Fei Z, Li G, Staub J, Kilian A, van der Vossen EAG, Wu Y, Guo J, He J, Jia Z, Ren Y, Tian G, Lu Y, Ruan J, Qian W, Wang M, Huang Q, Li B, Xuan Z, Cao J, Asan, Wu Z, Zhang J, Cai Q, Bai Y, Zhao B, Han Y, Li Y, Li X, Wang S, Shi Q, Liu S, Cho WK, Kim JY, Xu Y, Heller-Uszynska K, Miao H, Cheng Z, Zhang S, Wu J, Yang Y, Kang H, Li M, Liang H, Ren X, Shi Z, Wen M, Jian M, Yang H, Zhang G, Yang Z, Chen R, Liu S, Li J, Ma L, Liu H, Zhou Y, Zhao J, Fang X, Li G, Fang L, Li Y, Liu D, Zheng H, Zhang Y, Qin N, Li Z, Yang G, Yang S, Bolund L, Kristiansen K, Zheng H, Li S, Zhang X, Yang H, Wang J, Sun R, Zhang B, Jiang S, Wang J, Du Y, Li S (2009) The genome of the cucumber, Cucumis sativus L. Nature Genetics advance online publication.

Izawa I, Nishizawa M, Ohtakara K, Inagaki M (2002) Densin-180 interacts with delta-catenin/neural plakophilin-related armadillo repeat protein at synapses. Journal of Biological Chemistry 277:5345–50.

Jiao Y, Robison AJ, Bass MA, Colbran RJ (2008) Developmentally regulated alternative splicing of densin modulates protein-protein interaction and subcellular localization. Journal of Neurochemistry 105:1746–1760.

Krucker T, Siggins GR, Halpain S (2000) Dynamic actin filaments are required for stable long-term potentiation (LTP) in area CA1 of the hippocampus. Proceedings

of the National Academy of Sciences of the United States of America 97:6856–6861.

Lyford GL, Yamagata K, Kaufmann WE, Barnes CA, Sanders LK, Copeland NG, Gilbert DJ, Jenkins NA, Lanahan AA, Worley PF (1995) Arc, a growth factor and activity-regulated gene, encodes a novel cytoskeleton-associated protein that is enriched in neuronal dendrites. Neuron 14:433–445.

Margulies M, Egholm M, Altman W, Attiya S, Bader J, Bemben L, Berka J, Braverman M, Chen Y, Chen Z, et al. (2005) Genome sequencing in open microfabricated high density picoliter reactors. Nature 437:376.

Marioni J, Mason C, Mane S, Stephens M, Gilad Y (2008) RNA-seq: An assessment of technical reproducibility and comparison with gene expression arrays. Genome Research 18:1509–1517.

Matsuzaki M, Honkura N, Ellis-Davies G, Kasai H (2004) Structural basis of long-term potentiation in single dendritic spines. Nature 429:761–766.

Medina-Marino A (2009) Construction and Initial Characterization of the Densin Knockout Mouse. Ph.D. thesis, California Institute of Technology.

Messaoudi E, Kanhema T, Soulé J, Tiron A, Dagyte G, da Silva B, Bramham CR (2007) Sustained Arc/Arg3.1 synthesis controls long-term potentiation consolidation through regulation of local actin polymerization in the dentate gyrus in vivo. Journal of Neuroscience 27:10445–55.

Mortazavi A, Williams BA, McCue K, Schaeffer L, Wold B (2008) Mapping and quantifying mammalian transcriptomes by RNA-Seq. Nature Methods 5:621–628.

Nakagawa T, Engler JA, Sheng M (2004) The dynamic turnover and functional roles of alpha-actinin in dendritic spines. Neuropharmacology 47:734–745.

Ohtakara K, Nishizawa M, Izawa I, Hata Y, Matsushima S, Taki W, Inada H, Takai Y, Inagaki M (2002) Densin-180, a synaptic protein, links to PSD-95 through its direct interaction with MAGUIN-1. Genes to Cells 7:1149–60.

Okamoto KI, Nagai T, Miyawaki A, Hayashi Y (2004) Rapid and persistent modulation of actin dynamics regulates postsynaptic reorganization underlying bidirectional plasticity. Nature Neuroscience 7:1104–1112.

Plath N, Ohana O, Dammermann B, Errington ML, Schmitz D, Gross C, Mao X, Engelsberg A, Mahlke C, Welzl H, Kobalz U, Stawrakakis A, Fernandez E, Waltereit R, Bick-Sander A, Therstappen E, Cooke SF, Blanquet V, Wurst W, Salmen B, Bösl MR, Lipp HP, Grant SGN, Bliss TVP, Wolfer DP, Kuhl D (2006) Arc/Arg3.1 is essential for the consolidation of synaptic plasticity and memories. Neuron 52:437–44.

Quitsch A, Berhörster K, Liew CWW, Richter D, Kreienkamp HJJ (2005) Postsynaptic shank antagonizes dendrite branching induced by the leucine-rich repeat protein Densin-180. Journal of Neuroscience 25:479–487.

Rinta-Valkama J, Aaltonen P, Lassila M, Palmén T, Tossavainen P, Knip M, Holthöfer H (2007) Densin and filtrin in the pancreas and in the kidney, targets for humoral

autoimmunity in patients with type 1 diabetes. Diabetes/metabolism research and reviews 23:119–126.

Roger B, Al-Bassam J, Dehmelt L, Milligan RA, Halpain S (2004) MAP2c, but not tau, binds and bundles F-actin via its microtubule binding domain. Current Biology 14:363–371.

Rosenblatt J, Agnew BJ, Abe H, Bamburg JR, Mitchison TJ (1997) Xenopus actin depolymerizing factor/cofilin (XAC) is responsible for the turnover of actin filaments in Listeria monocytogenes tails. Journal of Cell Biology 136:1323–1332.

Sanabria H, Swulius M, Kolodziej S, Liu J, Waxham M (2009) {beta} CaMKII Regulates Actin Assembly and Structure. Journal of Biological Chemistry 284:9770.

Schafer DA (2004) Regulating actin dynamics at membranes: a focus on dynamin. Traffic 5:463–9.

Shendure J, Porreca G, Reppas N, Lin X, McCutcheon J, Rosenbaum A, Wang M, Zhang K, Mitra R, Church G (2005) Accurate multiplex polony sequencing of an evolved bacterial genome. Science 309:1728.

Simon SA, Zhai J, Nandety RS, McCormick KP, Zeng J, Mejia D, Meyers BC (2009) Short-Read Sequencing Technologies for Transcriptional Analyses. Annual Review of Plant Biology 60:305–333.

Steward O, Wallace CS, Lyford GL, Worley PF (1998) Synaptic activation causes the mRNA for the IEG Arc to localize selectively near activated postsynaptic sites on dendrites. Neuron 21:741–751.

Strack S, Robison AJ, Bass MA, Colbran RJ (2000) Association of calcium/calmodulin-dependent kinase II with developmentally regulated splice variants of the postsynaptic density protein densin-180. Journal of Biological Chemistry 275:25061–25064.

Sultan M, Schulz M, Richard H, Magen A, Klingenhoff A, Scherf M, Seifert M, Borodina T, Soldatov A, Parkhomchuk D, et al. (2008) A global view of gene activity and alternative splicing by deep sequencing of the human transcriptome. Science 321:956.

Trachtenberg JT, Chen BE, Knott GW, Feng G, Sanes JR, Welker E, Svoboda K (2002) Long-term in vivo imaging of experience-dependent synaptic plasticity in adult cortex. Nature 420:788–794.

Walikonis RS, Oguni A, Khorosheva EM, Jeng CJ, Asuncion FJ, Kennedy MB (2001) Densin-180 forms a ternary complex with the (alpha)-subunit of Ca2+/calmodulin-dependent protein kinase II and (alpha)-actinin. Journal of Neuroscience 21:423–433.

Wall PK, Leebens-Mack J, Chanderbali AS, Barakat A, Wolcott E, Liang H, Landherr L, Tomsho LP, Hu Y, Carlson JE, Ma H, Schuster SC, Soltis DE, Soltis PS, Altman

N, dePamphilis CW (2009) Comparison of next generation sequencing technologies for transcriptome characterization. BMC Genomics 10:347+.

Wang L, Xu J, Wu Q, Dai J, Ye X, Zeng L, Ji C, Gu S, Zhao RC, Xie Y, Mao Y (2003) Cloning and characterization of a novel splice variant of the brain-specific protein densin-180. Int J Mol Med 11:257–60.

Wilhelm BT, Landry JR (2009) RNA-Seq—quantitative measurement of expression through massively parallel RNA-sequencing. Methods 48:249–257.

Wilhelm BT, Marguerat S, Watt S, Schubert F, Wood V, Goodhead I, Penkett CJ, Rogers J, Bähler J (2008) Dynamic repertoire of a eukaryotic transcriptome surveyed at single-nucleotide resolution. Nature 453:1239–43.

Wyszynski M, Kharazia V, Shanghvi R, Rao A, Beggs AH, Craig AM, Weinberg R, Sheng M (1998) Differential regional expression and ultrastructural localization of alpha-actinin-2, a putative NMDA receptor-anchoring protein, in rat brain. Journal of Neuroscience 18:1383–1392.

Wyszynski M, Lin J, Rao A, Nigh E, Beggs AH, Craig AM, Sheng M (1997) Competitive binding of alpha-actinin and calmodulin to the NMDA receptor. Nature 385:439–442.

Chapter 2

Differential transcription in the densin knockout mouse as measured by RNA-Seq

Holly Beale, Andrew Medina-Marino, Ali Mortazavi, Barbara Wold, Mary Kennedy

2.1 Introduction

The postsynaptic density (PSD) is a dense mesh of neurotransmitter receptors, signal transduction molecules, and scaffold proteins localized to the postsynaptic portion of a synapse. Specificity of binding within the PSD has important consequences, enabling selective activation of proteins by positioning particular calcium-activated molecules near calcium influx. The microdomain of the initial calcium event governs the downstream signaling events, causing alterations not only in nearby cytoskeleton by also in gene expression.

Densin is a large, abundant postsynaptic protein that is tightly bound in the PSD. It is a LRR And PDZ domain-containing (LAP) protein with 16 leucine rich repeat (LRR) domains, a C-terminal PDZ domain, and a mucin-like domain that is

glycosylated with large sialic acid residues, which are only found on extracellular protein domains (Walikonis et al., 2001). Densin binds MAGUIN-1, α-actinin, δ-catenin and shank (Izawa et al., 2002; Nakagawa et al., 2004; Ohtakara et al., 2002; Quitsch et al., 2005; Wyszynski et al., 1997). It also binds CaMKII in an activity-dependent manner: The affinity increases dramatically when CaMKII is autophosphorylated, as it is after LTP (Strack et al., 2000; Walikonis et al., 2001). The densin knockout mouse displays behaviors that suggest neuropathy. It clasps (tucks its limbs into its body) when suspended by its tail, a behavior that is common in many types of neuropathy. It also has seizures when injected with pentobarbital, a γ-aminobutyric acid$_A$ receptor (GABA$_A$R) agonist that is used as a general anesthetic, also called Nembutal (personal communication, T. Luong). Neuronal cultures from the knockout mouse have 25 percent less autophosphorylated CaMKII than found in wild-type neuronal cultures. Furthermore, the CaMKII autophosphorylation is more responsive to glutamate receptor stimulating conditions; it increases twice as much as it does in wild-type cultures (H. Carlisle, personal communication). Densin could affect a number of cellular processes through its validated binding partners, and the phenotype of the knockout suggests the importance of the protein to synaptic biochemistry and neuronal function.

Three factors motivated us to analyze the transcriptome of the densin knockout mouse. First, synaptic regulation of transcription is well established (Flavell and Greenberg, 2008), and the loss of densin could disrupt synaptic activity. Second, an analysis of pathways affected by the loss of densin could identify other cellular

roles for densin. Third, the densin knockout mouse displays seizures in response to pentobarbital, which could indicate disruption of GABAergic transmission. We hoped to narrow the potential causes of the densin knockout phenotypes by taking a broad view and analyzing all transcripts.

We measured transcription levels using RNA-Seq, a technique in which transcript levels are measured by short-read sequencing. RNA-Seq produces millions of short sequences, called reads. The number of reads corresponding to a given transcript are used as a measurement of the abundance of that transcript, after normalization for the length of the transcript and the total number of reads generated for all sequences.

Transcription has been studied in other mice with postsynaptic proteins deleted using microarray techniques. When microarray and RNA-Seq are used to detect differentially expressed (DE) genes in the same samples in the same laboratory, they only agree on approximately fifty percent of the genes identified by either method. Moreover, early studies suggest that RNA-Seq is the more accurate method (Marioni et al., 2008; Sultan et al., 2008). Microarray results therefore provide only a tenuous prediction of RNA-Seq results, particularly when comparing work from different labs on different genotypes.

With these caveats in mind, microarray studies of PSD protein knockout mice have produced some interesting findings. Ras-GRF1 is a ras guanine nucleotide exchange factor that is enriched at the PSD and phosphorylated by CaMKII (Sturani et al., 1997). Gene expression was analyzed in hippocampal tissue laser-dissected from 10 μm transverse brain sections of Ras-GRF1 knockout mice (Fernández-Medarde et al.,

2007). Thirty-six DE transcripts were identified, none of them other ras or guanine nucleotide exchange factor (GEF) genes. Of the DE transcripts, most (27) were decreased. Two were PSD proteins as categorized by Cheng et al. (2006): 14-3-3 zeta and CSNK1D (casein kinase 1 delta). Many of the DE genes are known to participate in signal transduction pathways downstream of Ras-GFR1, particularly Ras/G protein signaling and microtubule organization pathways.

Hippocampal samples from mice heterozygous for a CaMKIIα null mutation have also been analyzed by microarray methods (Yamasaki et al., 2008). Two thousand transcripts were reported to be DE, nine of which were specifically named by the authors. None of the nine were PSD proteins as categorized by Cheng et al. (2006). Further analysis indicated a 30 percent decrease in NMDA receptors as measured by radiolabeled receptor agonist. Analysis of expression patterns of these genes in wild-type animals, along with behavioral and electrophysiological experiments, led the researchers to conclude that the effects were strongly localized to the dentate gyrus (Yamasaki et al., 2008).

Although microarray results are not a strong predictor of RNA-Seq results, an extrapolation of these microarray results to our RNA-Seq experiment would suggest that we might find DE genes that are downstream in signal transduction pathways, and that do not necessarily directly bind densin. A much greater number of DE genes were identified in the CaMKIIα heterozygous mice than in RAS-GRF knockout mice. While this might be due to different methods of analysis, two other possibilities are of interest. First, the number of DE genes could be a function of the size of downstream

signal transduction pathways. Second, the number of DE genes could be a function of the magnitude of the downstream signal transduction effects.

In the present study, we report the transcriptional effects of the loss of the protein densin. We find changes in the densin binding partner CaMKIIα, in immediate early genes (IEGs) known to be regulated by synaptic activity, and in $GABA_AR$ subunits. These findings are the outcome of a new application of this technology; we are aware of no published reports using RNA-Seq analysis to compare gene expression in the brains of knockout and wild-type mice.

2.2 Materials and Methods

Generating densin knockout mice

Densin knockout mice were generated as previously described (Medina-Marino, 2009). Briefly, a 9.9 kb sequence containing densin (lrrc7) exon 3, which includes the translation start codon, was cloned from strain 129S1/SvImJ. The sequence was modified to add a hygromycin selection cassette and loxP sequences to enable Cre-catalyzed recombination. After the construct was electroporated into CJ7 ES cells and recombination confirmed, clones with normal karyotypes were expanded and injected into 129B6 blastocysts, which were implanted into pseudo-pregnant mothers. Chimeric offspring were bred to C57BL/6 EIIa-cre$^{+/+}$ expressing female mice, generating either knockout or conditional knockout offspring. All experiments discussed here compare non-conditional knockout mice and their wild-type siblings.

The densin knockout mouse line is maintained in the heterozygous state. Genotype is determined by polymerase chain reaction (PCR) amplification with primers 5′- GAGATGCTCTCAAGATAGACATG-3′, 5′-CTCAATTCTGAAGCCAGTAG-3′ and 5′-ACAGAACTGGCTTCTGTCCAC-3′ followed by gel electrophoresis. The product of the deletion allele is 257 bases; the product of the wild-type allele is 187 bases.

RNA Sequencing

Ten adult male mice were used for RNA-Seq analysis. Forebrain samples were harvested from two pairs of mice, with each pair consisting of one wild-type and one

densin knockout mouse from the same litter, 11-12 weeks old. Forebrain samples include olfactory bulb, cerebral cortex, hippocampal formation, striatum, palladium, thalamus, hypothalamus and midbrain, while excluding pons, medulla and cerebellum. Hippocampal samples were harvested from six littermates, three knockout and three wild-type, 16 weeks old. The densin knockout mice described above were outcrossed twice with C57BL/6 strain. All litters used for RNA-Seq were the product of this outcross.

Total RNA was prepared from tissue that was flash frozen in liquid nitrogen, weighed, minced in mirVana lysis buffer (from mirVana miRNA Isolation Kit, Catalog No. AM1560, Ambion, Foster City, CA) and sheared using 20g and 25g needles successively. miRNA Homogenate Additive from the mirVana miRNA Isolation Kit was added to a concentration of 10 percent, mixed and the solution was incubated on ice for ten minutes. Total RNA was extracted with phenol/chloroform, ScriptGuard RNase Inhibitor was added, and concentration was measured with the Nanodrop quantification system (Thermo Scientific, Waltham, MA). Genomic DNA was digested with Baseline Zero DNase (Epicentre Biotechnologies). Phenol/chloroform extraction was repeated and RNA was precipitated overnight with ethanol at 4° Celsius. ScriptGuard was then added and RNA concentration measured as before.

A cDNA fragment library was prepared as previously described (Mortazavi et al., 2008). Briefly, mRNA was purified from total RNA by two cycles of hybridization to oligo(dT) beads (Dynal). These transcripts were fragmented by metal ion-catalysis. First-strand cDNAs were synthesized with random hexamer primers (Invitrogen cat.

no. 48190-011) using the SuperScript Double-Stranded cDNA Synthesis Kit (Invitrogen cat. no. 11917-010) according to manufacturer's instructions. The second strand was synthesized by nick-translation in custom buffer (Illumina). Different 5′ and 3′ adapters were ligated to the double stranded cDNA, and then amplified with primers complementary to the adapters to enrich the sample for successfully ligated fragments. The fragment library was size selected from an agarose gel for fragments of between 175 and 225 bases in length.

The cDNA fragment library was diluted to 3, 4 or 8pM and loaded on the flow cell at the cluster station (Illumina). The following steps were carried out within the flow cell, the surface of which contains covalently bound primers. These primers are complementary to the adapter sequences previously ligated to the cDNA fragments. The combined fragment-adapter oligonucleotides were flowed over the surface and hybridized to the primer. Taq polymerase was added to extend the primer, creating a covalently-bound oligonucleotide complementary to the original fragment. The two strands were denatured and the original fragment washed away.

The free ends of the newly extended oligonucleotide were hybridized to a primer covalently bound to the surface of the flow cell, forming a bridge. The second primer was extended, the two strands denatured, and each could hybridize with another nearby complementary primer. Subsequent rounds of extension and denaturation generated numerous adjacent copies of the original fragment. After the final extension, all fragments were denatured and one of the primers was cleaved by restriction digest, resulting in a cluster of numerous single-stranded copies of the original fragment. Free

3′ ends were blocked to prevent further priming. In preparation for sequencing, the sequencing primer was added.

The flow cell was transferred to the sequencer (Illumina's Genome Analyzer). Primers were extended one base at a time with fluorescently-labeled, reversibly-terminated nucleotides; the fluorophore is cleavable and termination was accomplished by addition of an azide group to the 3' oxygen of the 2' deoxyribose sugar that prevents further synthesis until is it cleaved (Metzker, 2009). After each extension, the flow cell was imaged, and the identity of the newly added base was determined from its fluorescence signal. The sequence of a single fragment was generated from the series of bases identified at a single location. Each extension was followed by cleavage of the fluorescent label and terminator, after which another round of extension was begun. The number of sequencer runs and resultant reads for each of our samples are shown in Table 2.1.

Table 2.1: Libraries prepared from the forebrain and hippocampus of wild-type and densin knockout mice were sequenced. The number of unique reads for each sequence run is shown, in millions. Forebrain tissue was obtained from four mice: wild-type 1 (WT1) and knockout 1 (KO1), which were littermates; and WT2 and KO2, which were littermates from a different litter than WT1 and KO1. Hippocampal tissue was obtained from six mice from a single litter: wild-type animals 3–5 (WT3–5) and knockout animals 3–5 (KO3–5).

	Forebrain				Hippocampus					
	WT1	KO1	WT2	KO2	WT3	KO3	WT4	KO4	WT5	KO5
	5.9	7.6	9.5	6.1	7.7	6.2	10.6	6.9	8.6	8.2
	7.6	6.8	9.1	9.4	4.3	3.5				
			5.2	7.8						
Total reads	13.5	14.4	23.8	23.3	12.0	9.7	10.6	6.9	8.6	8.2

Data Analysis

The computer program Bowtie (Langmead et al., 2009) was used to align sequences to the mouse genome (mm9, US National Center for Biotechnology Information build 37). ERANGE (Mortazavi et al., 2008) was used to derive measurements of the abundance of each transcript. Transcripts were identified in the University of California Santa Cruz (UCSC) Known Genes database (Hsu et al., 2006).

ERANGE counts the number of sequences (reads) within each gene. To improve the accuracy of comparisons of abundance among transcripts, the length of a transcript is taken into account. Longer transcripts have more corresponding reads than similarly expressed shorter transcripts. Consequently, ERANGE divides the number of reads attributed to a gene by the length of the corresponding transcript in kilobases.

To improve the accuracy of comparisons across flow cells, the total number of reads in a run is considered. Factors not related to transcript abundance in the original sample can alter the efficiency of the sequencing process, as shown by variability in the number of total reads generated in each lane of each run of the Solexa sequencer. This variability can be caused by errors in measurement of concentration of input and by the density of the oligos coating the flow cell. The total number of reads produced by a run of the sequencer is used as a normalization factor to account for variability both in the sample and in the preparation and sequencing processes. ERANGE implements this normalization by dividing the number of reads assigned to each gene by the total number of reads produced by that run of the sequencer

in millions of reads. The final unit is "Reads per Kilobase (of the total transcript length) per Million (total reads reported by the sequencer)," abbreviated **RPKM**.

Reads can match one or more positions in the reference sequence (in this case, the mouse genome). ERANGE can assign fractions of reads to multiple genes in a probabilistic manner when genes match at multiple positions. However, in order to avoid false positive changes in similar transcripts, our analysis excludes reads that match at multiple positions.

We used the following programs in this analysis: R (http://www.R-project.org) for calculations and visualization (R Development Core Team, 2008), Ingenuity Pathway Analysis (http://www.ingenuity.com) for pathway analysis, and Princeton Slim GO Mapper (http://go.princeton.edu) for identifying patterns in gene ontology classifications. We obtained correlations between brain structures and transcript expression from the Allen Brain Atlas (Lein et al., 2007).

Because the precision of RNA-Seq increases with the abundance of the transcript, the standard deviation is dependent on the abundance of the transcript as well. In order to identify significant changes, we calculated a smoothed moving average and standard deviation.

The transcript abundance measurements (in RPKM) were transformed using a base 2 logarithmic scale. We subtracted the transcript abundance in the experimental condition from the transcript abundance in the control condition and plotted the change against the control condition in a Tukey mean-difference (Bland-Altman) plot, similar to the MA (microarray) plot. For each transcript, the mean and standard

deviation of the change in abundance was calculated based on the 500 transcripts with the most similar abundance in the control condition. Due to the large number of transcripts that are similarly expressed, this averaged mean was still highly variable as shown in Figure 2.1. We applied a local regression to the mean and standard deviation using the LOWESS (locally weighted scatterplot smoothing) method with a span of 66 percent of the data points (f=.66). We identified significant changes in transcript abundance as those changes with a z-score above two (i.e. more than two standard deviations from the smoothed local mean) (Quackenbush, 2002).

Three comparisons of gene expression were performed: knockout forebrain was compared to wild-type forebrain, knockout hippocampus was compared to wild-type hippocampus, and wild-type forebrain was compared to wild-type hippocampus.

The lists of DE genes were analyzed with Ingenuity Pathway Analysis (IPA, http://www.ingenuity.com), a proprietary service that identifies relationships between groups of genes based on a curated global interaction network. Each list of DE genes contains the gene symbol and the number of standard deviations between the change in expression for that specific gene and the mean change of similarly expressed transcripts. The lists were uploaded to IPA. Genes for which IPA had interaction information were mapped to their counterparts in IPA's global network model. Genes that were not mapped often corresponded to loci for which an official symbol had not been designated (e.g. 1110059M19Rik, LOC100042459). The relationships between mapped genes in the IPA global network model were assessed and weighted by the number of standard deviations. Groups of connected genes were

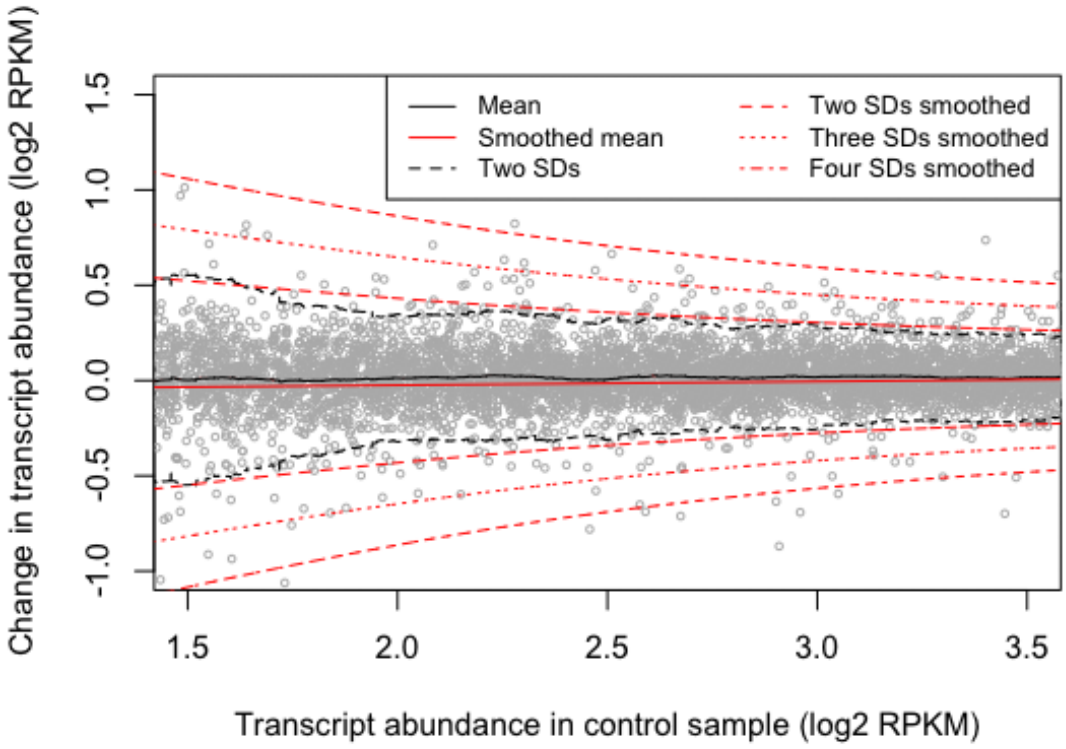

Figure 2.1: Smoothed mean and standard deviation lines permit more consistent identification of differentially expressed genes. The change in transcript abundance in log2 RPKM units is plotted against the transcript abundance in the control sample; these points are shown in grey. The mean change in transcript abundance is calculated for each transcript from the five hundred transcripts most similarly expressed in the control sample. This method was applied to each comparison of RPKM values; the samples shown here are wild-type forebrain (control) and densin knockout forebrain (experimental).

returned as networks with a score based on a P value; a higher score indicates a lower probability that the network is included by chance. The analysis was performed with settings specifying that direct and indirect relationships (those which do not require physical contact) be considered. Relationships identified in human, rat and mouse, as well as all tissues and cell lines were included.

We investigated whether DE genes were most highly expressed in particular brain structures. The Allen Mouse Brain Atlas project has generated anatomical expression data for many genes using automated *in situ* hybridization. From this data, they quantified the intensity and density of expression in different brain structures (Lein et al., 2007), normalizing by expression of a ubiquitously expressing gene in each structure. Quantitation of intensity is intended to correlate with microarray-type measurements; it is the average expression per cell normalized by the number of cells in the region that express a ubiquitously expressed gene. Density measures the percent of cells in a region that express the transcript. Density is the number of expressing cells in a region divided by the number of cells in the region that express a ubiquitously expressing gene (Allen Institute for Brain Science, 2006). We downloaded the data in XML format, parsed the files and organized the information in a relational format. We compared the intensity and density for five brain structures

Gene ontology annotations describe the function, localization or cellular component of a gene product. We used the Princeton web implementation of GOTermFinder (Boyle et al., 2004) to evaluate the annotations of DE genes. GOTermFinder uses high-level terms to identify commonalities in a list of genes. The scientific support for an annotation is assigned an evidence code, such as "Inferred from Direct Assay" and "Inferred from Electronic Annotation." No evidence codes were excluded from our analysis.

2.3 Results

RNA transcript abundance was measured in densin knockout and wild-type mice using ultra-high-throughput sequencing of RNA (RNA-Seq). Five pairs of mice were used, each consisting of a densin knockout mouse and a wild-type littermate. Transcript levels were measured in libraries prepared from the forebrain of two pairs. Hippocampal transcripts levels were measured in libraries prepared from three pairs, all of which came from the same litter. The data generated by RNA-Seq were analyzed to identify genes which were DE between wild-type and knockout animals; these lists were further analyzed to identify patterns of co-regulation.

2.3.1 Processing sequence data

As described in Materials and Methods, RNA-Seq produces a list of sequences, called reads, present in the pool of transcripts. Table 2.1 summarizes the number of reads obtained from each sample, including forebrains of wild-type (WT) and knockout (KO) littermates from litters 1 and 2 (WT1, KO1, WT2, KO2) and hippocampi from one litter including three wild-type and three knockout littermates: (WT3, KO3, WT4, KO4, WT5, KO5). Each read was aligned to the genome with a sequence alignment program called Bowtie, which is specialized for aligning millions of short reads to a genome (Langmead et al., 2009). Transcript abundance was calculated using ERANGE, which counts reads falling within gene models (the portion of a gene that codes for the transcript) (Mortazavi et al., 2008). This value was normalized by the length of the gene model as well as the total number of reads for all transcripts,

as described in Materials and Methods. The unit of transcript abundance is RPKM (Reads per Kilobase of transcript per Million bases sequenced).

2.3.2 Measuring gene expression

Precision of measurements

Precision of RNA-Seq results is affected by the number of times a library is measured (reflected in the reads produced) and by the abundance of each transcript. In order to measure the precision of the RNA-Seq results, we categorized transcript reads by abundance: not expressed, expressed below threshold (0.25 RPKM, discussed in the next section), and between the intervals of 0.25, 3, 30 and 300.

Figure 2.2 shows the large difference between the numbers of reads coming from the most abundant transcripts and those from moderately abundant transcripts. In a cDNA library prepared for RNA-Seq analysis of the densin knockout mouse, half of the library is composed of copies of just 7 percent of transcripts. Consequently, a random sample of transcripts will contain many examples of the most abundant transcripts, which are thus sequenced more frequently. More abundant transcripts will therefore be measured with greater precision than less abundant ones.

In order to understand the effects of the predominance of abundant transcripts on the precision of the experiment, we assessed the precision of this data set by combining reads from three sequencing runs of a single library in random order. We then calculated transcript abundance from the first four million reads, from the first eight million reads, and so on for each increment shown in Table 2.2. For each

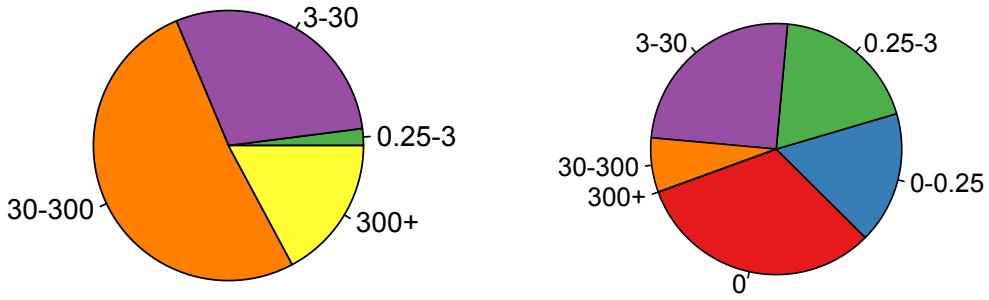

(a) Sequencer reads grouped by transcript abundance (RPKM)

(b) Genes grouped by transcript abundance (RPKM)

Figure 2.2: Seven percent of transcripts account for over half of all reads. Transcripts were categorized by abundance: Not expressed (0 RPKM), expressed below threshold (0<x<0.25), and expressed between the intervals of 0.25, 3, 30 and 300, intervals chosen for comparison with Mortazavi et al. (2008). Plot (a) illustrates the fraction of the sequencer reads from wild-type mouse forebrain by each abundance category. Plot (b) illustrates the fraction of mRNA-producing genes corresponding to each abundance categories. The orange segment in (a) shows fifty-one percent of all reads are derived from transcripts with an abundance measurement between 30 and 300 RPKM. However, those transcripts comprise only seven percent of mRNA-producing genes.

increment, we noted the number of measurements that were within 5 percent of the final value: the measurement calculated with all the reads available for that sample.

Table 2.2 shows an example of the measurements for a single gene, *Gabra2*, which codes for the $GABA_AR$ subunit $\alpha 2$. The abundance of the *Gabra2* transcript is within 5 percent of its final value (6.39 RPKM) when 8, 28, 32 or 36 million reads are included in calculations. Many genes show a trend like this, increasing precision as the measurement is based on more reads.

The fraction of all transcripts within 5 percent of their final value is plotted against the number of reads used to calculate the abundance in Figure 2.3. More highly abundant transcripts are precisely measured with fewer reads, as indicated by the blue and purple lines. Of all transcripts expressed above 3 RPKM, 99 percent are

Table 2.2: The abundance measurements of the γ-aminobutyric acid$_A$ receptor subunit $\alpha 2$ transcript are increasingly precise as more reads are included in the calculation.

Million reads use in calculations	4	8	12	16	20	24	28	32	36	40
Transcript abundance (RPKM)	6.89	6.61	5.74	5.75	5.89	6.07	6.09	6.1	6.28	6.39
Percent final value	107.8	103.4	89.8	90.0	92.2	95	95.3	95.5	98.3	100.0

within 5 percent of their final abundance measurement (indicated by the green, blue and purple lines). Thus we conclude that by pooling our samples we have sufficient depth of sequencing to analyze genes that are expressed at greater than 3 RPKM.

Measurements of known quantities of transcripts

In order to determine the number of transcripts represented by one RPKM, we added reference transcripts to our samples and compared the resulting transcript abundance measurements to the known concentrations. The seven reference transcripts, derived from Arabidopsis and phage lambda, ranged in length from 325 to 11,936 bases and in concentration from 50,000 to 500 $\times$ 10^8 transcripts per 100ng of experimental transcripts. The measured abundance is highly correlated with the number of transcripts. One RPKM corresponds, on average, to 150,000 transcripts (Figure 2.4). The high correlation and small error indicates that RPKM is a consistent measure of the number of samples in a transcript and that measurements are linear across different transcripts.

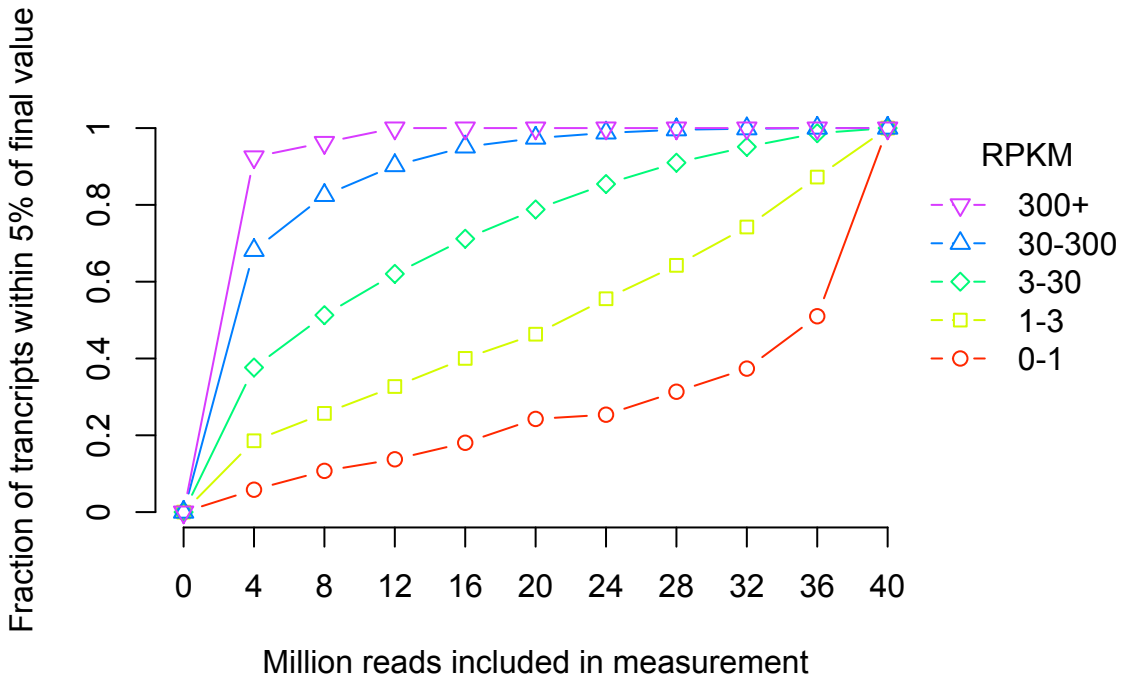

Figure 2.3: Transcripts more abundant than 3 RPKM are precisely measured. The abundance of each transcript was calculated with increasing numbers of sequencer reads. Precise measurement was defined as a measurement within 5 percent of the final value, and transcripts were grouped by abundance category. For each increment of reads, the fraction of precise measurements for an abundance category was plotted against the number of reads used in the calculation. Ninety-nine percent of transcripts more abundant than 3 RPKM are precisely measured to within 5 percent of their final value.

To estimate the noise in the measurements, we considered the transcript levels that are reported not to be expressed in brain: Hnf4a, Myf5, Myf6, Myod1, and Myog. The average transcript level for these five genes was 0.025 RPKM. We used a ten-fold increase of that threshold, 0.25, as a conservative threshold of expression when evaluating patterns of expression in the entire transcriptome. Because of the results

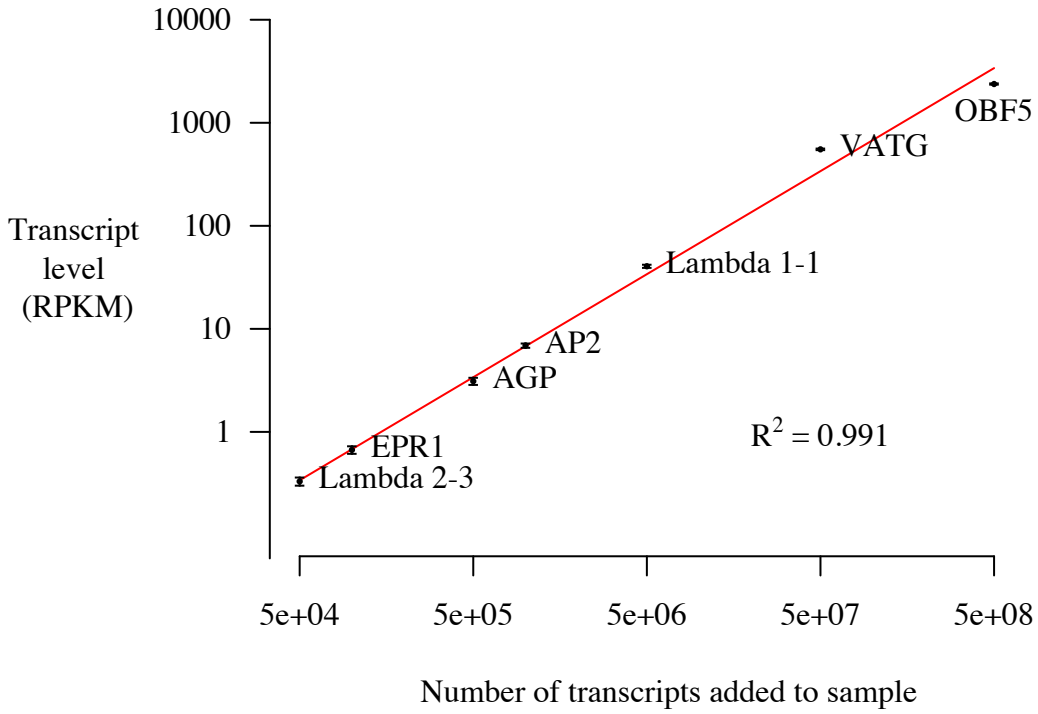

Figure 2.4: Validation of RPKM as a consistent unit of measure. The measured transcript abundance, in RPKM, is plotted against the number of known Arabidopsis and phage lambda reference transcripts. Seven different reference transcripts were added to mouse brain samples and sequenced together with the mouse brain transcripts. The measured transcript abundance of these transcripts is highly linearly correlated with the number of reference transcripts spiked in to the sample (R^2=0.991). The red line indicates where 1 RPKM consists of 150,000 transcripts. Error bars indicate standard error of the mean. The high correlation and small error indicates that RPKM is a consistent measure of the number of samples in a transcript. Reference transcripts were measured in the four forebrain samples.

of our precision analysis, we limited analysis of transcript abundance of individual genes to those expressed over 3 RPKM in either of the compared samples.

Range of gene expression levels within a single animal

The RNA-Seq measures the abundance of each transcript in a sample. We measured the abundance of 33,114 transcripts in samples from 10 mice. In the forebrain samples

from the wild-type mice, 10,625 of the 33,114 transcripts considered are not expressed (zero RPKM). Another 5,749 are expressed below threshold (0.25), calculated as described in section 2.3.2. There are 16,737 transcripts above threshold.

Figure 2.5 presents an overview of the distribution of the transcript abundance in the forebrain of wild-type mice. Transcript measurements were binned, and the log of the number of genes in each bin is indicated on the ordinate. For clarity, 5 genes with RPKM above 1000 were omitted. The histogram shows that majority of transcript levels are less than 50 RPKM (31,822 transcripts). The distribution of RPKM values is heavily skewed toward lower values. As expression levels increase, the number of genes expressed at that level drops.

Figure 2.6 shows the data depicted in 2.5 at higher resolution, focussing on the distribution of transcripts expressed between the lower threshold, 0.25, and twenty RPKM. The transcript measurements are binned, and the number of genes in each bin is indicated on the ordinate. Transcript levels represented in this plot were measured in the forebrains of wild-type mice. Together, Figures 2.5 and 2.6 show that most genes that are expressed in forebrain are expressed at less than 20 RPKM.

2.3.3 Differential gene expression

Most genes are similarly expressed

Although some genes are DE, expression is quite similar between individuals of the same or different genotypes. Figure 2.7 depicts the relationship of transcript levels in the forebrain of a densin knockout mouse and a wild-type littermate. For each

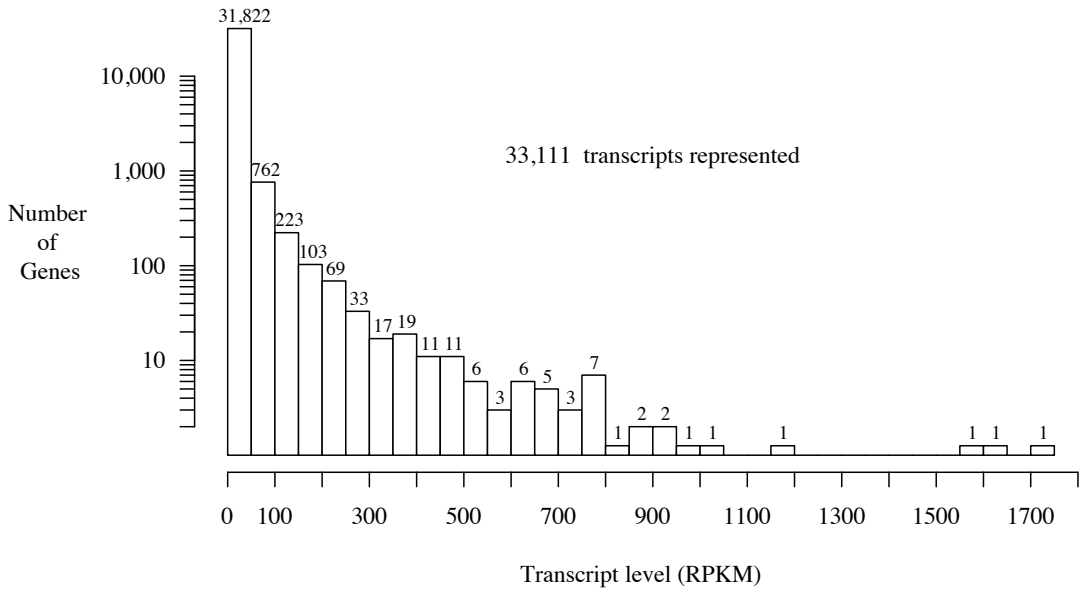

Figure 2.5: Most genes expressed in the brain exhibit low transcript abundance. The transcript levels measured for each gene were binned, and the number of genes in each bin is indicated on the ordinate. This plot shows the transcript level measured in the forebrains of wild-type mice. The majority of transcript levels are less than 50 RPKM; the higher the expression level, the fewer genes expressed at that level

transcript, the amount of transcript in the knockout is plotted on the y-axis against the amount in the wild-type on the x-axis. The plot is divided into hexagons, and the number of transcripts falling within each hexagon is represented by a shade of gray. Darker gray indicates a greater density of transcripts. The legend indicates the range of the number of transcripts represented by each shade. The diagonal trend indicates that many transcripts are similarly abundant in each animal. The correlation between the two samples is 0.998. The clustering of the darkest hexagons in the lower left of the graph indicates that transcripts expressed at low levels are prevalent. The region

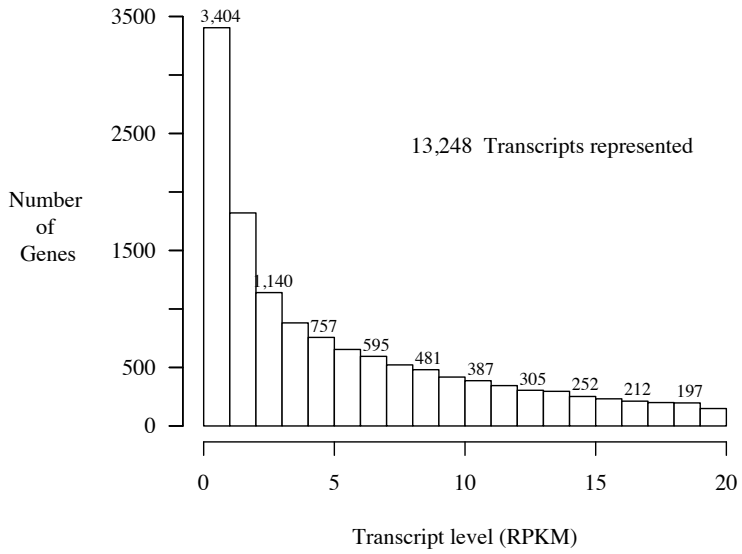

Figure 2.6: Most genes expressed in forebrain are expressed at levels near the detection threshold. The transcript levels between a conservative detection threshold, 0.25 RPKM, and 20 RPKM are binned, and the number of genes in each bin is plotted. Transcript levels represented in this plot were measured in the forebrains of wild-type mice; values below 0.25 and above twenty were excluded. The cutoff of 0.25 was used to decrease the likelihood of false positives.

of Figure 2.7a with the highest concentration of genes is shown at higher resolution in Figure 2.7b.

The largest changes in transcript abundance are observed between brain areas (Figure 2.8). Each square contains a scatterplot of transcript levels for two samples. Points are binned as in Figure 2.7. In forebrain samples, littermates share an id number; for example, wild-type (WT) 1 and knockout (KO) 1 are littermates. All hippocampal samples come from the same litter. The side of each square represents 1000 RPKM. Boxes with a yellow background contain comparisons between forebrain samples. Consistent with the highly correlated forebrain measurements in Figure

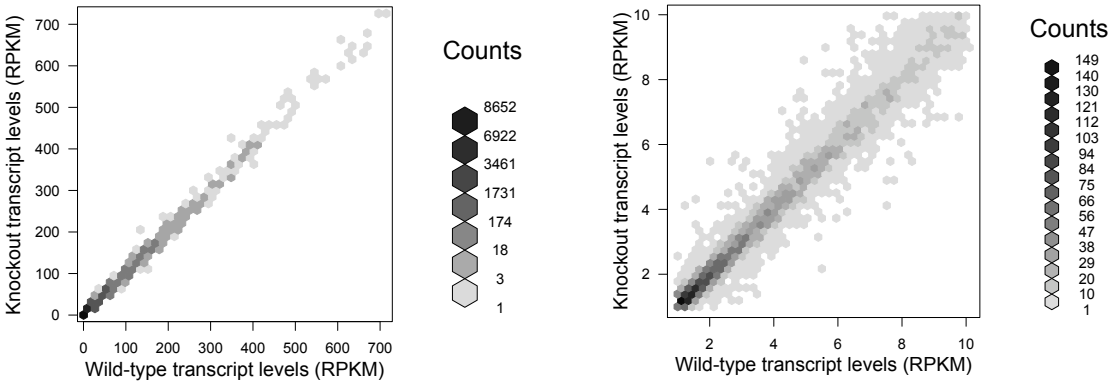

(a) Correlation of most values

(b) Higher resolution view of the correlation of low abundance transcripts

Figure 2.7: The majority of transcripts are expressed at similar levels across in wild-type and densin knockout forebrain. Transcript abundance in the forebrain of densin knockout mice is plotted against the equivalent value in wild-type mice. Nearby points are binned. The number of points in a hexagon are indicated by the intensity of gray; darker areas contain more points. (a) All genes expressed under 700 RPKM are plotted. The R squared value is 0.998, indicating a high correlation of gene expression across genotype. (b) Transcript abundance measurements between 0.25 and 10 RPKM are also highly correlated between the densin knockout and wild-type mice. As in previous figures, low transcript levels are prevalent. At higher resolution, changes in expression in the knockout are more visible.

2.7, the correlation between each individual sample is extremely high. Boxes with a blue background contain comparisons between hippocampal samples. Boxes with a green background contain comparisons between the hippocampal and forebrain samples, where the most variability is apparent. The list of genes DE between the hippocampus and forebrain in wild-type animals is discussed in Chapter 7, Appendix B. The most highly correlated group is the forebrain samples (R^2 between 0.991 and 0.998), followed by the hippocampal samples (R^2 between 0.941 and 0.995). The correlation between hippocampus and forebrain samples ranges from 0.853 to 0.956.

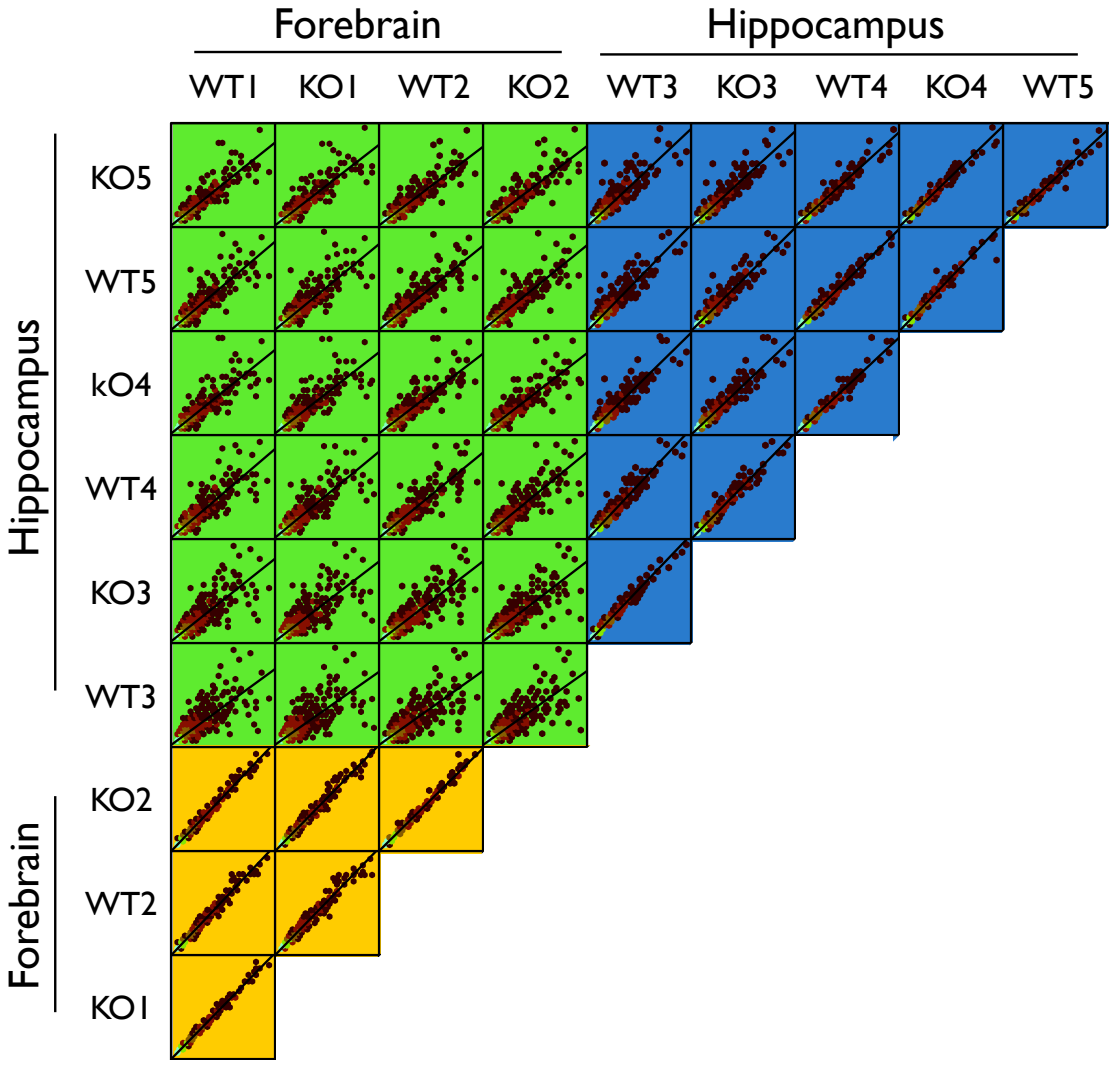

Figure 2.8: The largest changes in transcript levels were observed between brain regions. Each square contains a scatterplot showing transcript levels for two samples. The points are binned as in Figure 2.7. The side of each square represents 1000 RPKM. The background color of the plot indicates the samples being compared: yellow for two forebrain samples, blue for two hippocampal samples, and green for one forebrain and one hippocampal sample. The lowest correlation is between the forebrain and hippocampus; thus, the difference in expression between the hippocampus and forebrain is greater than the difference caused by the loss of densin.

Identification of differentially expressed genes

We investigated the effects of the absence of densin on gene expression by analyzing transcript abundance in densin knockout and wild-type mice. We investigated these

effects in the forebrain and in the hippocampus. The densin mice are maintained as heterozygotes, and litters can include wild-type mice as well as mice heterozygous and homozygous for the null densin allele. We were therefore able to use wild-type littermates as controls for the densin knockout mice. The results of each comparison are presented below; individual genes are discussed in subsequent sections.

Results from each brain region and genotype were pooled to maximize precision of measurement and thus accurately identify DE genes. For each pooled sample (wild-type forebrain, knockout forebrain, wild-type hippocampus, knockout hippocampus), differences in expression were visualized by plotting the change in expression against the expression in the control condition, as in an MA (microarray) plot. The mean and the standard deviation of the changes were smoothed and used to identify DE genes as described in Materials and Methods.

The changes in expression in the forebrain of densin knockout mice are compared to expression wild-type mice in Figure 2.9. The smoothed mean change is adjacent to zero, indicating that the same proportion of genes increased or decreased between the two conditions. The most highly DE genes were selected from those that changed by at least 4 standard deviations. This subset was selected by an index consisting of the product of the magnitude of the expression and distance from the mean in standard deviations. The metallothioneins (MTs) are the most highly ranked outliers.

Changes of expression in the hippocampus are depicted in Figure 2.10 on page 60. Transcript abundance measurements in the hippocampus are the pooled results from three mice for each genotype. All six mice were littermates. The mean change is very

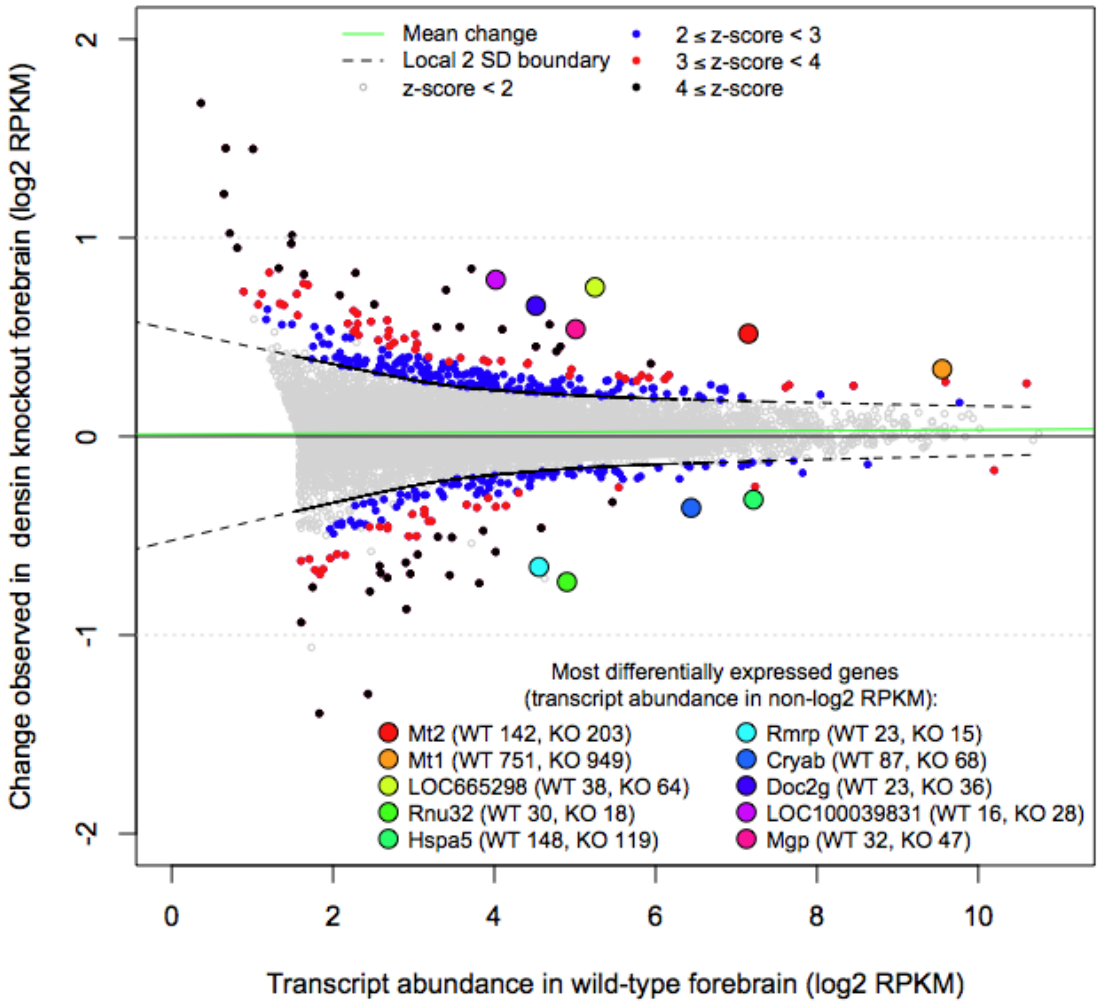

Figure 2.9: Metallothioneins are differentially expressed in the forebrain of densin knockout versus wild-type mice. The change of expression observed in transcript abundance in the forebrain of densin knockout mice is plotted against the abundance of the same transcript in the forebrain of wild-type mice. The smoothed local mean and local standard deviation are indicated by green and dotted black lines, respectively. Changes in gene expression greater than two standard deviations from the mean differential expression are shown in blue, more than three standard deviations in red; four in black. The ten most DE genes are plotted as indicated. Key to named genes: Mt2 (metallothionein 2), Mt1 (metallothionein 1), Hspa5 (heat shock protein 5), Rmrp (RNA component of mitochondrial RNAase P), Cryab (crystallin, alpha B), Doc2g (double C2, gamma).

close to zero; there was no general trend of increase or decrease. The distribution is similar to that seen in the forebrain.The increased expression of MT3 in the hippocampus is particularly notable in light of the increases in MT1 and MT2 expression in the forebrain. Having identified DE genes, we next characterized commonalities among them.

2.3.4 Patterns of differential expression

We analyzed gene expression data from the densin knockout mouse using two general approaches. For the first, we used pattern identification methods to generate unbiased hypotheses about the inter-relation of the DE genes. These methods included identification of brain structures enriched for DE transcripts, known interactions among DE gene products, and common characteristics of DE genes, which we identified using gene ontology annotations. The second approach consisted of analyzing the expression levels of genes that could be affected by the loss of densin by a known characteristic, such as co-localization of gene products, interaction of a gene product with densin, a gene product which has been implicated in the phenotypic behaviors of the densin knockout mouse, or proximity of the genes on the chromosome. This approach is discussed in section 2.3.5.

Brain structures

Because of the variety of structures in the forebrain, we sought to identify those affected by the altered gene expression identified in the forebrain. We used data from the Allen Mouse Brain Atlas (ABA) to identify brain regions likely to exhibit the

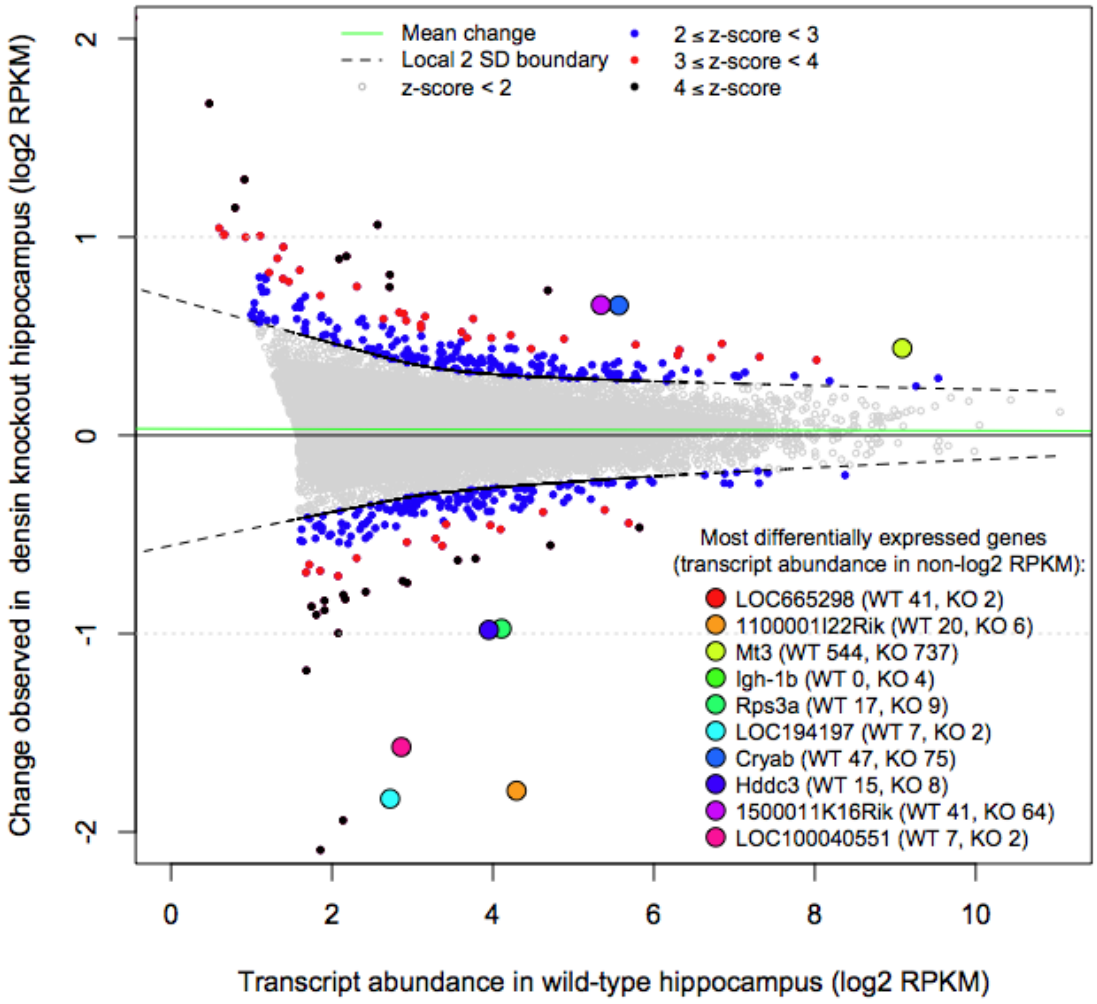

Figure 2.10: Metallothionein (MT) 3 is upregulated in the hippocampus of densin knockout relative to wild-type mice. The hippocampus displays a similar pattern of DE genes as in the forebrain, although the variability is generally greater in the hippocampus. MT3 expression is increased in the hippocampus of densin mice relative to wild-type mice. In the forebrain, MT1 and MT2 are among the most highly DE genes, and like MT3 in the hippocampus, MT1 and MT2 are increased in the forebrain in densin knockout mice relative to the wild-type mice. Key: Mt3 (metallothionein 3), Igh-1b (immunoglobulin heavy chain 1b (serum IgG2c)), Rps3a (ribosomal protein S3A), Cryab (crystallin, alpha B), Hddc3 (HD domain containing 3).

DE genes. We reasoned that if expression of the DE genes was concentrated in a particular region, this might indicate a locus of change in the densin knockout mouse.

The ABA contains the results of large-scale *in situ* hybridization studies of thousands of transcripts (Lein et al., 2007). They also quantify the intensity and density of expression in different brain structures (Allen Institute for Brain Science, 2006). Because the information was not available in the form required for our analysis, we generated scripts that parsed the XML-formatted data and aggregated it into a format that could be queried. Consequently, we could compare relative expression in different brain structures for 3,225 genes.

In the densin knockout mice, 418 transcripts were DE in the forebrain with a z-score of more than two. Of these, we have ABA data for 283 of them. For each, we compared the reported *in situ* hybridization intensity in five mutually exclusive structures: hippocampus, striatum, thalamus, hypothalamus and midbrain. These comparisons are represented in Figure 2.11. Each row represents the intensity of one transcript in the five structures. The region with the lowest expression is represented by a thin red bar; the one with the highest with a green bar, and other structures by intermediate colors. The rows are then sorted to group common expression patterns together. As indicated by the prevalence of green in the hippocampal column, genes affected by the loss of densin are more highly expressed in the hippocampus than in the other structures analyzed.

We quantified the difference in expression between brain structures. The ABA intensity values reported for the hippocampus are significantly different from those

reported in any of the other structures; the greatest p value of t tests between values reported for the hippocampus and any other structure is less than 0.01. The same tests performed on density values indicate a trend, but not a significant difference, in density of expression; the greatest p value in those comparisons is less than 0.07. The analysis of the intensity values indicates that the genes we identified as DE in the forebrain are significantly more expressed in the hippocampus than in the hypothalamus, thalamus, striatum or midbrain. Repeating the analysis with randomly chosen groups of expressed genes produces the same result, reflecting the high frequency of DE gene expression in the hippocampus. This suggests that the hippocampus is a promising region to look for the effects of the loss of densin.

Networks

Having identified the hippocampus as a structure of high abundance of DE genes in that structure, we sought to identify interactions between the DE genes. We queried a curated interaction network (Ingenuity Pathway Analysis) and identified networks of highly interconnected genes in that structure (Figure 2.12 on page 64). The network is centered around Iκb which is significantly upregulated in both forebrain and hippocampus of densin knockout mice. Networks are ranked by the fraction of DE genes involved in the network compared to the fraction expected by chance as well as by the magnitude of the difference in transcription level. Although Iκb is the most highly ranked network, it includes few of the most DE genes.

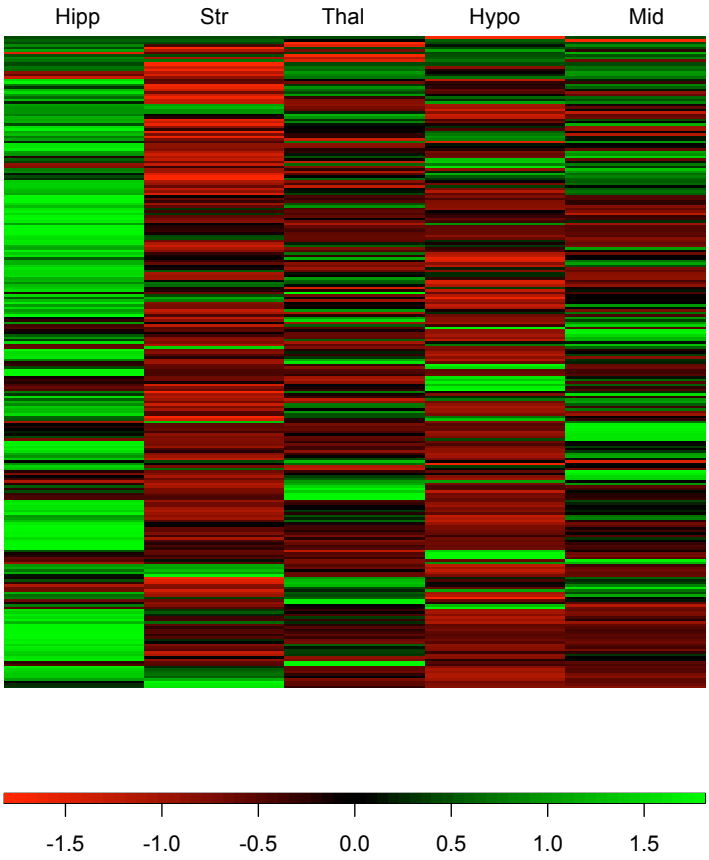

Figure 2.11: Genes differentially expressed in the forebrains of densin knockout mice are highly expressed in the wild-type hippocampus. We used data from the ABA to identify structures enriched for genes identified as DE in the forebrain of densin knockout versus wild-type mice. One brain region is represented in each column (Hipp=hippocampus, Str=striatum, thal=Thalamus, Hypo=hypothalamus, Mid=midbrain). Each row corresponds to a DE gene ($z>2$). The ABA intensity values are separately color coded for each gene. Higher expression is represented by green, and lower expression by red. The trend of bright green in the hippocampus indicates that many of the genes are more highly expressed there than in other structures. The intensity values measured in the hippocampus differ from all other structures ($p<0.01$). No other columns significantly differed.

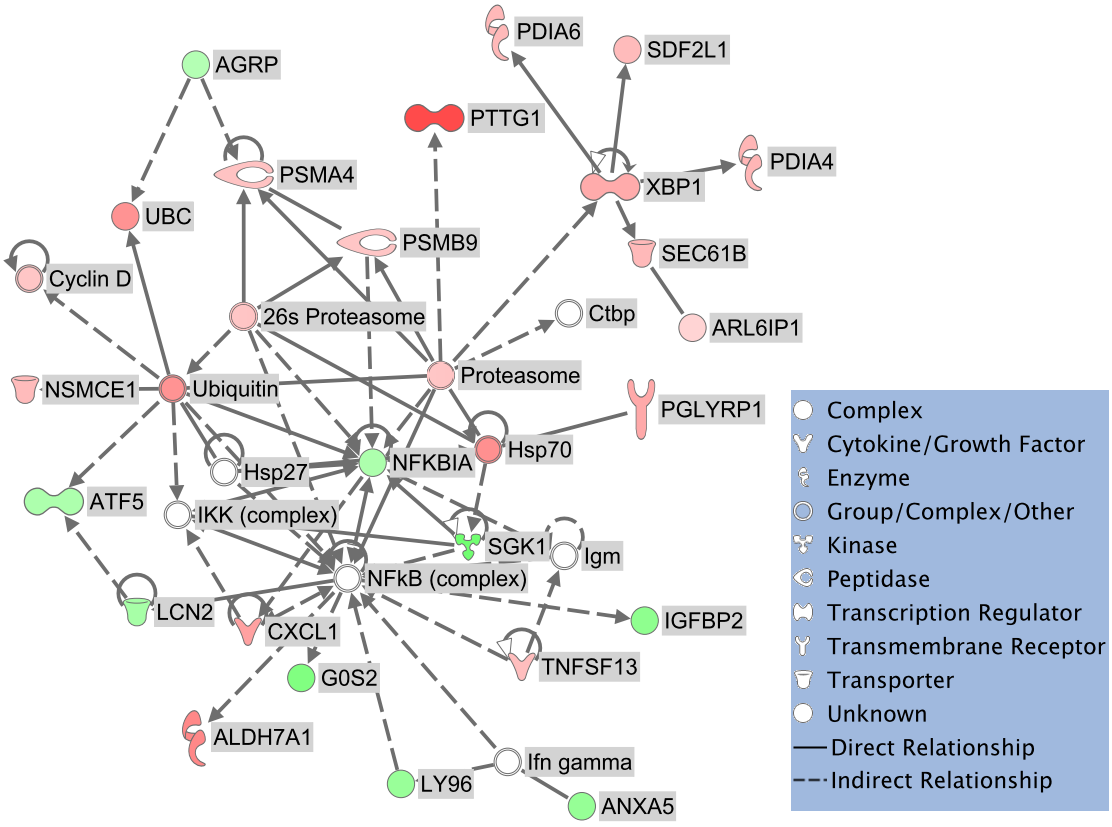

Figure 2.12: The NFκB pathway is a central hub connecting many genes differentially expressed in the densin knockout mouse. Networks among genes DE in the forebrain of the densin knockout versus wild-type mice were identified by querying a curated interaction network (Ingenuity Pathway Analysis). The shapes of the genes correspond to the function of the genes. Green shapes indicate upregulated genes; red, downregulated. Brighter colors indicate a greater difference in transcription level between densin knockout and wild-type mice. White shapes are genes included to demonstrate possible indirect connections. For example, the inclusion of NFκB allows a connection between ALDH7A1 and GOS2. The network shown here is centered around Iκb, which is DE in both forebrain and hippocampus of densin knockout mice. This network includes many genes implicated in neurological and cardiovascular disease.

2.3.5 Differential expression in densin-related genes

We next considered genes that are associated with densin by the binding of their product, by their presence in the PSD, by implication of the phenotypic behavior, or by proximity on the chromosome.

Densin binding partners

Out of the 33,000 transcripts measured, we first analyzed transcript levels of known binding partners of densin. These measurements are reported in Table 2.3. In the hippocampus, CaMKIIα, Shank1, and Shank3 are all upregulated with z-scores of more than 2. In the forebrain sample, no significant change is seen in expression.

Table 2.3: Hippocampal gene expression is upregulated in the densin knockout mouse for three protein binding partners of densin. Compared to the gene expression in the hippocampus wild-type mice, CaMKIIα, Shank1 and Shank3 each increase in expression with a z-score of greater than two.

Gene expression of densin binding partners

	Forebrain				Hippocampus			
	Wt	Ko			Wt	Ko		
Gene	(RPKM)		z>2	z	(RPKM)		z>2	z
Actn1	21.5	20.0		-1.3	20.0	22.7		1.2
Actn2	7.9	8.7		1.0	3.9	4.2		0.3
Actn4	41.3	42.1		0.0	29.9	32.3		0.7
Camk2a	483.7	533.2		1.7	612.2	726.9	*	2.1
Camk2b	235.9	253.9		1.1	261.4	267.9		-0.1
Ctnnd1	10.4	10.6		0.1	11.8	11.6		-0.3
Ctnnd2	40.2	40.0		-0.4	35.8	35.4		-0.3
Shank1	32.6	35.1		0.9	46.5	56.5	*	2.0
Shank2	15.2	14.2		-1.2	19.8	22.7		1.3
Shank3	36.8	36.0		-0.6	23.6	29.3	*	2.1

Key: Wt (wild-type), Ko (knockout), z (z-score), Actn1 (actinin, alpha 1), Actn2 (actinin alpha 2), Actn3 (actinin alpha 3), Actn4 (actinin alpha 4), Camk2a (calcium/calmodulin-dependent protein kinase II alpha), Camk2b (calcium/calmodulin-dependent protein kinase II, beta), Cnksr3 (Cnksr family member 3), Ctnnd1 (catenin (cadherin associated protein), delta 1), Ctnnd2 (catenin (cadherin associated protein), delta 2), Shank1 (SH3/ankyrin domain gene 1), Shank2 (SH3/ankyrin domain gene 2), Shank3 (SH3/ankyrin domain gene 3)

Proteins present in the PSD

We tested whether the loss of densin disproportionately affected the expression of other PSD proteins using a list of genes identified by analysis of proteins in the PSD fraction (Cheng et al., 2006). This PSD-fraction set of genes may differ from the true set of PSD protein-coding genes because PSD fractions can contain contaminants, and transient or low-abundance components can be absent from the fraction (Sheng and Hoogenraad, 2007). Of the 271 PSD-fraction genes, 13 were DE in the densin knockout; 9 in the hippocampus and 4 in the forebrain (Table 2.4 on the next page). Most of the PSD-fraction genes are expressed above 3 RPKM, and so most were tested for differential expression. The PSD-fraction genes comprise two percent all genes expressed above 3 RPKM and two percent of DE genes. Thus, PSD-fraction genes are not more likely to be DE in the densin knockout than other genes.

$\mathbf{GABA_A}$ receptors

Densin knockout mice commonly have seizures when injected with pentobarbital, a $GABA_AR$ agonist that is used as a general anesthetic (personal communication, T. Luong, H. Carlisle). Therefore, we are particularly interested in the abundance of transcripts coding for $GABA_AR$ subunits. Surprisingly, transcript levels of three $GABA_AR$ subunits ($\alpha 2$, $\alpha 5$ and $\beta 1$) are significantly lower in densin knockout mice relative to wild-type mice (Table 2.5).

Table 2.4: PSD genes are differentially expressed in densin knockout mice. When compared to wild-type mice, densin knockout mice express 13 transcripts differentially (z>2): nine in the hippocampus and four in the forebrain.

Gene expression of PSD proteins

	Forebrain				Hippocampus			
Gene	Wt (RPKM)	Ko (RPKM)	z>2	z	Wt (RPKM)	Ko (RPKM)	z>2	z
Apoe	1550.7	1865.1	*	3.9	826.5	943.0		1.5
Camk2a	483.7	533.2		1.7	612.2	726.9	*	2.1
Camk4	16.4	18.2		1.2	11.7	14.7	*	2.1
Dgkz	110.7	107.5		-0.9	74.5	92.2	*	2.3
Fxyd5	7.7	10.1	*	2.8	5.9	5.8		-0.3
Gda	20.3	17.7	*	-2.2	45.7	41.7		-1.3
Gpsm1	19.0	22.4	*	2.1	8.1	8.8		0.6
Hapln4	39.1	41.8		0.8	24.7	32.7	*	2.8
Mapk1	80.4	74.1		-1.8	117.3	99.3	*	-2.5
Opcml	20.3	18.6		-1.5	44.4	37.7	*	-2.1
Shank1	32.6	35.1		0.9	46.5	56.5	*	2.0
Shank3	36.8	36.0		-0.6	23.6	29.3	*	2.1
Sparc	199.0	210.8		0.8	128.3	157.9	*	2.3

Key: Wt (wild-type), Ko (knockout), z (z-score), * (z-score > 2), Apoe (apolipoprotein E), Camk2a (calcium/calmodulin-dependent protein kinase II alpha), Camk4 (calcium/calmodulin-dependent protein kinase IV), Dgkz (diacylglycerol kinase zeta), Fxyd5 (FXYD domain-containing ion transport regulator 5), Gda (guanine deaminase), Gpsm1 (G-protein signalling modulator 1 (AGS3-like, C. elegans)), Hapln4 (hyaluronan and proteoglycan link protein 4), Mapk1 (mitogen-activated protein kinase 1), Opcml (opioid binding protein/cell adhesion molecule-like), Shank1 (SH3/ankyrin domain gene 1), Shank3 (SH3/ankyrin domain gene 3), Sparc (secreted acidic cysteine rich glycoprotein).

Immediate Early Genes

Transcription of several IEGs, including Arc, Egr1 (Zif268), Fos, Junb and Nptx2, are upregulated in the hippocampus of densin knockout mice relative to the hippocampus of wild-type mice. As shown in Table 2.6, all of the IEGs genes DE in the hippocampus of densin knockout mice are increased, suggesting a persistently activated state. Jund1 is upregulated in the forebrain but not the hippocampus, and Npas4 is down-

Table 2.5: Three γ-aminobutyric acid$_A$ receptor (GABA$_A$R) subunits are significantly decreased in densin knockout mice. Transcript levels are decreased in both forebrain and hippocampal samples, but the decrease only reach significance (z-score>2) for GABA$_A$R subunits α2 (Gabra2) and β1 (Gabrb1) in the hippocampus and GABA$_A$R subunit α5 (Gabra5) in the forebrain.

Gene expression of γ-aminobutyric acid$_A$ receptor subunits

	Forebrain				Hippocampus			
	Wt	Ko			Wt	Ko		
Gene	(RPKM)		z>2	z	(RPKM)		z>2	z
Gabra2	11.7	10.6		-1.4	56.5	40.9	*	-4.1
Gabra5	31.5	27.5	*	-2.4	63.3	59.8		-0.9
Gabrb1	8.4	8.1		-0.6	26.9	21.8	*	-2.4

Key: Wt (wild-type), Ko (knockout), z (z-score), * (z-score > 2)

regulated in the forebrain. Although none of the genes are DE in both forebrain and hippocampus, it is notable that Arc, Egr1, Fos and Npas4 all change in the opposite directions in the two regions. Arc, Egr1, Fos are significantly upregulated in the hippocampus and downregulated in the forebrain; the reverse is true for Npas4.

IEGs are transcribed shortly after a stimulus and those that are transcribed in response to synaptic activity (e.g. Arc and Fos) can be triggered by an animal's exposure to a novel environment (Guzowski et al., 1999). When we identified the pattern of increased expression of IEGs in the knockout mice, we evaluated the possibility that the densin knockout mice were exposed to a novel environment for longer than were the wild-type mice. However, wild-type and knockout mice were raised in the same facility and sacrificed in random order in the dissection room.

Table 2.6: Immediate early genes expression is increased in the hippocampus of densin knockout mice. Arc, Egr1 (Zif268), Fos, Junb and Ntpx2 (Narp) have significantly higher transcript levels in the hippocampus of densin knockout mice than in the hippocampus of wild-type mice (z>2). Other changes include an increase of Jund1 in the densin knockout forebrain (z=2.6) and a decrease in Npas4 in the forebrain (z=-3.5). Several immediate early genes are DE in the opposite direction in the forebrain and hippocampus. Npas4 is decreased in the forebrain (z= -3.5) and increased in the hippocampus (z=1.8); Arc levels are increased in the hippocampus (z=5.3) and decreased in the forebrain (z=-1.8). Other immediate early genes are not DE: Pcdh8, Ptgs2 (Cox-2) and Homer1 (Loebrich and Nedivi, 2009).

Gene expression of some immediate early genes

	Forebrain				Hippocampus			
Gene	Wt (RPKM)	Ko (RPKM)	z>2	z	Wt (RPKM)	Ko (RPKM)	z>2	z
Arc	86.8	79.9		-1.8	25.7	42.6	*	5.3
Egr1	83.1	79.3		-1.1	33.9	42.0	*	2.2
Fos	25.0	24.6		-0.5	4.3	7.9	*	4.1
Homer1	16.8	15.6		-1.2	18.4	17.8		-0.5
Junb	59.9	64.6		1.0	16.1	20.9	*	2.5
Jund1	116.1	136.1	*	2.6	49.4	54.6		0.9
Npas4	9.1	6.8	*	-3.5	2.2	3.1		1.8
Nptx2	36.8	41.7		1.7	12.2	16.9	*	3.0
Nrn1	118.0	118.3		-0.3	111.8	115.8		0.1
Pcdh8	11.4	12.2		0.7	10.8	12.3		1.1
Ptgs2	2.8	3.1		0.8	5.2	5.2		-0.2

Key: Wt (wild-type), Ko (knockout), z (z-score), * (z-score > 2), Arc (activity regulated cytoskeletal-associated protein), Bdnf (brain derived neurotrophic factor), Egr1 (early growth response 1), Fos (FBJ osteosarcoma oncogene), Homer1 (homer homolog 1 (Drosophila)), Junb (Jun-B oncogene), Pcdh8 (protocadherin 8), Nptx2 (neuronal pentraxin 2), Nrn1 (neuritin 1), Ptgs2 (prostaglandin-endoperoxide synthase 2)

Genes with reduced protein levels

Preliminary data from immunoblots indicates that the densin knockout mouse has decreased levels of several PSD proteins in the forebrain homogenate. However, none of the corresponding transcripts are are significantly decreased in either the forebrain

or the hippocampus of densin knockout mice. Thus, the changes observed in these protein levels may not be the result of changes in transcription.

Effect of homologous recombination

The process of making the knockout animal did not change the expression of genes near the site of genomic manipulation. The transcript levels of genes near densin are plotted in Figure 2.13. In each case the difference between the expression of knockout and wild-type genes is less than two standard deviations from the mean. Thus, we observe no perturbation of local transcription due to the homologous recombination used to make the densin knockout.

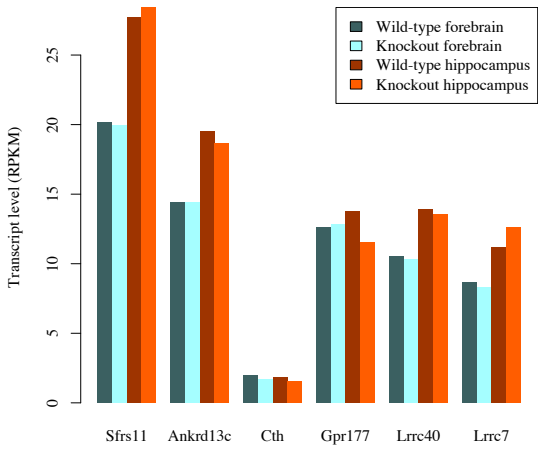

Figure 2.13: No significant differences in transcript levels between densin knockout and wild-type mice are observed in genes proximal to the densin locus.. The average transcript level measured for the genes listed on the abscissa are plotted. The average transcript level for each sample is shown: wild-type and knockout forebrain, and wild-type and knockout hippocampus. In each case the difference between the expression of the knockout and wild-type genes is less than two standard deviations from the mean. We observe no perturbation of local transcription due to the homologous recombination used to make the densin knockout.

2.4 Discussion

In order to understand more about the postsynaptic protein densin, we used RNA-Seq, a recently developed method of global transcriptional analysis, to analyze changes in gene expression in mice missing the gene that codes for densin (*Lrrc7*). Differences in gene expression between the brains of densin knockout mice and their wild-type littermates indicate that the loss of densin results in upregulation of its binding partner CaMKIIα and several IEGs, including Arc and Jund1, and downregulation of $GABA_AR$ subunit $\alpha 2$. These results, together with supporting observations of the behavioral phenotype of the knockout mouse, extend previous knowledge of densin function and implicate it in homeostatic regulation of excitatory and inhibitory currents. In addition, the interaction network analysis highlights a central role for the NFκB signaling pathway in coordinating the DE genes in the densin knockout.

2.4.1 Implementation of RNA-Seq

RNA-Seq is a recently-developed method of measuring transcript abundance by sequencing. No consensus exists for optimal depth of sequencing, data normalization methods or methods of identifying DE genes, nor have the options been extensively compared.

The depth of sequencing in an RNA-Seq experiment determines the precision of measurement. We were able to precisely measure transcripts of above 3 RPKM with approximately 40 million reads. We used 0.25 RPKM as a conservative lower threshold of measurement. Of transcripts above 0.25 RPKM, we precisely measured 63

percent of them, accounting for 97 percent of all reads. The domination of mRNA samples by highly abundant transcripts is a crucial consideration both for experimental design and biological models.

We normalized raw reads by the length of the transcript and by the number of reads produced by a run of the sequencer. Two further normalizations were considered. The first normalization is a log2 conversion, commonly used in microarray analysis to normalize gene expression measurements along the dimension of abundance (a skewed distribution; most genes are expressed at low levels) as well as normalizing the distribution of difference in gene expression (also a skewed distribution: changes in genes with low expression have greater variation than more highly expressed genes). Both of these distributions are reduced but not eradicated by the log2 transformation.

Further transformations have been developed which change values in a locally weighted manner, which further improves the normalization of variance (notably Huber et al. (2003)). Because microarray data are usually not compared between transcripts, the data loss resulting from this type of variable transformation is insignificant for microarray analysis. However, inter-transcript comparisons are an advantage of the RNA-Seq technique, and the locally-weighted transformations lose that advantage. Therefore we used only the log2 transformation, and selected a method for identifying DE genes that accounts for abundance-dependent changes in distribution.

These data analysis methods allowed us to capitalize on the precision available to us without losing relationships among the data. Measuring the fraction of values that approached their final value allowed us to confidently use 97 percent of the

reads that unambiguously matched a transcript region in the genome. In lieu of local data transformation, which changes the relationships between transcripts, we used a method of identifying DE genes that was sensitive to local changes in distribution.

2.4.2 Effects of the loss of densin on brain transcription

Using RNA-Seq, we investigated changes in brain transcription in mice missing the postsynaptic protein densin. We compared transcript expression in the forebrain and hippocampus of densin knockout mice to that in wild-type mice. We found dysregulation of a number of genes.

The DE genes had a number of other commonalities. When the expression pattern of the genes was analyzed using localization data from the ABA, they were significantly more likely to be more highly expressed in the hippocampus than in the striatum, thalamus, hypothalamus or midbrain ($p<0.01$). If, as this suggests, the loss of densin has a larger effect on the hippocampus than on other brain regions, densin may be more important to the function of the hippocampus than to other brain regions. This implication is consistent with preliminary results of behavioral test suggesting a memory deficit in the densin knockout mice.

Three GABA receptor subunits are significantly decreased: $\alpha 2$ and $\beta 1$ in the hippocampus and $\alpha 5$ in the forebrain. If this corresponds to a decrease in surface GABA receptors, densin knockout mice may have decreased inhibitory tone compared to wild-type mice.

A number of IEGs are upregulated in the hippocampus of the knockout mice: Arc, Egr1 (Zif268), Fos, Junb and Nptx2 (Narp). The overexpression in the hippocampus does not occur in the forebrain: The levels of Arc, Egr1 and Fos all decrease in the forebrain, although not to a significant extent. The increase in IEG expression and the decrease in GABAR subunit expression suggest that the hippocampi of densin knockout mice are in a persistent state of overstimulation.

Another pattern also suggests stimulation: Several genes coding for proteins in the heat shock family are also dysregulated. Heat shock proteins (HSPs) are molecular chaperones that respond to stress, reducing the harmful effects of misfolded proteins. Many are induced in response to stressful conditions, but high expression of HSPs can be detrimental (Feder and Hofmann, 1999). Cryab, a member of the small HSP family, is among the most DE in both the forebrain and the hippocampus of the densin knockout, but it changes in opposite directions in the two regions. Like Arc, Egr1 and Fos, Cryab is upregulated in the hippocampus and downregulated in the forebrain. It is widely expressed, but expression is also heat-inducible. Another of the most DE genes is HSP 5 (Hspa5, also called BiP or GRP78). Like Cryab, it is downregulated in the knockout forebrain. Hspa5 is a glucose-regulated protein and a member of the HSP70 family. It is induced in response to heat and other stresses. Hspa5 is also called "immunoglobulin heavy chain-binding protein"; Igh-1b (immunoglobulin heavy chain 1b (serum IgG2c) is another DE gene in the knockout. In the hippocampus of wild-type mice, Igh-1b is not expressed (0 RPKM) while in the knockout it is expressed at 4 RPKM. This may be part of an inflammatory

response, as NFKBIA (Iκb) is upregulated in both the forebrain and hippocampus of densin knockout mice. The analysis of interactions among differentially regulated genes places Iκb at the center of the resulting network. The NFκB pathway is a key regulator of transcription responses to extracellular stimuli such as cytokines and growth factors. Importantly, this pathway in neurons is also stimulated by NMDA, calcium influx, and seizures (Boersma and Meffert, 2008).

In the forebrain, Mt1 and Mt2 were both significantly upregulated in the densin knockout. Co-regulation of these genes has been previously observed: both are upregulated after 3,4-methylenedioxymethamphetamine (MDMA) treatment (Xie et al., 2004). Moreover, intravitreous NMDA injection upregulates Mt2. Thus, the Mt2 upregulation in the densin knockout could be the result of the hyperexcitability indicated by the increased CaMKII transcripts and tendency toward seizure (Suemori et al., 2006).

Amid this set of indicators of over-activated excitatory mechanisms are two apparently incompatible observations. Transcripts of three $GABA_AR$ subunits are decreased, and densin knockout mice are likely to have seizures in response to administration of the GABA agonist pentobarbital. A decrease in GABA receptor expression is compatible with decreased inhibition and the general shift toward excitability suggested by the DE genes discussed above, but increased sensitivity to a $GABA_AR$ agonist does not predict decreased $GABA_AR$ subunit expression or enhanced excitation.

Although induction of seizure by pentobarbital is not commonly reported, several $GABA_A$-regulating drugs are biphasic in effect. They either cause initial proconvulsive effects and subsequent anticonvulsive effects, or the dosage response curve includes both proconvulsive and anticonvulsive ranges (Garant et al., 1995; Stuchlík, 2001). Seizures induced by the withdrawal of pentobarbital are extensively used as an experimental paradigm. It is not implausible that alterations in general excitatory tone could alter the effect of pentobarbital treatment in densin knockout mice.

On the other hand, the same caveats apply to interpreting the differential expression in the $GABA_AR$ genes as other genes: the change in transcript level may not correspond to a change in protein level. Although there is a positive overall correlation, reports of correlation vary, by gene ontology category, with R^2 values from 0.2 to 0.8 (Greenbaum et al., 2003; Kadota et al., 2003). Furthermore, proteins and mRNA have different degradation mechanisms and half-lives, both of which affect abundance. Finally, the loss of even major regulatory proteins can have silent phenotypes (Marder and Goaillard, 2006; Piedras-Rentería et al., 2004).

Densin may be involved in the regulation of dendritic structure. Shank transcription is upregulated in the hippocampus of the densin knockout mouse. Shank is a densin binding partner and core PSD scaffold that is involved in PSD organization. Densin overexpression causes excessive dendritic branching, an effect rescued by co-expression of Shank (Quitsch et al., 2005). Shank also interacts with δ-catenin, which is also a binding partner of densin (Izawa et al., 2002). These results suggest a model in which densin regulates dendritic branching via δ-catenin in a Shank-dependent

manner (Quitsch et al., 2005). Studies of neuronal branching in the densin knockout mouse are ongoing.

2.4.3 Implications for densin

We have identified a striking and pervasive trend of upregulation of activity- and stress-regulated genes in the hippocampus of the densin knockout mouse. This may be the result of changes in phospho-CaMKIIα localization. Since densin is hypothesized to be a CaMKIIα docking site in the PSD, the loss of densin may disrupt CaMKIIα localization.

The suggestion that densin is a docking site for CaMKIIα in the PSD comes from the following evidence: densin binds to alpha-actinin, suggesting it could be localized independently of CaMKII, and densin can bind α-actinin and CaMKIIα simultaneously. Furthermore, the affinity of CaMKIIα for densin increases when CaMKIIα is autophosphorylated, as it is after LTP induction (Strack et al., 2000; Walikonis et al., 2001). Thus, densin binds CaMKIIα differentially, depending on the phosphorylation state of CaMKIIα, and could thus effect downstream signal transduction.

The brains of densin knockout mice have a lower steady state level of phospho-CaMKIIα protein than wild-types, but phospho-CaMKIIα levels increase more after stimulation in the knockout. Specifically, under steady-state conditions, neuronal cell cultures derived from densin knockout mice have lower phospho-CaMKIIα levels than wild-type cultures. However, the increase in phospho-CaMKII levels induced

by glutamate receptor-stimulation conditions is twice as great in densin knockout cultures as it is in wild-type cultures (H. Carlisle, personal communication).

Taken together, the foregoing observations suggest a model in which a substantial fraction of autophosphorylated CaMKIIα binds to densin. In the absence of densin, less autophosphorylated CaMKIIα is bound to the PSD, causing more CaMKIIα to be exposed to phosphatases, which lower the steady state levels of phospho-CaMKII. Under glutamate receptor stimulating conditions, however, more unphosphorylated CaMKIIα is available to be autophosphorylated, and phospho-CaMKIIα levels increase. This increase triggers signal transduction pathways, generating an excitatory state. This persistent excitatory state leads to increased expression of some genes that are induced by synaptic stimulation and stress, such as the IEGs, HSPs and NFκB signaling pathway identified in our DE gene network analysis.

We have combined RNA-Seq data with wet-lab experiments to shape our hypotheses of densin function. The seizure response to pentobarbital led to the search for a possible mechanism in the transcript data; the discovery of GABA downregulation and IEG upregulation in the transcript data will lead to a further set of wet lab experiments.

References

Allen Institute for Brain Science (2006) Informatics data processing. Allen Brain Atlas.

Boersma MC, Meffert MK (2008) Novel roles for the NF-kappaB signaling pathway in regulating neuronal function. Sci Signal 1:pe7.

Boyle EI, Weng S, Gollub J, Jin H, Botstein D, Cherry JM, Sherlock G (2004) GO TermFinder-open source software for accessing Gene Ontology information and finding significantly enriched Gene Ontology terms associated with a list of genes. Bioinformatics 20:3710–3715.

Cheng D, Hoogenraad CC, Rush J, Ramm E, Schlager MA, Duong DM, Xu P, Wijayawardana SR, Hanfelt J, Nakagawa T, Sheng M, Peng J (2006) Relative and Absolute Quantification of Postsynaptic Density Proteome Isolated from Rat Forebrain and Cerebellum. Molecular Cellular Proteomics 5:1158–1170.

Feder M, Hofmann G (1999) Heat-shock proteins, molecular chaperones, and the stress response: evolutionary and ecological physiology. Annual Review of Physiology 61:243–282.

Fernández-Medarde A, Porteros A, de las Rivas J, Núñez A, Fuster JJ, Santos E (2007) Laser microdissection and microarray analysis of the hippocampus of RasGRF1 knockout mice reveals gene expression changes affecting signal transduction pathways related to memory and learning. Neuroscience 146:272–285.

Flavell SW, Greenberg ME (2008) Signaling mechanisms linking neuronal activity to gene expression and plasticity of the nervous system. Annual Review of Neuroscience 31:563–90.

Garant DS, Xu SG, Sperber EF, Moshé SL (1995) Age-related differences in the effects of GABAA agonists microinjected into rat substantia nigra: pro- and anticonvulsant actions. Epilepsia 36:960–965.

Greenbaum D, Colangelo C, Williams K, Gerstein M (2003) Comparing protein abundance and mRNA expression levels on a genomic scale. Genome Biol 4:117.

Guzowski JF, McNaughton BL, Barnes CA, Worley PF (1999) Environment-specific expression of the immediate-early gene Arc in hippocampal neuronal ensembles. Nature Neuroscience 2:1120–1124.

Hsu F, Kent WJ, Clawson H, Kuhn RM, Diekhans M, Haussler D (2006) The UCSC Known Genes. Bioinformatics 22:1036–1046.

Huber W, von Heydebreck A, Sueltmann H, Poustka A, Vingron M (2003) Parameter estimation for the calibration and variance stabilization of microarray data. Statistical applications in genetics and molecular biology 2:3.

Izawa I, Nishizawa M, Ohtakara K, Inagaki M (2002) Densin-180 interacts with delta-catenin/neural plakophilin-related armadillo repeat protein at synapses. Journal of Biological Chemistry 277:5345–50.

Kadota K, Tominaga D, Asai R, Takahashi K (2003) Correlation analysis of mRNA and protein abundances in human tissues. Genome Letters 2:139–148.

Langmead B, Trapnell C, Pop M, Salzberg SL (2009) Ultrafast and memory-efficient alignment of short DNA sequences to the human genome. Genome Biology 10:R25.

Lein ES, Hawrylycz MJ, Ao N, Ayres M, Bensinger A, Bernard A, Boe AF, Boguski MS, Brockway KS, Byrnes EJ, Chen L, Chen L, Chen TM, Chin MC, Chong J, Crook BE, Czaplinska A, Dang CN, Datta S, Dee NR, Desaki AL, Desta T, Diep E, Dolbeare TA, Donelan MJ, Dong HW, Dougherty JG, Duncan BJ, Ebbert AJ, Eichele G, Estin LK, Faber C, Facer BA, Fields R, Fischer SR, Fliss TP, Frensley C, Gates SN, Glattfelder KJ, Halverson KR, Hart MR, Hohmann JG, Howell MP, Jeung DP, Johnson RA, Karr PT, Kawal R, Kidney JM, Knapik RH, Kuan CL, Lake JH, Laramee AR, Larsen KD, Lau C, Lemon TA, Liang AJ, Liu Y, Luong LT, Michaels J, Morgan JJ, Morgan RJ, Mortrud MT, Mosqueda NF, Ng LL, Ng R, Orta GJ, Overly CC, Pak TH, Parry SE, Pathak SD, Pearson OC, Puchalski RB, Riley ZL, Rockett HR, Rowland SA, Royall JJ, Ruiz MJ, Sarno NR, Schaffnit K, Shapovalova NV, Sivisay T, Slaughterbeck CR, Smith SC, Smith KA, Smith BI, Sodt AJ, Stewart NN, Stumpf KR, Sunkin SM, Sutram M, Tam A, Teemer CD, Thaller C, Thompson CL, Varnam LR, Visel A, Whitlock RM, Wohnoutka PE, Wolkey CK, Wong VY, Wood M, Yaylaoglu MB, Young RC, Youngstrom BL, Yuan XF, Zhang B, Zwingman TA, Jones AR (2007) Genome-wide atlas of gene expression in the adult mouse brain. Nature 445:168–76.

Loebrich S, Nedivi E (2009) The function of activity-regulated genes in the nervous system. Physiological Reviews 89:1079–103.

Marder E, Goaillard JM (2006) Variability, compensation and homeostasis in neuron and network function. Nature Reviews Neuroscience 7:563–574.

Marioni J, Mason C, Mane S, Stephens M, Gilad Y (2008) RNA-seq: An assessment of technical reproducibility and comparison with gene expression arrays. Genome Research 18:1509–1517.

Medina-Marino A (2009) Construction and Initial Characterization of the Densin Knockout Mouse. Ph.D. thesis, California Institute of Technology.

Metzker M (2009) Sequencing technologies—the next generation. Nature Reviews Genetics 11:31–46.

Mortazavi A, Williams BA, McCue K, Schaeffer L, Wold B (2008) Mapping and quantifying mammalian transcriptomes by RNA-Seq. Nature Methods 5:621–628.

Nakagawa T, Engler JA, Sheng M (2004) The dynamic turnover and functional roles of alpha-actinin in dendritic spines. Neuropharmacology 47:734–745.

Ohtakara K, Nishizawa M, Izawa I, Hata Y, Matsushima S, Taki W, Inada H, Takai Y, Inagaki M (2002) Densin-180, a synaptic protein, links to PSD-95 through its direct interaction with MAGUIN-1. Genes to Cells 7:1149–60.

Piedras-Rentería E, Pyle J, Diehn M, Glickfeld L, Harata N, Cao Y, Kavalali E, Brown P, Tsien R (2004) Presynaptic homeostasis at CNS nerve terminals compensates

for lack of a key Ca2+ entry pathway. Proceedings of the National Academy of Sciences 101:3609–3614.

Quackenbush J (2002) Microarray data normalization and transformation. Nature Genetics 32 Suppl:496–501.

Quitsch A, Berhörster K, Liew CWW, Richter D, Kreienkamp HJJ (2005) Postsynaptic shank antagonizes dendrite branching induced by the leucine-rich repeat protein Densin-180. Journal of Neuroscience 25:479–487.

R Development Core Team (2008) R: A Language and Environment for Statistical Computing. R Foundation for Statistical Computing, Vienna, Austria.

Sheng M, Hoogenraad CC (2007) The postsynaptic architecture of excitatory synapses: a more quantitative view. Annu Rev Biochem 76:823–47.

Strack S, Robison AJ, Bass MA, Colbran RJ (2000) Association of calcium/calmodulin-dependent kinase II with developmentally regulated splice variants of the postsynaptic density protein densin-180. Journal of Biological Chemistry 275:25061–25064.

Stuchlík A (2001) Single systemic dose of vigabatrin induces early proconvulsant and later anticonvulsant effect in rats. Neuroscience Letters 312:37–40.

Sturani E, Abbondio A, Branduardi P, Ferrari C, Zippel R, Martegani E, Vanoni M, Denis-Donini S (1997) The Ras Guanine nucleotide Exchange Factor CDC25Mm is present at the synaptic junction. Experimental cell research 235:117–123.

Suemori S, Shimazawa M, Kawase K, Satoh M, Nagase H, Yamamoto T, Hara H (2006) Metallothionein, an Endogenous Antioxidant, Protects against Retinal Neuron Damage in Mice. Invest Ophthalmol Vis Sci 47:3975–3982.

Sultan M, Schulz M, Richard H, Magen A, Klingenhoff A, Scherf M, Seifert M, Borodina T, Soldatov A, Parkhomchuk D, et al. (2008) A global view of gene activity and alternative splicing by deep sequencing of the human transcriptome. Science 321:956.

Walikonis RS, Oguni A, Khorosheva EM, Jeng CJ, Asuncion FJ, Kennedy MB (2001) Densin-180 forms a ternary complex with the (alpha)-subunit of Ca2+/calmodulin-dependent protein kinase II and (alpha)-actinin. Journal of Neuroscience 21:423–433.

Wyszynski M, Lin J, Rao A, Nigh E, Beggs AH, Craig AM, Sheng M (1997) Competitive binding of alpha-actinin and calmodulin to the NMDA receptor. Nature 385:439–442.

Xie T, Tong L, McCann U, Yuan J, Becker K, Mechan A, Cheadle C, Donovan D, Ricaurte G (2004) Identification and Characterization of Metallothionein-1 and-2 Gene Expression in the Context of ({+/-}) 3, 4-Methylenedioxymethamphetamine-Induced Toxicity to Brain Dopaminergic Neurons. Journal of Neuroscience 24:7043–50.

Yamasaki N, Maekawa M, Kobayashi K, Kajii Y, Maeda J, Soma M, Takao K, Tanda K, Ohira K, Toyama K, Kanzaki K, Fukunaga K, Sudo Y, Ichinose H, Ikeda M,

Iwata N, Ozaki N, Suzuki H, Higuchi M, Suhara T, Yuasa S, Miyakawa T (2008) Alpha-CaMKII deficiency causes immature dentate gyrus, a novel candidate endophenotype of psychiatric disorders. Molecular Brain 1:6.

Chapter 3

Cofilin regulation by NMDA receptor activation

Holly Beale, Holly Carlisle, Mary Kennedy

3.1 Introduction

The majority of excitatory synapses in the brain are located on dendritic spines. Larger synapses are located on larger spines and are stronger. These properties–synapse size and strength, and spine size–are coordinately regulated in part by salient patterns of synaptic activity. Some of the proteins that regulate actin polymerization and thus determine spine morphology are known. Moreover, abnormalities in spine morphology are linked to mental retardation and cognitive disorders (Carlisle and Kennedy, 2005). Fragile X syndrome (FXS), which is an inherited form of mental retardation and autism, is associated with increased dendritic spines, a greater proportion of which are long and immature (O'Donnell and Warren, 2002). Inactivation of the *fragile X mental retardation 1 (Fmr1)* gene in mice recapitulates the spine phenotype seen in humans with FXS. These mice also display hyperactivity, stereotypy,

and hypoanxiety phenotypes that may be analogous to behaviors in FXS patients (Dutch-Belgian Fragile, 1994). The converse phenotype of spine morphology is seen in mice that express a dominant negative form of p21-activated kinase (PAK), a regulator of spine morphology (Hayashi et al., 2007): These mice have decreased spine density, fewer long spines, and fewer immature spines than do wild-type mice. By crossing the PAK strain with the *Fmr1* knockout, investigators partially rescued the spine density, hyperactivity, stereotypy and hypoanxiety phenotypes, and completely rescued the impaired cortical long term potentiation (LTP) (Hayashi et al., 2007). This demonstrates the therapeutic insight that can be gained by basic research into the regulation of dendritic spine morphology.

Our research into the regulation of spine morphology focused on the actin-severing protein cofilin, a strong modulator of actin dynamics, whose activity has been implicated in LTP and long term depression (LTD) (Fukazawa et al., 2003; Zhou et al., 2004). Treatment of primary hippocampal cultures with the drug N-methyl-D-aspartate (NMDA), which stimulates NMDA receptors, activates upstream actin regulators Rac (a small GTPase) and PAK (Carlisle et al., 2008). In other systems, an increase in phospho-PAK leads to an inactivation of cofilin by phosphorylation (Aleksic et al., 2009). In primary mouse hippocampal cultures, however, NMDA treatment increases phospho-PAK and decreases phospho-cofilin. Cofilin is dephosphorylated within 15 seconds of NMDA receptor activation (Carlisle et al., 2008). This result suggests that there is an activity-dependent phosphatase regulating cofilin activity. Thus, it was of interest to identify that phosphatase.

In selecting candidate phosphatases, we considered the broadly active phosphatases, protein phosphatase 1 (PP1), protein phosphatase 2A (PP2A) and calcineurin, as well as the cofilin-specific phosphatases, slingshot and chronophin (Figure 3.1). PP1 and PP2A are responsible for much of the phosphatase activity in mammalian cells. Calcineurin is regulated by calcium and is thus a good candidate for a process triggered by the opening of the calcium-permeable NMDA receptor channel. These three phosphatases have well-characterized small-molecule inhibitors: PP1 and PP2A are inhibited by okadaic acid, and calcineurin is inhibited by FK506 and Cyclosporin A (CsA).

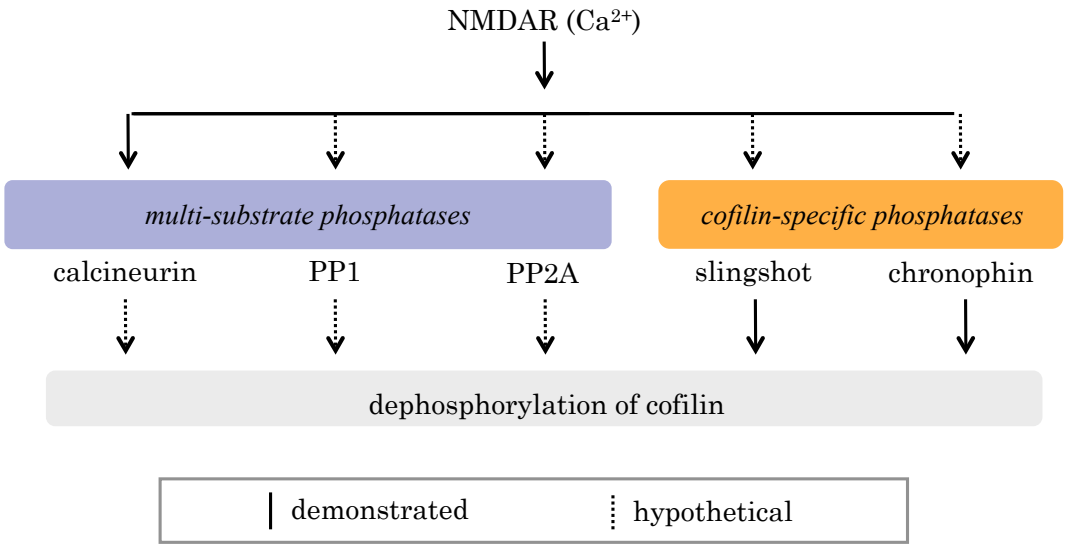

Figure 3.1: Candidate cofilin phosphatases are illustrated. We considered both broadly-active and specific phosphatases. Slingshot and chronophin specifically dephosphorylate cofilin (Gohla et al., 2005; Huang et al., 2008; Nagata-Ohashi et al., 2004; Nishita et al., 2004; Niwa et al., 2002; Wang et al., 2005)

Although two cofilin-specific phosphatases, slingshot and chronophin, are both known to directly dephosphorylate cofilin, they have yet to be extensively character-

ized in neurons. Slingshot dephosphorylates cofilin in HeLa, COS-7, and 293T cells, as well as in cell-free conditions (Nagata-Ohashi et al., 2004; Nishita et al., 2004; Niwa et al., 2002; Wang et al., 2005). Chronophin dephosphorylates cofilin in bovine brain cytosol, Hela cells, and cell-free conditions (Gohla et al., 2005; Huang et al., 2008). To test the role of these phosphatases in cultured neurons, we investigated using RNA interference (RNAi) to decrease protein levels.

3.2 Materials and Methods

3.2.1 Cell culture and treatment

Cell cultures were generated and treated as described in Carlisle et al. (2008). Briefly, primary mouse hippocampal neurons were prepared from embryonic day 16 or day 17 mice, and grown for 13-14 days *in vitro* (DIV). Cells for immunocytochemistry studies were plated on glass coverslips. Cultures were pretreated with phosphatase inhibitor for 30 minutes; FK506 (50 nM) or CsA (50 nM) were used to inhibit the phosphatase calcineurin, and okadaic acid (1 μM) was used to inhibit the phosphatases PP1 and PP2A. Cultures were washed, allowed to recover for two minutes on a plate warmer, and then treated with 25 μM NMDA (Tocris; Ellisville, MO) for 15 seconds, or one, three, or five minutes. Cells were then lysed with in a solution with 3 percent SDS.

3.2.2 Fluorescence immunocytochemistry

After 14 DIV, cells were fixed with paraformaldehyde and methanol as described in (Vazquez et al., 2004) with blocking buffer from Li-Cor buffer used in place of buffer with normal goat serum. Slingshot-1L (ECM Biosciences)antibody signal was visualized with a Zeiss Axiovert 200 microscope with a Plan-Apochromat 63x/1.4 (oil) objective lens. Images were captured with a high-resolution CCD camera (Axiocam MRm, Zeiss, Jena, Germany), controlled by Zeiss AxioVision 3.1 software.

3.2.3 Immunoblot

Samples were heated to 95°C for three minutes in 3 percent SDS and 40 mM β-glycerophosphate and fractionated via SDS-PAGE. Proteins were transferred to nitrocellulose membranes in 25 mM Tris, 190 mM glycine, and 20 percent methanol; blocked in Odyssey Blocking Buffer; and probed with antibodies against one of the following: phospho-cofilin (Cell Signaling), actin (Sigma), cofilin (BD Transduction Labs), synGAP (developed in our laboratory; Oh et al., 2004), phospho-Thr423 PAK (Cell Signaling), PAK1 (Cell Signaling), GAPDH (Sigma), PSD-95 (Affinity Bioreagents), Synaptophysin (Abcam), Chronophin (Cell Signaling), Slingshot-1L (ECM Biosciences), PAK2 (Cell Signaling), or LIMK1 (Cell Signaling). The secondary antibody used was IRDye (Rockland). Antibodies were diluted in Odyssey Blocking Buffer; and membranes were scanned with an Odyssey scanner (Li-Cor).

3.2.4 Mouse PSD preparation with sucrose gradient

We prepared the crude mouse-brain postsynaptic density fraction from 10 mice in the manner described in Carlin et al. (1980), with modifications described in Cho et al. (1992). In brief, mouse brain tissue was homogenized in buffered isotonic sucrose with protease inhibitors and then centrifuged at 1400 X g for 10 minutes. Homogenate samples were taken from the supernatant. The remaining supernatant was applied to sucrose density gradients and centrifuged. Synaptosome samples were taken from the band between 1.0 and 1.2M sucrose; the remainder of the band was incubated with 0.5 percent Triton X-100 (Pierce), stirred for 15 minutes at 4° Celsius, and centrifuged at 36,800 X g for 45 minutes. The resulting pellet was the postsynaptic density (PSD).

3.3 Results

3.3.1 Analysis of synaptic localization

To determine which phosphatases are located in the PSD, we performed a crude synaptosome and PSD fractionation from mouse forebrain (Figure 3.2). To analyze the purity of the preparation, we measured the relative enrichment of PSD-95 and synaptophysin in the PSD fraction. Analysis by immunoblot showed that the protein PSD-95 is enriched in the synaptosome fraction and significantly enriched in the PSD fraction to a similar extent found in preparations from rat forebrain (Apperson et al., 1996). Conversely, the pre-synaptic protein synaptophysin is nearly undetectable in

the PSD fraction, demonstrating that the fraction is relatively free of presynaptic contaminants.

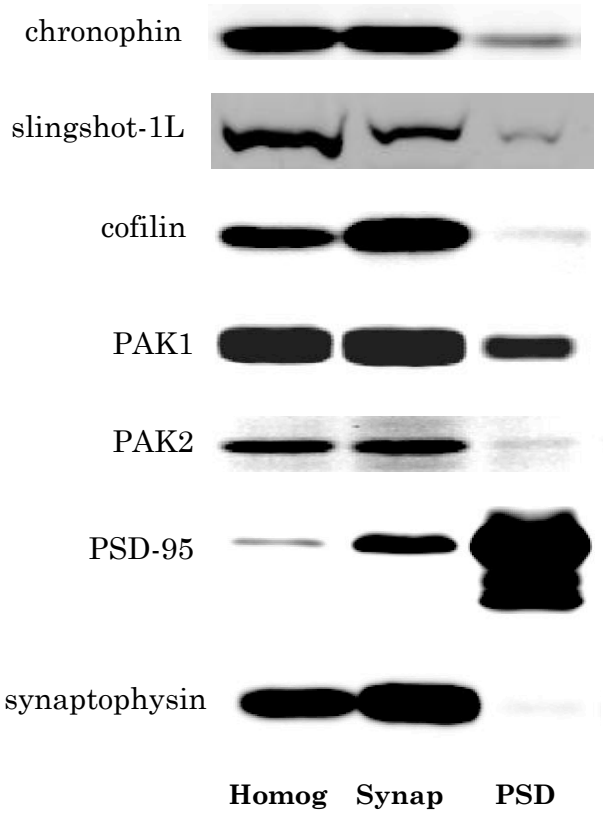

Figure 3.2: Slingshot and chronophin are present in the crude synaptosomal fraction. Immunoblots from a PSD preparation are shown. Brain homogenate was run in the first lane, the synaptosomal fraction in the second, and the PSD fraction in the third. Chronophin and slingshot are present in the synaptosome, and thus are potential mediators of NMDA-induced cofilin dephosphorylation. Both are also present at low levels in the PSD fraction. The large PSD95 band in the PSD fraction indicates successful enrichment of the postsynaptic density. The decrease in synaptophysin between the synaptosome and PSD fractions indicates the extensive depletion of presynaptic proteins.

Two candidate phosphatases, chronophin and slingshot, are both present in the synaptosome fraction. Because equal amounts of total protein were loaded in each lane, enrichment can be determined by the relative size of the bands in the different fractions. These results showed that chronophin protein levels are similar in the

homogenate and synaptosome fractions, while slingshot is slightly decreased in the synaptosome fraction. Both phosphatases are also present in the PSD fraction, although at lower levels. Thus, chronophin and slingshot are potential mediators of NMDA-induced cofilin dephosphorylation.

PAK and cofilin are also present in the synaptosome fraction. PAK1 and PAK2 show little change between the homogenate and synaptosome fraction, while cofilin is enriched in the synaptosome fraction. All of the proteins are depleted in the PSD relative to the synaptosome fraction. This does not exclude interactions with PSD proteins; proteins that are present in the postsynaptic compartment but are loosely bound to core PSD proteins can be easily stripped from the PSD during the triton solubilization step.

To further characterize the subcellular localization of slingshot, we used immunocytochemistry to visualize its distribution in hippocampal cultures. Slingshot staining is punctate in dendrites and close to the cell membrane in the cell body (Figure 3.3). Since cofilin regulates actin structures, which are also located close to the cell membrane, these findings are consistent with a role for slingshot in the regulation of cofilin and thus actin.

3.3.2 Small molecule phosphatase inhibitors

To identify the activity-dependent phosphatases that mediate NMDA-induced dephosphorylation of cofilin, we applied phosphatase inhibitors to primary hippocampal cell cultures. Since bath application of NMDA causes a decrease in cofilin phospho-

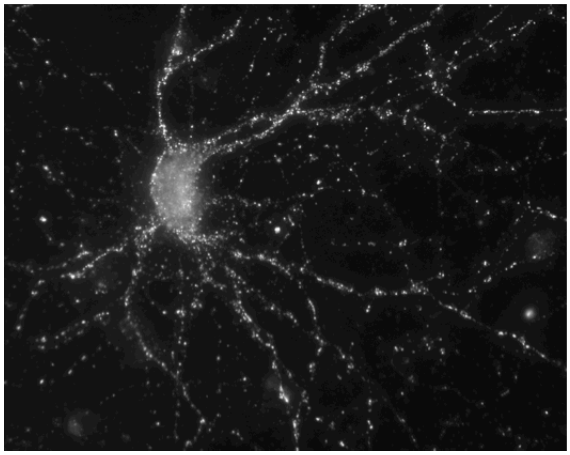

Figure 3.3: SSH antibody showed punctate staining pattern at the in dendrites and close to the cell membrane in the cell body

rylation, we reasoned that inhibition of involved phosphatases would perturb that response. Therefore, the NMDA-induced dephosphorylation of cofilin was determined in both the presence and absence of phosphatase inhibitors. We inhibited PP1 and PP2A with okadaic acid, and calcineurin with FK506 or CsA. Inhibitors were applied to the cell cultures 30 minutes before the NMDA treatment.

We measured phospho-protein levels in the absence of NMDA to assess the role of the phosphatases in steady-state conditions, and measured them again at 15 seconds, and at one, three, and five minutes after NMDA treatment. Phospho-protein levels are expressed as a percent of those in the control cultures that were treated with neither phosphatase inhibitor nor NMDA. Although these experiments depend on measuring phospho-cofilin, we also measured phosphorylation of PAK isoforms 1–3 to confirm the activation of the actin-regulatory pathways observed in Carlisle et al. (2008) and to assess the specificity of the effects of phosphatases.

Inhibition of calcineurin

While calcineurin inhibitors increase phospho-cofilin by 12 percent before the addition of NMDA (Figure 3.4), calcineurin inhibition does not change the trend of cofilin dephosphorylation after NMDA treatment. The proportion of dephosphorylation is similar in the presence and absence of calcineurin inhibition. Thus, although calcineurin regulates steady-state phosphorylation of cofilin, it does not appear to be the activity-dependent phosphatase that activates cofilin in response to NMDA treatment.

Inhibiting calcineurin has little effect on phospho-PAK1-3 levels. Pretreatment with calcineurin inhibitors FK506 or CsA does not change the steady-state phosphorylation of PAK1 (Figure 3.5). Nor does pretreatment with FK506 or CsA change the phosphorylation of PAK1 in response to 25 μM NMDA treatment. Consequently, we conclude that calcineurin does not regulate the phosphorylation of PAK1 under these conditions.

Inhibition of PP1/PP2A

We performed similar studies with the PP1/PP2A inhibitor okadaic acid. Steady-state levels of phospho-cofilin doubles in response to the phosphatase inhibitor. However, the addition of NMDA still decreases phospho-cofilin, which indicates that neither PP1 nor PP2A mediate NMDA-induced dephosphorylation of cofilin.

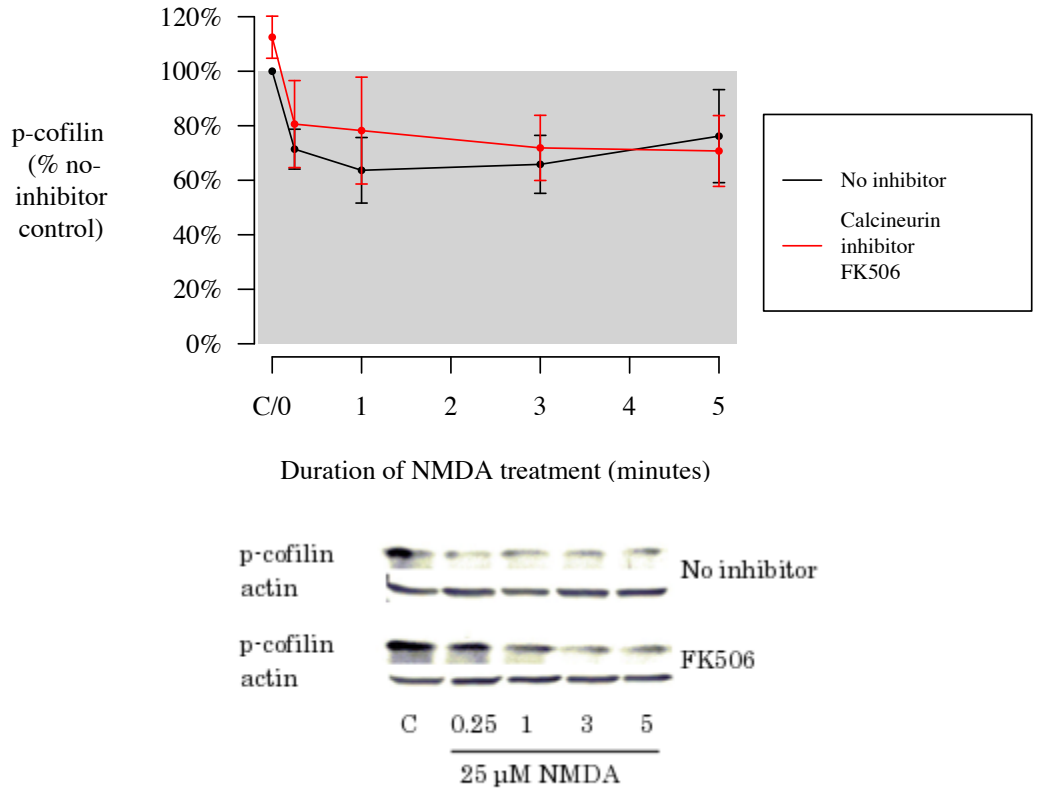

Figure 3.4: Calcineurin regulates steady-state phosphorylation of cofilin but not NMDA-induced dephosphorylation of cofilin. Phospho-cofilin levels are plotted on the ordinate as a percent of the phospho-cofilin levels in the control sample (indicated by the gray box; the control cultures were treated with neither phosphatase inhibitor nor NMDA). Duration of NMDA treatment is plotted on the abscissa. Thirty-minute pretreatment with FK506, a calcineurin inhibitor, caused an increase of 12 percent in steady-state phospho-cofilin. When NMDA was added in addition to FK506, phospho-cofilin levels decreased, indicating that calcineurin is not mediating NMDA-induced dephosphorylation of cofilin. Representative western blots of FK506 and control (no inhibitor treatment) are shown for each NMDA treatment condition. Statistics include results of CsA treatment (not shown), which were indistinguishable from the FK506 results. Error bars indicate standard error of the mean.

The effect of inhibiting PP1/PP2A on PAK1-3 is dramatic: Steady-state PAK1-3 phosphorylation increases a hundred-fold. The further addition of NMDA in the presence of okadaic acid does not further increase phospho-PAK1-3 (Figure 3.7).

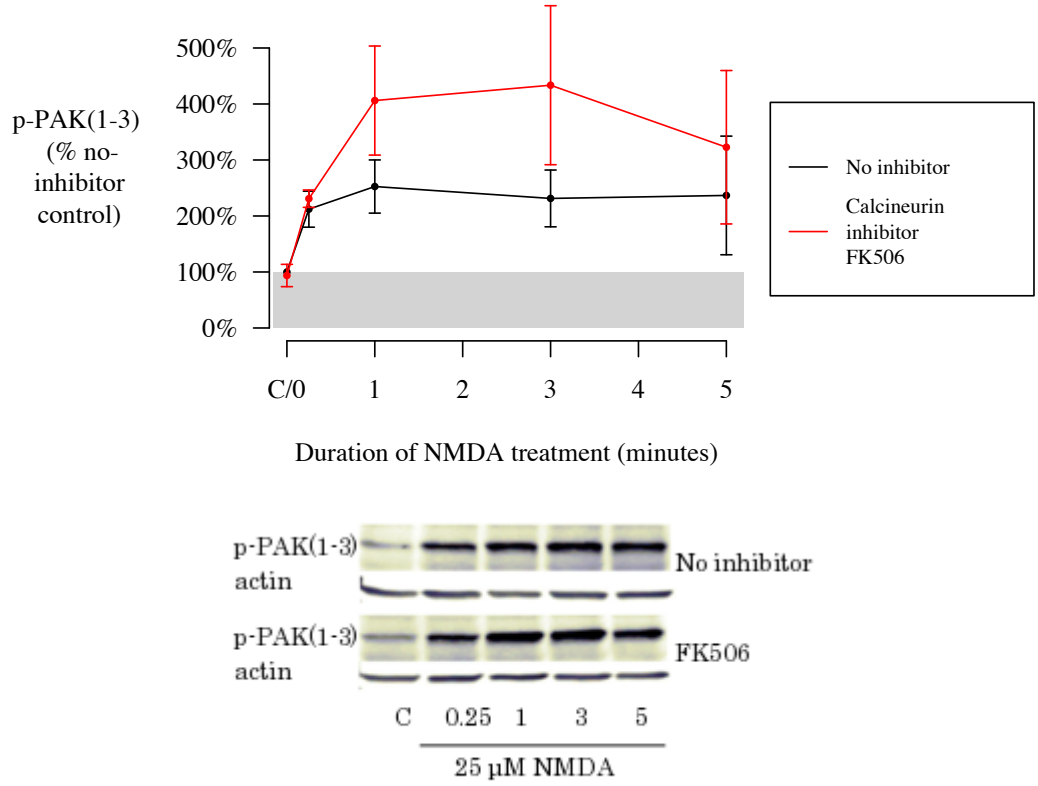

Figure 3.5: Calcineurin does not regulate steady-state levels of phosphorylation of PAK1-3. Phospho-PAK1-3, as a percent of control (indicated by the gray box), is plotted against the duration of the NMDA treatment. Calcineurin inhibitor FK506 does not change steady-state phospho-PAK1-3 levels (time point 0), and phospho-PAK1-3 levels increase in response to NMDA treatments in the presence and absence of the calcineurin inhibitor. Representative western blots of FK506 and control (no inhibitor applied) are shown for each NMDA treatment condition. Statistics include results of CsA treatment (not shown), which were indistinguishable from FK506 results. Error bars indicate standard error of the mean.

These findings indicate that PP1 and/or PP2A actively suppress steady-state phosphorylation of PAK1-3 under these experimental conditions. It also reveals that a kinase is constitutively phosphorylating PAK1-3, maintaining the phosphorylation of PAK1-3 in a state of dynamic equilibrium.

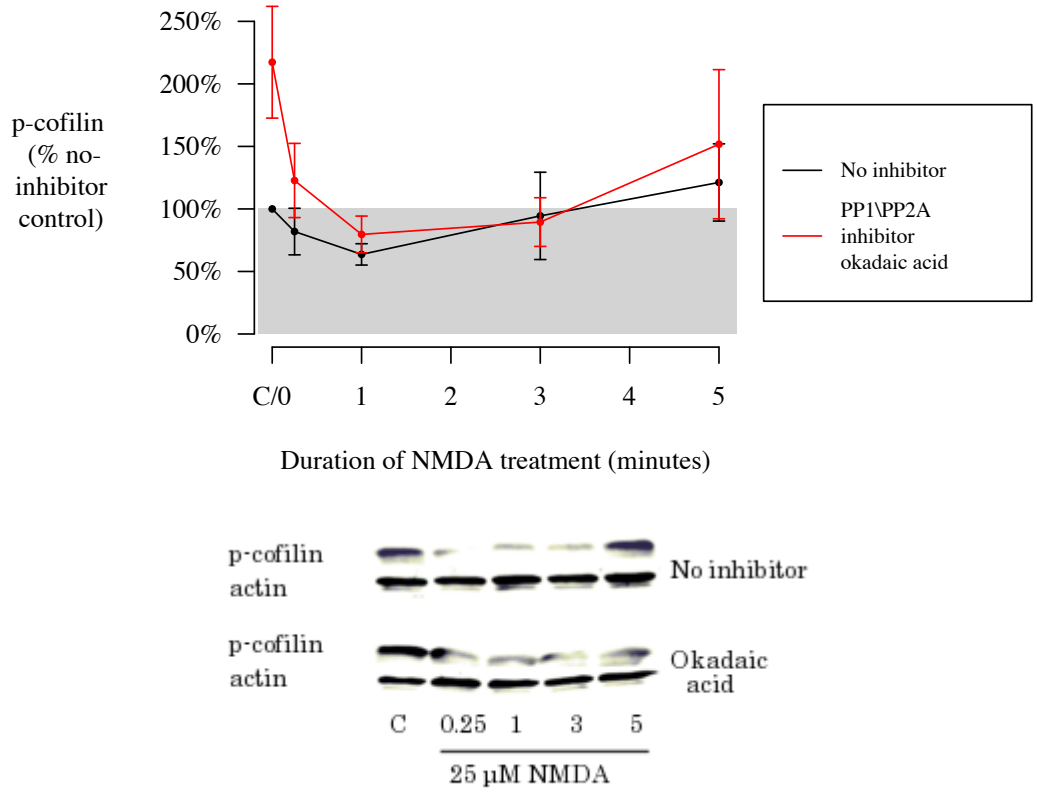

Figure 3.6: PP1 and/or PP2A regulates steady-state phosphorylation of cofilin but not NMDA-induced dephosphorylation of cofilin. Phospho-cofilin, as a percent of control (indicated by the gray box), is plotted against the duration of the NMDA treatment. Okadaic acid increases steady-state phospho-cofilin levels (time point 0), but phospho-cofilin is still dephosphorylated in response to a bath application of NMDA. Okadaic acid does not mediate NMDA-induced dephosphorylation of cofilin. Representative western blots of each condition are shown. Error bars indicate standard error of the mean.

3.3.3 Knockdown of slingshot

No small molecule inhibitors are available for chronophin and slingshot. Therefore, to reduce the levels of these proteins, we investigated different methods of RNAi. We utilized membrane-permeable short interfering RNA (siRNA) oligonucleotides that do not require a separate transfection reagent (Accell, Dharmacon). Transfection

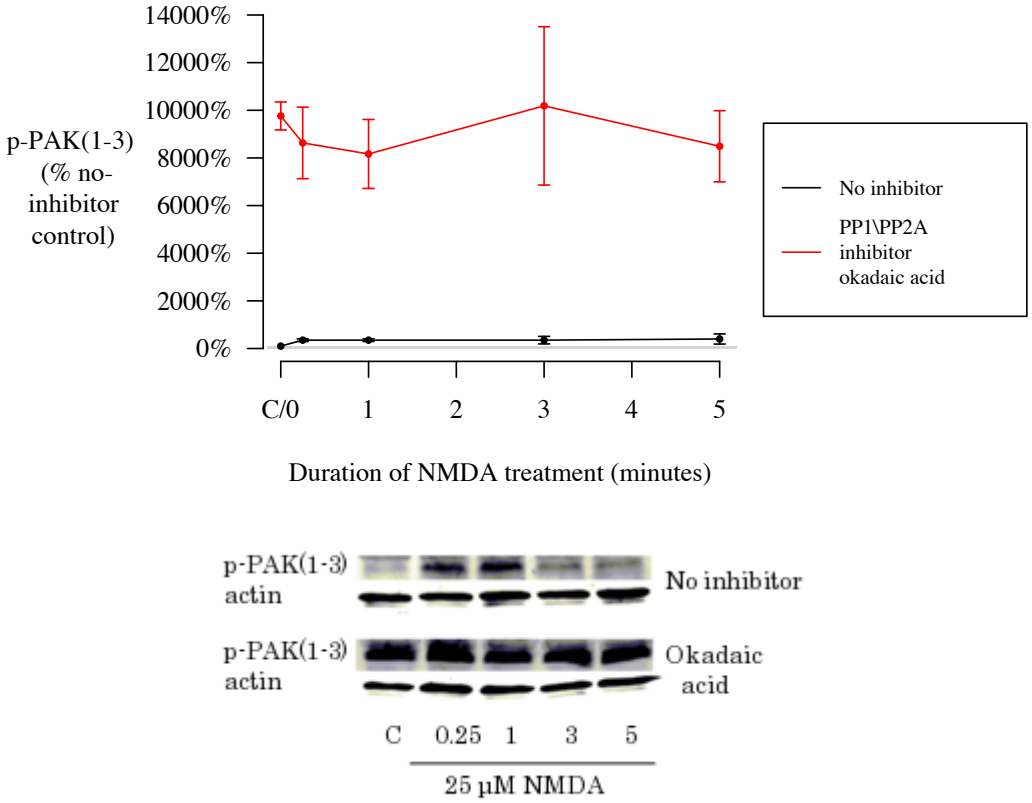

Figure 3.7: PP1 or PP2A strongly suppresses the steady-state phosphorylation of p-PAK(1-3). p-PAK(1-3), as a percent of control (indicated by the gray box), is plotted against the duration of the NMDA treatment. Okadaic acid increases steady state pPAK1-3 levels by a factor of 100. Representative western blots of each condition are shown. Error bars indicate standard error of the mean.

reagents are often toxic and inappropriate for cultures intended for signal transduction experiments experiments that require mature, healthy neurons.

The positive control siRNA oligonucleotide, targeted against GAPDH, decreases the protein level in the neurons. Neurons were grown for 11 DIV and the GAPDH siRNA applied for 48 or 72 hours. At 72 hours, GAPDH protein levels are decreased by 60 percent compared to cultures treated with a non-targeting siRNA (Figure

3.8). Although the method decreases protein levels, a 60 percent reduction may be insufficient for some purposes.

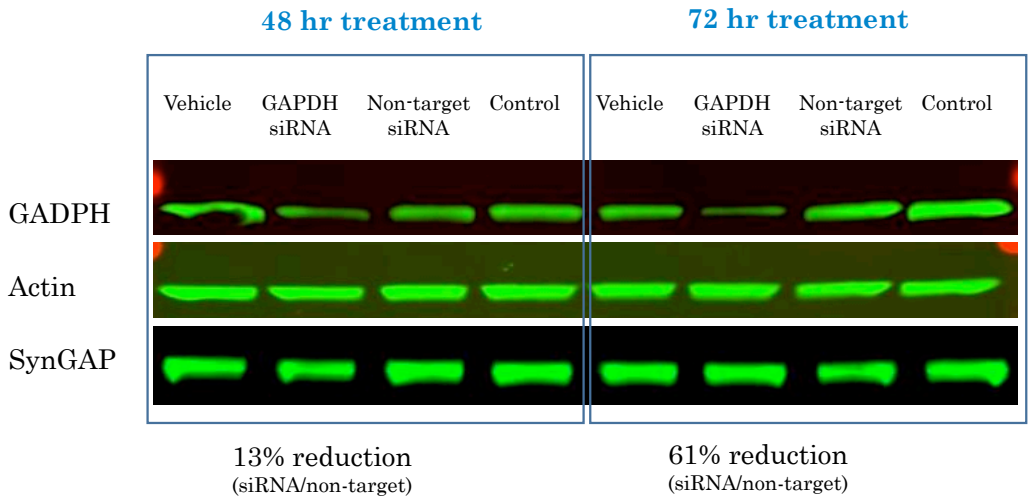

Figure 3.8: GAPDH protein was reduced by 60 percent after 72 hour treatment with siRNA. Western blots of treated and untreated samples are shown. GAPDH was targeted for knockdown with Accel siRNA. To assess the effect of the siRNA system for effects on important regulators of our experimental system, we also measured actin and SynGAP, a regulator of synaptic signaling. In the left group, vehicle or siRNA was applied to cultures for 48 hours; in the right, for 72 hours. In the GAPDH siRNA lane, the GAPDH band is visible low in both the 48- and 72-hour conditions. The total reduction of GAPDH was 61 percent after 72 hours of treatment, when normalized to the non-targeting siRNA treatment.

Unfortunately, the siRNA oligonucleotides targeting slingshot are ineffective at reducing slingshot protein levels (Figure 3.9).

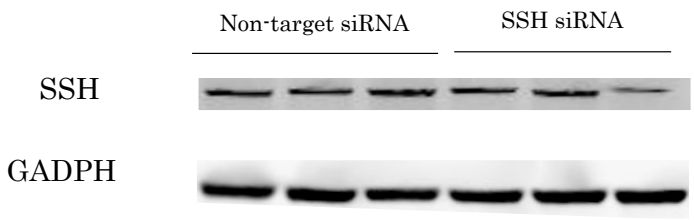

Figure 3.9: Slingshot siRNA did not decrease slingshot protein levels. Cultures were incubated with slingshot (SSH) or non-targeted siRNA oligonucleotides for 72 hours. Western blots of treated and untreated samples are shown. GAPDH was used as a loading control. Slingshot levels are not consistently reduced. This blot is representative of those from other experiments in which oligonucleotides were applied for longer and shorter times, as well as to neuronal cultures of different ages.

3.4 Discussion

Synaptic plasticity is accompanied by extensive cytoskeletal modification. NMDA receptors mediate several forms of synaptic plasticity, and signal transduction leading to cytoskeletal modification can be studied by applying the NMDA receptor agonist, NMDA, to neuronal cultures. This treatment decreases phosphorylation of cofilin, a protein that depolymerizes actin filaments when it is dephosphorylated (Carlisle et al., 2008). This NMDA-mediated decrease in phospho-cofilin led us to hypothesize that an activity-regulated phosphatase dephosphorylates cofilin. Activation of PAK, a kinase, leads to phosphorylation of cofilin in non-neuronal systems (Edwards et al., 1999). However, we demonstrated that applying NMDA to hippocampal cultures activates PAK while decreasing phospho-cofilin levels. These results suggest that the canonical PAK-LIMK-Cofilin signaling pathway described in other systems might not be present in spines.

We hypothesized that stimulation of neuronal NMDA receptors activates a cofilin-phosphatase that mediates the observed dephosphorylation of cofilin. When PP1/2A or calcineurin are inhibited, the amount of phosphorylated cofilin is still decreased in response to NMDA application. Thus, neither PP1/2A nor calcineurin is likely to mediate the decrease in phospho-cofilin (Table 3.1). We found that two cofilin-specific phosphatases, slingshot and chronophin, are localized at the synapse, suggesting they are candidates for mediating the decrease in cofilin phosphorylation observed after NMDA stimulation.

Table 3.1: Effect of phosphatase inhibitors on phosphorylation of PAK and cofilin.

	Calcineurin Inhibitors		PP1/PP2A Inhibitors	
Protein	steady-state	NMDA	steady-state	NMDA
phospho-cofilin	increased	no change	highly increased	no change
phospho-PAK1-3	increased	no change	highly increased	?

To confirm the activation of actin-regulatory pathways by NMDA, we measured phosphorylation of PAK isoforms 1–3 and phospho-cofilin. We observed a hundred-fold increase in basal phospho-PAK1-3 when PP1 and PP2A are inhibited with okadaic acid. This observation is consistent with prior demonstrations of increases in phospho-PAK in neutrophils in response to okadaic acid (Westphal et al. 1999; Zhan et al. 2003, but see Chan et al. 2008). The present findings also further support the hypothesis that PAK1-3 does not phosphorylate cofilin in spines.

Due to the increased phosphorylation of PAK1-3 when PP1 and PP2A are inhibited, we were unable to definitively assess the effect of adding NMDA. Measurements of the increased phosphorylation signal have an error margin larger than the magnitude of the NMDA-dependent increase observed when PP1 and PP2A are not inhibited. Thus, it is difficult to observe an NMDA-dependent increase in the signal. An alternate consideration concerns the total amount of PAK that can be phosphorylated. If PAK is maximally phosphorylated when PP1 and PP2A are inhibited, there may be no further response to NMDA.

Although we did not identify the phosphatase involved in the NMDA-dependent dephosphorylation of cofilin, this evidence indicates that the most promiscuous phos-

phatases are not likely candidates. We also confirmed the presence of two cofilin-specific phosphatases in the system.

As discussed in the introduction, a dominant negative form of PAK can rescue cytoskeletal and behavioral deficits in a mouse model of Fragile X syndrome. However, our work shows that the PAK signaling observed in most other systems is altered in neurons, as a hundred-fold increase in phospho-PAK does not increase phospho-cofilin levels in neurons. Understanding neuron-specific regulation of PAK and cofilin is critical for implementation of treatments that will target PAK and cofilin regulation.

References

Aleksic M, Walcher D, Giehl K, Bach H, Grüb M, Durst R, Hombach V, Marx N (2009) Signalling processes involved in C-peptide-induced chemotaxis of CD4-positive lymphocytes. Cellular and Molecular Life Sciences 66:1974–1984.

Apperson ML, Moon IS, Kennedy MB (1996) Characterization of Densin-180, a New Brain-Specific Synaptic Protein of the O-Sialoglycoprotein Family. Journal of Neuroscience 16:6839–6852.

Carlin RK, Grab DJ, Cohen RS, Siekevitz P (1980) Isolation and characterization of postsynaptic densities from various brain regions: enrichment of different types of postsynaptic densities. Journal of Cell Biology 86:831–45.

Carlisle H, Kennedy M (2005) Spine architecture and synaptic plasticity. Trends in Neurosciences 28:182–187.

Carlisle HJ, Manzerra P, Marcora E, Kennedy MB (2008) SynGAP regulates steady-state and activity-dependent phosphorylation of cofilin. Journal of Neuroscience 28:13673–83.

Chan P, Lim L, Manser E (2008) PAK Is Regulated by PI3K, PIX, CDC42, and PP2C {alpha} and Mediates Focal Adhesion Turnover in the Hyperosmotic Stress-induced p38 Pathway. Journal of Biological Chemistry 283:24949.

Cho KO, Hunt CA, Kennedy MB (1992) The rat brain postsynaptic density fraction contains a homolog of the Drosophila discs-large tumor suppressor protein. Neuron 9:929–42.

Dutch-Belgian Fragile X (1994) Consortium. FMR1 knockout mice: a model to study fragile X mental retardation. Cell 78:23–33.

Edwards DC, Sanders LC, Bokoch GM, Gill GN (1999) Activation of LIM-kinase by Pak1 couples Rac/Cdc42 GTPase signalling to actin cytoskeletal dynamics. Nature Cell Biology 1:253–9.

Fukazawa Y, Saitoh Y, Ozawa F, Ohta Y, Mizuno K, Inokuchi K (2003) Hippocampal LTP is accompanied by enhanced F-actin content within the dendritic spine that is essential for late LTP maintenance in vivo. Neuron 38:447–460.

Gohla A, Birkenfeld J, Bokoch GM (2005) Chronophin, a novel HAD-type serine protein phosphatase, regulates cofilin-dependent actin dynamics. Nature Cell Biology 7:21–9.

Hayashi K, Ohshima T, Hashimoto M, Mikoshiba K (2007) Pak1 regulates dendritic branching and spine formation. Journal of Neurobiology 67:655–669.

Huang TY, Minamide LS, Bamburg JR, Bokoch GM (2008) Chronophin mediates an ATP-sensing mechanism for cofilin dephosphorylation and neuronal cofilin-actin rod formation. Developmental Cell 15:691–703.

Nagata-Ohashi K, Ohta Y, Goto K, Chiba S, Mori R, Nishita M, Ohashi K, Kousaka K, Iwamatsu A, Niwa R, Uemura T, Mizuno K (2004) A pathway of neuregulin-induced activation of cofilin-phosphatase Slingshot and cofilin in lamellipodia. Journal of Cell Biology 165:465–71.

Nishita M, Wang Y, Tomizawa C, Suzuki A, Niwa R, Uemura T, Mizuno K (2004) Phosphoinositide 3-kinase-mediated activation of cofilin phosphatase Slingshot and its role for insulin-induced membrane protrusion. Journal of Biological Chemistry 279:7193–8.

Niwa R, Nagata-Ohashi K, Takeichi M, Mizuno K, Uemura T (2002) Control of actin reorganization by Slingshot, a family of phosphatases that dephosphorylate ADF/cofilin. Cell 108:233–46.

O'Donnell WT, Warren ST (2002) A decade of molecular studies of fragile X syndrome. Annual Review of Neuroscience 25:315–38.

Vazquez LE, Chen HJ, Sokolova I, Knuesel I, Kennedy MB (2004) SynGAP regulates spine formation. Journal of Neuroscience 24:8862–72.

Wang Y, Shibasaki F, Mizuno K (2005) Calcium signal-induced cofilin dephosphorylation is mediated by Slingshot via calcineurin. Journal of Biological Chemistry 280:12683–12689.

Westphal R, Coffee Jr R, Marotta A, Pelech S, Wadzinski B (1999) Identification of kinase-phosphatase signaling modules composed of p70 S6 kinase-protein phos-

phatase 2A (PP2A) and p21-activated kinase-PP2A. Journal of Biological Chemistry 274:687.

Zhan Q, Ge Q, Ohira T, Van Dyke T, Badwey J (2003) p21-activated kinase 2 in neutrophils can be regulated by phosphorylation at multiple sites and by a variety of protein phosphatases. Journal of Immunology 171:3785.

Zhou Q, Homma KJ, Poo MmM (2004) Shrinkage of dendritic spines associated with long-term depression of hippocampal synapses. Neuron 44:749–757.

Chapter 4

Arc protein interactions

Holly Beale, Mary Kennedy

4.1 Introduction to Arc

Brain function depends on synaptic plasticity, which is the ability of synapses to increase or decrease the amplitude of the signals they relay. Maintaining changes in synaptic strength over hours requires gene expression (Alberini, 2009). A gene with characteristics that are particularly suggestive for playing a role in maintaining changes in synaptic strength is Arc (also known as Arg3.1), an immediate early gene (IEG) named for its *a*ctivity *r*egulated and *c*ytoskeleton-associating properties. Within minutes of stimuli that trigger changes in synaptic strength, Arc is transcribed and this transcript is transported to the stimulated portion of the dendrite (Steward et al., 1998). When Arc is not present, as in the Arc knockout mouse, both memory and long term potentiation (LTP), a form of induced change in synaptic strength, are impaired. (Guzowski et al., 2000). To better understand the role of the Arc protein

in changes in synaptic strength, we studied its binding to other proteins involved in LTP.

Several known binding partners of Arc have been described in the literature, including endophilin, dynamin, MAP2, and CaMKII (which phosphorylates Arc) (Chowdhury et al., 2006; Donai et al., 2003; Fujimoto et al., 2004). An interaction with an actin-binding protein is suggested by the co-sedimentation observed with crude, but not purified, filamentous actin (Lyford et al., 1995). An interaction with 14-3-3ζ is also suggested by the results of a yeast-two hybrid assay (Lyford, 1998).

14-3-3ζ regulates cofilin, which depolymerizes actin, a process that is required for the cytoskeletal remodeling associated with synaptic potentiation. Thus, Arc could support synaptic potentiation by binding to 14-3-3ζ. 14-3-3 proteins often regulate signal transduction pathways by binding serine/threonine phosphorylated proteins, thus preventing dephosphorylation. Because 14-3-3ζ binds phosphorylated cofilin, it prevents dephosphorylation and activation of cofilin (Gohla and Bokoch, 2002). If Arc does, in fact, bind 14-3-3ζ, this may change the binding affinity between 14-3-3ζ and phospho-cofilin, thus altering the amount of cofilin that can depolymerize actin filaments.

I used pull-down experiments and generated an Arc fragment cDNA library to investigate possible Arc binding interactions. Candidate binding partners included: 1) proteins that had been identified by a yeast two-hybrid screen, 2) proteins that play a large role in the regulation of synaptic plasticity, and 3) CaMKII, which has been reported to bind Arc (Donai et al., 2003).

4.2 Materials and Methods

4.2.1 Protein expression

The pGEX-Arc construct was the gift of Paul Worley. On sequencing the plasmid, we found that our results did not agree with the sequence submitted by the same source to *PubMed*. Specifically, the resulting protein sequence contained the changes P17L (base 50), L209V (base 625), E318G (base 953) (Figure 4.1). The plasmid was mutated back to the reported consensus sequence with the QuikChange Multi Site-Directed Mutagenesis Kit (Stratagene). Frozen glycerol glutathione-S-transferase (GST) and GST-Arc stocks in BL21 *E. coli* cells were prepared and stored at -80° Celsius. For expression, thawed culture was diluted at 1:200 in Luria broth with 100 μg/ml carbenicillin and incubated with shaking (250 rpm) at 37° Celsius overnight. The overnight preculture was diluted at 1:40 into Luria broth and grown to OD_{600} =0.7. Temperature was reduced to 37° Celsius, and IPTG was added to 125 μM. Cultures were grown for six more hours. Pellets were stored at -80° Celsius.

4.2.2 Protein purification

A bacterial pellet overexpressing GST-Arc or GST (control) was resuspended in 10 ml lysis buffer (phosphate-buffered saline (PBS: 137 mM NaCl, 2.7 mM KCl, 4.3 mM Na_2HPO_4, 1.47 mM KH_2PO_4), 1mM EDTA, Complete protease inhibitor (Roche)). The bacterial cells were sonicated on ice for 3 minutes at 30% intensity. Two-second bursts of sonication were followed by 2-second rest periods. The total duration of

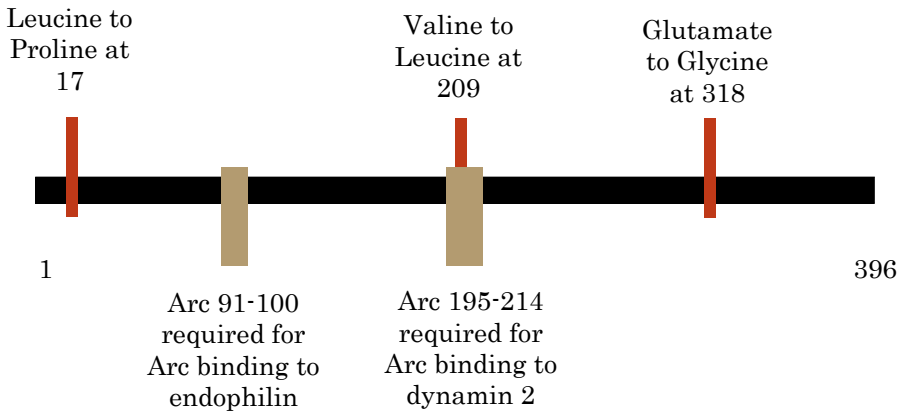

Figure 4.1: Amino acid locations of Arc mutations, displayed with binding sites for endophilin and dynamin identified by Chowdhury et al. (2006).

sonication and rest intervals was six minutes. All subsequent steps took place at 4° Celsius. Triton X-100 (Triton; Pierce) was added to to a concentration of 1%, and phenylmethylsulphonyl fluoride (PMSF) was added to a final concentration of 10 mM. The sample was stirred for 10 minutes after which it was centrifuged at 15,000 X g for 15 minutes. The supernatant was filtered with a 45 μm filter and then a .45 μm filter. GST and GST-fusion proteins were purified from the solubilized bacterial-cell lysate with affinity chromatography:10 ml of supernatant was incubated with 2 ml bed volume of glutathione bead slurry (Sigma G4510) for 1 hour, rotating end-over-end. The protein-bead mixture was spun down in a clinical centrifuge for 30 seconds. GST and GST-Arc beads were washed 4 times in 10 ml PBST (PBS and 1% Triton), rotating 5 min end-over-end. The last wash was removed, reducing the volume to 4 ml (50% slurry). Beads were triturated and 1 ml 50% slurry was aliquoted into four tubes (500 μl bed volume each). Each tube was spun down, and the supernatant

removed and discarded. Protein was batch eluted with 500 μl elution buffer (510 mM reduced glutathione (GSH; Sigma G4251) in 50 mM Tris-HCl, pH 9.5) incubated for 5 minutes with end-over-end rotation. The beads were spun down briefly, the supernatant removed and saved. The elution was repeated 4 times with fresh buffer. The five eluates were combined and injected into three 12-ml 10 K MWCO Slide-A-Lyzer Dialysis Cassettes (Pierce). The sample was dialyzed in 2 L of dialysis buffer (50 mM Tris pH 7.5, 1 mM EDTA) overnight with stirring. Each experiment was performed with freshly purified protein.

To increase the proportion of full-length GST-Arc to GST-Arc fragment, some purified protein samples were subjected to size exclusion chromatography instead of dialysis. The sample was applied to a Superdex 200 10/300 GL column (GE Healthcare Life Sciences) and eluted with 50 mM Tris pH 7.5, 1 mM EDTA and 0.15 M NaCl.

In an alternate method employed to increase the proportion of full-length GST-Arc to GST-Arc fragment, GSH-agarose beads were used to deplete the GST-Arc fragment. After dialysis, GST-Arc solution was twice incubated with GSH-agarose beads for five minutes. The beads were discarded and the supernatant retained.

4.2.3 Pull-down experiments

Glutathione (GSH)-agarose beads were incubated with either GST or GST-Arc with GSH-agarose beads (Sigma G4510) for one hour at 4° Celsius with rotation. Beads were analyzed by SDS-PAGE gels which were stained for total protein (GelCode Blue

Stain, Pierce), revealing that GSH has a much lower affinity for GST-Arc than for GST. Incubating beads with more concentrated GST-Arc solution resulted in more GST-Arc binding to beads. Consequently, we used the maximum concentration of GST-Arc available. Each experiment was performed with freshly purified protein, so the concentration of GST-Arc varied, and thus the amount of GST-Arc that coupled to the GSH-agarose beads varied.

Detecting whether interactors bound to GST-Arc more than they bound to GST required comparison between equimolar amounts of GST bait. To increase the likelihood of equimolar conditions, we serially diluted agarose beads after incubating them with bait. Beads incubated with with GST were were labeled "100% loaded beads." An aliquot of these beads was diluted 1:1 with fresh GSH-agarose beads (those that had never been incubated with bait protein) and labeled "50% loaded beads." These were in turn diluted 1:1 and labeled "25% loaded beads."

The input for the experiment was deoxycholate (DOC)-solubilized brain-membrane fraction prepared from mice that had been sacrificed via cervical dislocation. The forebrain was isolated, the olfactory bulbs and cerebellum were removed, and the remaining tissue tissue added to 2.4 ml of homogenization buffer (4 mM HEPES-NaOH pH 7.4, 0.32 M sucrose, Complete protease inhibitors, adjusted to pH 7.4 with 1 N NaOH). The tissue was homogenized with ten strokes of the tissue grinder at 1,000 RPM and centrifuged for ten minutes at 1,000 g. The resulting supernatant was centrifuged at 100,000 x g for one hour to isolate the membrane fraction, which was then resuspended in 50 mM pH 9 Tris-HCl with Complete protease inhibitor and 1

mM EDTA. DOC was added to 1% and the membrane fraction was solubilized at 37° Celsius for 45 minutes in a rotating bath incubator. The fast spin (100,000 x g for one hour) was repeated and the supernatant was retained. Triton was added to 1%. The pH of the solution was brought up to pH 7.5 by addition of 50 mM pH 7 Tris-HCl with Complete protease inhibitor and 1 mM EDTA. NaCl was added to 150 mM. The solution incubated with glutathione-agarose beads loaded with GST or GST-Arc. The beads and solubilized brain-membrane fraction were incubated at 4° Celsius for two hours with end-over-end rotation, after which the beads were washed 4 times. Proteins were eluted with sample loading buffer (3% SDS, 10% glycerol, 5% beta-mercaptoethanol, 0.002% bromophenol blue, 0.125 M pH 7.5 Tris HCl) and loaded into an SDS-acrylamide gel. Immunoblots were probed with antibodies against CaMKIIα (Affinity Bioreagents), GluR1 (Chemicon), synGAP (developed in our laboratory; Oh et al., 2004) and PSD-95 (Affinity Bioreagents).

4.2.4 Yeast two-hybrid Arc mini-library

The pGEX-Arc plasmid was diluted to 0.2 mg/ml. The solution was sonicated on ice for 0.2 second bursts at 20% intensity on followed by 1.5-seconds rests; total duration of sonication and rest intervals was five minutes. The output was concentrated (Zymo Clean & Concentrator), and subjected to agarose gel electrophoresis. Bands of 0.3-0.5 kilobases were excised and purified (Zymoclean Gel DNA Recovery Kit). Fragments were blunted and ligated into the pUC19 and then subcloned into

the pGADT7 (activating domain) plasmid (Clontech). A subset was sequenced to determine coverage.

4.3 Results

4.3.1 Protein purification

We purified the fusion protein GST-Arc for use as bait in pull-down experiments. On sequencing the plasmid, we found that it did not agree with the sequence submitted by the source lab to PubMed. Specifically, it contained the mutations L209V (base 605), E318G (base 953), E377G (base 1153). Multisite-directed mutagenesis was employed to change the bases back to the PubMed sequence.

Expression of GST-Arc produced the full-length (75 kDa) protein and a 30 kDa fragment composed of GST (26 kDa) and a small piece of Arc. Initially, the insoluble fraction of the bacterial lysate contained a greater proportion of full-length product than did the soluble fraction. To enrich the full-length protein, we optimized the expression of GST-Arc for solubility, yield and reduced proteolysis. Solubility and yield increased but the fragment remained, constituting on average 55% of the sample by mass.

We assessed two other methods of reducing the amount of GST-Arc fragment in the sample: size-exclusion chromatography, and depletion with GSH-agarose beads. Size-exclusion chromatography resulted in an increase of 10% in the fraction of the

sample comprised by full-length GST-Arc; however, this method also reduced the total amount of protein by 50%.

Depletion with GSH-agarose beads was more successful. The GST-Arc fragment has a much higher affinity for GSH-agarose than does the full-length protein, and longer incubations increase the amount of full-length protein on the bead. To take advantage of this, we depleted the GST-Arc fragment by incubating the protein solution with GSH-agarose beads for five minutes, and then retaining the supernatant. On average, two rounds of depletion increased the percent of total protein comprised by GST-Arc by 10-15% at the cost of a loss of 30% of the GST-Arc protein (Figure 4.2).

For subsequent pull-down experiments, we incubated GSH-agarose beads in the protein solution that had been bead-depleted of the Arc fragment. Because GSH-agarose has a greater affinity for the GST-Arc fragment than for full-length GST-Arc, the maximum enrichment of full-length GST-Arc was not maintained. Nevertheless, the proportion of full-length GST-Arc in the pull-down experiments was improved by depleting the GST-Arc fragment.

4.3.2 Interactions in brain lysate

To test for binding between Arc and candidate interactors, we performed GST pull-down experiments. GST-Arc was immobilized on glutathione-agarose beads which were then incubated with DOC-solubilized brain-membrane fraction. The presence of candidate interactors was measured by immunoblot. To assess whether binding

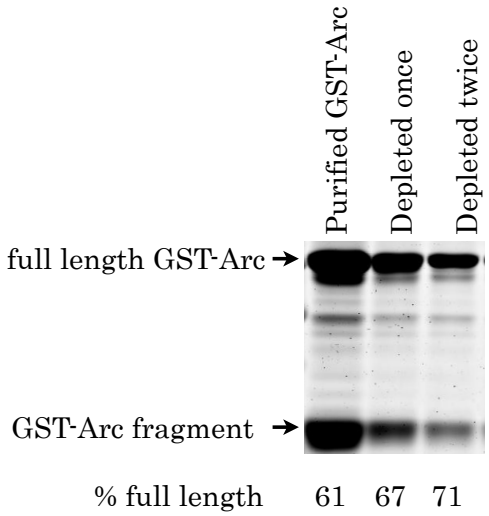

Figure 4.2: Brief incubation with glutathione (GSH) agarose beads depletes the GST-Arc fragment. GST-Arc expressed in *E. coli* is purified by GSH-agarose incubation and elution and analyzed by SDS-PAGE stained for total protein. The two most prominent species in the solution are full-length GST-Arc and a GST-Arc fragment of approximately 30 kiloDaltons (lane one). The fragment is depleted by an additional five-minute incubation with GSH-agarose beads; the supernatant is retained (lane 2). An additional incubation results in a further depletion of the fragment (lane 3). The depletion is the result of the affinity of GSH-agarose beads for the GST-Arc fragment, which is higher than the affinity of the beads for the full-length GST-Arc protein.

was specific to Arc, we compared the amount of protein pulled down by GST-Arc to that pulled down by GST alone.

To compare equimolar amounts of our bait proteins, GST and GST-Arc, we generated multiple samples by serially diluting our immobilized bait, measured the amount of bait protein in each sample, and selected equimolar samples for comparison. Specifically, we diluted bait-incubated GSH-agarose beads with non-incubated GSH-agarose beads (described in Materials and Methods section 4.2.3, shown in Figure 4.3). We analyzed the amount of bait protein in each sample using SDS-PAGE and total protein stain, measuring the relative mass of each bait species via densitometry. This

number was converted to a molar intensity by dividing the mass by the molecular weight of the species in kilodaltons (kDa).

Table 4.1 contains the densitometry measurements for the bead samples shown in Figure 4.3. In this example, the relative number of moles of GST in an aliquot composed only of beads incubated with GST is 26 (shown in the first column of the table, the GST sample), and a comparable molar amount of GST-fusion species is present in an aliquot composed only of beads incubated with GST-Arc (28; the sum of the molar intensity value listed for columns 4 and 6, full-length GST-Arc and GST-Arc fragment).

Table 4.1: Quantification of the mass and molar amounts of bait protein species in a pull-down experiment.

	GST			full-length GST-Arc		GST-Arc fragment	
Percentage of beads incubated with bait	100	50	25	100	50	100	50
Integrated intensity	684	374	162	314	195	713	447
Molar intensity	26	14	6	4	2	24	15

Figure 4.4 shows results from a pull-down experiment. SDS-PAGE lanes were loaded with the same samples described in Figure 4.3. The first lane contains the input, DOC-solubilized brain-membrane fraction, which contains the candidate interactors. Lanes 2–4 contain decreasing concentrations of GST immobilized on agarose and incubated with the input. Lanes 5–6 contain decreasing concentrations of GST-Arc immobilized on agarose and incubated with the input. Lanes 2 and 5 can be nearly directly compared; as indicated in Table 4.1, the relative number of moles of

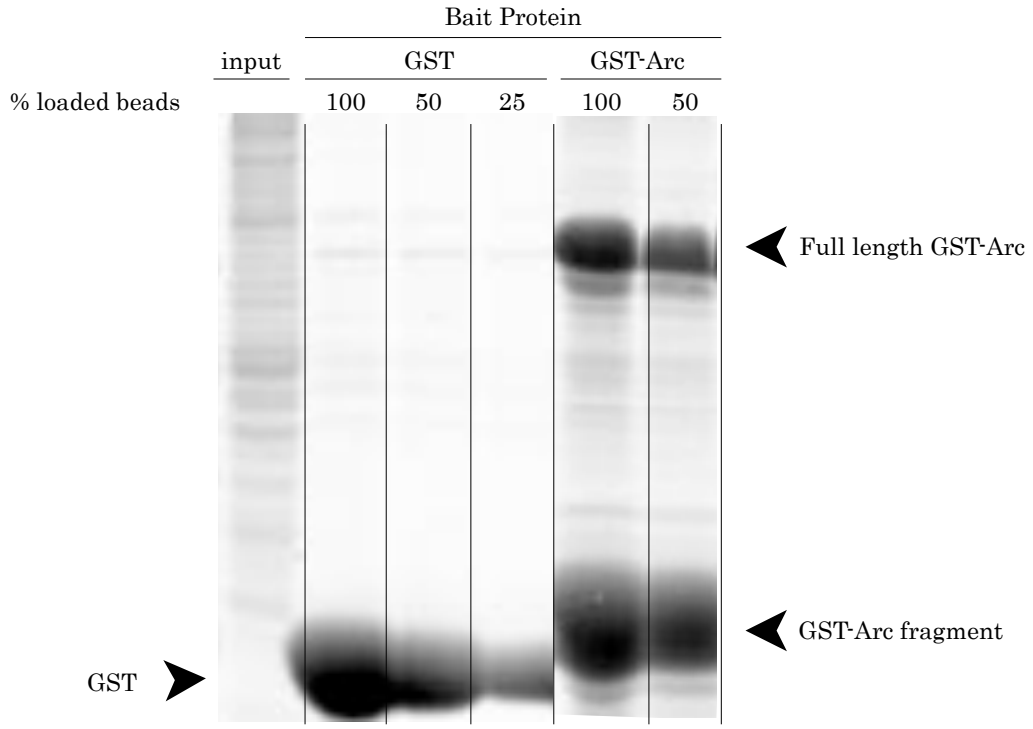

Figure 4.3: Total protein as visualized by SDS-PAGE allows selection of equimolar conditions. Samples from a GST-Arc pull-down experiment were analyzed: 1) DOC-solubilized brain-membrane fraction (input), which contains the potential interactors; 2-4) GST immobilized on glutathione-agarose beads, diluted to the percent indicated with fresh glutathione-agarose beads, incubated with input; 5-6) GST-Arc immobilized on glutathione-agarose beads, diluted to the percent indicated with fresh glutathione-agarose beads, incubated with input. Full-length GST-Arc (solid black arrowhead) is approximately 80 kDa; a prominent GST-Arc fragment (empty arrowhead) is approximately 30 kDa.

GST species is 26 in the GST-only conditions and 28 in the GST-Arc "100% loaded beads" conditions, with GST-Arc fragment comprising 26 of the 28 relative moles. Thus the bands of each interactor can be compared between the "100% loaded beads" lanes in this experiment, at least within an error range of 10% (a generous estimate of the difference in binding, possibly resulting from a 26:28 molar ratio).

The greater intensity of the CaMKIIα band in the GST-Arc 100 lane compared to the GST-100 lane indicates that more CaMKII bound GST-Arc than GST. Because the GST-Arc beads are only 1/7th as long as full-length GST-Arc (4/28; Table 4.1), the difference we see may be only 1/7th of the difference of CaMKII binding to GST-Arc and GST alone. This assumes CaMKII does not bind a region of Arc contained in the GST-Arc fragment, which contains approximately the first 40 amino acids of Arc.

Although we probed for CaMKIIα, the signal does not exclusively represent an interaction between CaMKIIα and Arc. First, because this pull-down was performed in brain-membrane fraction, an interaction between CaMKII and Arc could be mediated by an adapter protein. Secondly, the typical composition of a CaMKII holoenzyme in the forebrain is approximately three α subunits to one β subunit. An interaction with with either could be detected with the anti-CaMKIIα antibody.

Comparison of the GluR1 and SynGAP bands in this experiment shows that both of them bound more to GST-Arc than GST in this experiment. Since PSD-95 bands were not observed, the GST-Arc beads did not pull down large portions of the postsynaptic density (PSD).

Repeating this optimized experiment several times indicated an interaction between Arc and CaMKII at $p<.05$, and a trend indicating that Arc bound SynGAP and GluR1. However, the immunoblot bands were faint, and background was high, which added uncertainty to the quantification. Changes to the number and duration of bead wash steps decreased background, but also decreased signal. When exper-

iments implementing these changes were included, no interactions were statistically significant.

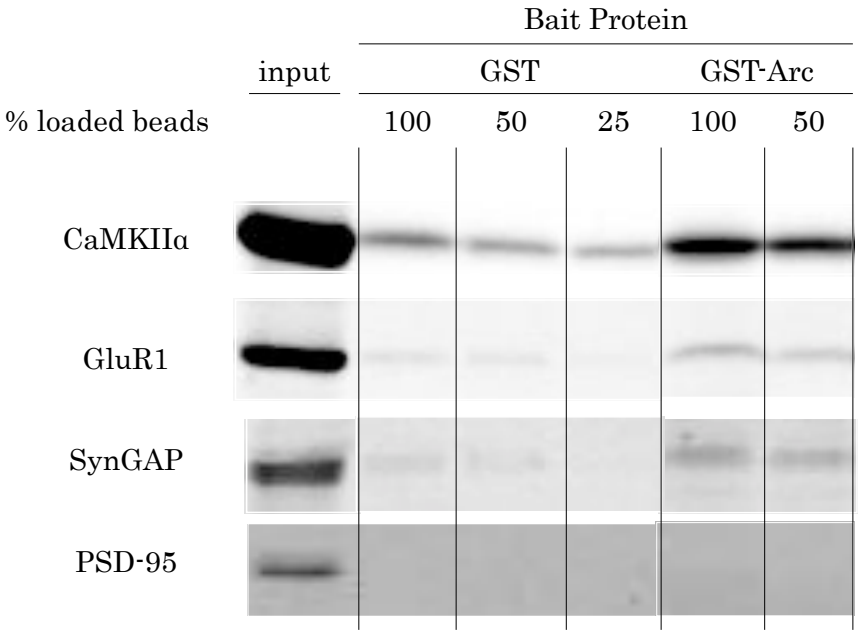

Figure 4.4: Immunoblot GST-Arc pull-down from brain-membrane fraction; not representative. Glutathione-agarose beads were incubated with GST or GST-Arc as described and subsequently incubated with deoxycholate (DOC)-solubilized brain-membrane fraction. After incubation, the beads were washed and loaded on to an SDS-PAGE gel, where the proteins were eluted with sample loading buffer. Input was also loaded on the gel. Immunoblots were probed for CaMKII, GluR1, SynGAP and PSD-95. GST-coated beads incubated with input were loaded in lanes 2 through 4; GST-Arc coated beads incubated with input were loaded in lanes 5 and 6. The percent loaded beads indicates whether the loaded beads were diluted with newly swollen glutathione beads. Relative enrichment was calculated as described in the text. This blot shows binding between Arc and CaMKII, and a small increase over background binding with GluR1 and SynGAP. However the results were inconsistent and were not present when we made changes to the post-incubation bead wash to reduce background.

4.3.3 Creation of Arc mini library

In preparation for identifying regions of Arc bound by other proteins, we generated an Arc fragment library to use in a modified yeast two hybrid technique as described in Kornau et al. (1995). Typically, a yeast two hybrid experiment identifies binding partners of a protein (the bait) by screening for interactions with proteins (the prey) expressed by a cDNA library from a tissue such as brain. Instead of identifying binding partners from an entire tissue, we planned to use the technique to identify fragments of Arc (the prey) that bind to a known interaction partner. For example, because CaMKII has been reported to interact with Arc, we planned to screen the Arc fragment library to see which fragments interact with CaMKII, to identify the region of the full-length Arc that binds CaMKII.

We generated the library by sonicating a plasmid that expresses Arc, thereby generating DNA fragments. These fragments were size-separated by agarose gel electrophoresis and isolated by excising the portion of gel corresponding to fragments of 300-500 bases. These fragments were purified from the gel, blunted, and ligated into a plasmid designed for yeast two hybrid experiments. To determine the length and coverage of the fragments, a subset of the plasmids were sequenced. Figure 4.5 shows the distribution of one set of fragments generated by this method. The fragments are distributed across the plasmid, including the Arc protein coding region.

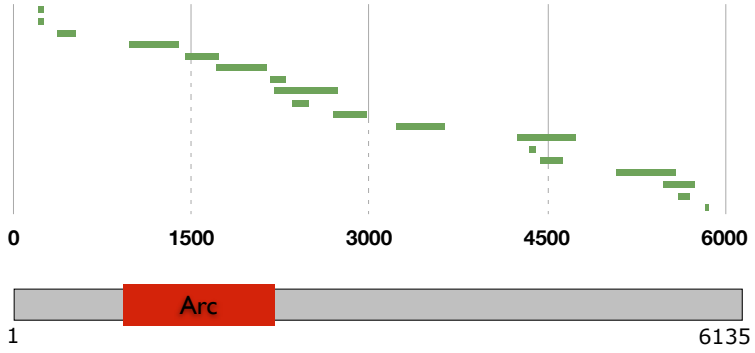

Figure 4.5: Distribution of preliminary fragment library

4.4 Discussion

Our assessment of the interactions between purified GST-Arc and several candidate regulators of synaptic potentiation and maintenance yielded inconclusive results. We tried to increase the signal to noise by making systematic changes to the protocol including modifications to protein expression, purification and pull-down experiment parameters. If interactions exist between Arc and any of CaMKII, SynGAP or GluR1; this system is not sensitive enough to detect them. The Arc fragment cDNA library, which was constructed for yeast-two-hybrid identification of binding regions, has been archived for later use.

Although Arc has been reported to bind with CaMKII (Donai et al., 2003), these two proteins did not bind under our conditions. The most parsimonious explanations for the difference between our results and those of Donai et al. are that: 1) Arc may not bind CaMKII in neurons and/or 2) Arc may bind weakly with CaMKII in all

conditions tested. Although both of these could be true, there is a great deal of evidence for a weak interaction.

Donai et al. reported binding between Arc and CaMKII under two different conditions: In one, purified GST-Arc and purified CaMKII holoenzymes co-immunoprecipitated; in the other, the Arc and CaMKIIα co-expressed in Nb2A cells (a mouse-derived neuroblastoma cell line) were co-immunoprecipitated. We tested for interactions between GST-Arc and CaMKII by incubating GST-Arc immobilized on GSH-agarose beads in mouse brain-membrane fraction.

It is possible that the interaction is weak in all conditions tested. The bands published in Donai et al. (2003) are extremely faint, and the number of tests represented by the depicted blots is not indicated. The bands in our immunoblots are faint as well. We consistently saw a faint interaction, although the difference in amounts of CaMKII interacting with GST and GST-Arc was inconsistent. Further confounding the assessment of the interaction is a potential interaction between GST and CaMKII predicted from their X-ray crystal structures (personal communication, T. Kinzer-Ursem, January 2010)

Finally, our difficulty in replicating the interaction represent the experience of others; this paper is now infrequently cited. The absence of the citation is most notable in the four papers published in a single issue of Neuron in 2006, characterizing the Arc knockout mouse and describing the first direct protein-protein interactions of Arc reported since the Donai paper was published in 2003 (Chowdhury et al., 2006; Plath et al., 2006; Shepherd et al., 2006; Verde et al., 2006).

How does Arc contribute to the maintenance of synaptic plasticity? This question, which motivated the work described in this chapter, remains unanswered: Although knockdown of Arc after inducing synaptic plasticity impairs the maintenance of LTP (Messaoudi et al., 2007), increasing Arc protein levels reduces the number of surface GluR1 receptors (Verde et al., 2006). The first implicates Arc in maintaining increases in synaptic transmission; the second implicates it in decreases in synaptic transmission.

One hypothesis resolves this apparent contradiction: Arc may act to reduce the strength of synapses adjacent to potentiated synapses, thus supporting homeostasis and preventing reversal of potentiation (Okuno et al., 2007; Verde et al., 2006). Preliminary data demonstrate 1) an interaction between Arc and CaMKIIβ that increases in affinity when calcium levels are decreased; and 2) CaMKIIβ-dependent translocation of Arc into spines and reduced surface GluR1 levels. The translocation occurs in neurons after they are stimulated and then silenced, conditions were chosen to replicate the approximate conditions of spines adjacent to potentiated synapses. It is suggested that Arc is targeted to non-potentiated synapses by minimally autophosphorylated CaMKIIβ and subsequently reduces synaptic strength through endocytosis of AMPA receptors (Okuno et al., 2007).

There are major caveats to this explanation: The preliminary data has not been extended and published. Additionally, the reported interaction with CaMKIIβ is not in agreement with the probable low affinity of the interaction between Arc and CaMKII described above. Although we probed for CaMKIIα in our pull-down exper-

iments from brain-membrane fraction, a high-affinity interaction between CaMKIIβ and Arc would also result in a positive signal for the α subunit, because the typical composition of a CaMKII holoenzyme in the forebrain is approximately three α subunits to one β subunit. Furthermore, in exploratory experiments, we used CaMKIIβ antibody to probe the results of pull-down experiments with GST-Arc and CaMKII holoenzymes purified from rat brain. We did not see an interaction between GST-Arc and CaMKIIβ in those experiments.

In spite of these caveats, the story is an excellent model of the elements required to reconcile Arc's biochemical and network features. It posits a mechanism by which Arc could be selectively localized to non-potentiated synapses, thus explaining, at least in part, the apparent contradiction between Arc's roles in decreasing synaptic strength and maintaining synaptic potentiation. It also demonstrates the components of the mechanism in a model system. While it may not be the ultimate explanation of Arc's contribution to the maintenance of synaptic plasticity, it certainly demonstrates the elements any such explanation must include.

References

Alberini CM (2009) Transcription factors in long-term memory and synaptic plasticity. Physiological Reviews 89:121–145.

Chowdhury S, Shepherd J, Okuno H, Lyford G, Petralia R, Plath N, Kuhl D, Huganir R, Worley P (2006) Arc/Arg3.1 interacts with the endocytic machinery to regulate AMPA receptor trafficking. Neuron 52:445–459.

Donai H, Sugiura H, Ara D, Yoshimura Y, Yamagata K, Yamauchi T (2003) Interaction of Arc with CaM kinase II and stimulation of neurite extension by Arc in neuroblastoma cells expressing CaM kinase II. Neuroscience Research 47:399–408.

Fujimoto T, Tanaka H, Kumamaru E, Okamura K, Miki N (2004) Arc interacts with microtubules/microtubule-associated protein 2 and attenuates microtubule-associated protein 2 immunoreactivity in the dendrites. Journal of Neuroscience Research 76:51–63.

Gohla A, Bokoch GM (2002) 14-3-3 regulates actin dynamics by stabilizing phosphorylated cofilin. Current Biology 12:1704–1710.

Guzowski JF, Lyford GL, Stevenson GD, Houston FP, McGaugh JL, Worley PF, Barnes CA (2000) Inhibition of activity-dependent arc protein expression in the rat hippocampus impairs the maintenance of long-term potentiation and the consolidation of long-term memory. Journal of Neuroscience 20:3993–4001.

Kornau HC, Schenker LT, Kennedy MB, Seeburg PH (1995) Domain interaction between NMDA receptor subunits and the postsynaptic density protein PSD-95. Science 269:1737–40.

Lyford G (1998) Characterization of Arc: a novel, neuronal immediate early gene that binds CaMKinase II. Ph.D. thesis, Johns Hopkins.

Lyford GL, Yamagata K, Kaufmann WE, Barnes CA, Sanders LK, Copeland NG, Gilbert DJ, Jenkins NA, Lanahan AA, Worley PF (1995) Arc, a growth factor and activity-regulated gene, encodes a novel cytoskeleton-associated protein that is enriched in neuronal dendrites. Neuron 14:433–445.

Messaoudi E, Kanhema T, Soulé J, Tiron A, Dagyte G, da Silva B, Bramham CR (2007) Sustained Arc/Arg3.1 synthesis controls long-term potentiation consolidation through regulation of local actin polymerization in the dentate gyrus in vivo. Journal of Neuroscience 27:10445–55.

Okuno H, Naruse H, Kawashima T, Fujii H, Nonaka M, Chowdhury S, Worley P, Bito H (2007) Synaptic targeting of Arc via high affinity interaction with Ca2+/calmodulin-dependent kinase II beta. Society for Neuroscience.

Plath N, Ohana O, Dammermann B, Errington ML, Schmitz D, Gross C, Mao X, Engelsberg A, Mahlke C, Welzl H, Kobalz U, Stawrakakis A, Fernandez E, Waltereit R, Bick-Sander A, Therstappen E, Cooke SF, Blanquet V, Wurst W, Salmen B, Bösl MR, Lipp HP, Grant SGN, Bliss TVP, Wolfer DP, Kuhl D (2006) Arc/Arg3.1 is

essential for the consolidation of synaptic plasticity and memories. Neuron 52:437–44.

Shepherd JD, Rumbaugh G, Wu J, Chowdhury S, Plath N, Kuhl D, Huganir RL, Worley PF (2006) Arc/Arg3.1 mediates homeostatic synaptic scaling of AMPA receptors. Neuron 52:475–484.

Steward O, Wallace CS, Lyford GL, Worley PF (1998) Synaptic activation causes the mRNA for the IEG Arc to localize selectively near activated postsynaptic sites on dendrites. Neuron 21:741–751.

Verde EMR, Lee-Osbourne J, Worley PF, Malinow R, Cline HT (2006) Increased expression of the immediate-early gene arc/arg3.1 reduces AMPA receptor-mediated synaptic transmission. Neuron 52:461–474.

Chapter 5

Discussion

This thesis describes the outcomes of biological processes that range in duration from seconds to months, including posttranslational modifications that occur within seconds of receptor stimulation, protein binding reactions that are allowed to reach completion over the course of hours, and gene expression in a knockout mouse several months old. The variety of biologically relevant time frames in these studies underscores the cumulative nature of experimental perturbations. This issue is particularly relevant with knockout mice.

The densin knockout mice used in our RNA-Seq experiments were adult mice. We aim to learn about densin by studying the effects of its absence, but we are studying an adult densin knockout mouse in which perturbations we observe occur over a lifetime without densin. By surveying cumulative changes we are less likely to miss the consequences a disruption in development than if we surveyed only at an earlier stage. However, we cannot easily examine the developmental defects in the adult.

Ideally, we could analyze the knockout mice at different developmental time points. Alternatively, we could analyze gene expression in conditional densin knockout mice, in which the loss of densin occurs after post-natal development is complete.

An ideal system would allow repeated measurements of the same sample after acute knockdown. For other purposes, gene silencing has been achieved *in vivo* within hours using oligodeoxynucleotides (Guzowski et al., 2000). The method of RNAi examined in Chapter 3, which was optimized for non-toxic transfection of post-mitotic cell cultures, required 72 hours for only 60 percent knockdown of GAPDH, the recommended positive control. An acute knockdown would make the loss of densin more synchronized, which would, in turn, make identification of changes in gene expression more robust than in the Cre-mediated systems described above. However, the existing acute knockdown systems are problematic in implementation, entirely apart from any issues of unintended gene regulation (Olejniczak et al., 2009).

The value of making repeated measurements of the same biological entity is substantial (see Arrasate et al., 2004). Typically the main barrier is destruction of the remaining sample in the process of making the measurement.

In summary, a range of genetic manipulations could be employed to extend the results presented in Chapter 2. Given the significant amounts of time and resources required for even the least involved of these options, the implementation will be based on the outcome of ongoing behavioral and biochemical experiments.

References

Arrasate M, Mitra S, Schweitzer E, Segal M, Finkbeiner S (2004) Inclusion body formation reduces levels of mutant huntingtin and the risk of neuronal death. Nature 431:805–810.

Guzowski JF, Lyford GL, Stevenson GD, Houston FP, McGaugh JL, Worley PF, Barnes CA (2000) Inhibition of activity-dependent arc protein expression in the rat hippocampus impairs the maintenance of long-term potentiation and the consolidation of long-term memory. Journal of Neuroscience 20:3993–4001.

Olejniczak M, Galka P, Krzyzosiak W (2009) Sequence-non-specific effects of RNA interference triggers and microRNA regulators. Nucleic Acids Research 38:1–16.

Chapter 6

Appendix A

Differentially expressed genes

	Forebrain				Hippocampus			
Gene	Wt (RPKM)	Ko (RPKM)	z>2	z	Wt (RPKM)	Ko (RPKM)	z>2	z
0610007P22Rik	11.6	14.4	*	2.5	5.7	7.1		1.5
0610012D17Rik	7.3	9.6	*	2.7	6.0	5.8		-0.4
0910001L09Rik	73.4	81.6		1.5	29.5	41.3	*	3.5
1100001I22Rik	30.6	32.8		0.8	19.6	5.7	*	-13.1
1110006G06Rik	17.9	18.4		0.2	7.6	9.8	*	2.0
1110019N10Rik	26.2	26.5		-0.1	13.5	17.4	*	2.4
1110034A24Rik	6.6	8.3	*	2.2	3.5	4.1		0.9
1110059M19Rik	0.8	1.0			4.5	3.3	*	-2.4
1190002H23Rik	20.6	20.9		-0.0	11.8	16.0	*	2.8
1190002J23Rik	8.9	11.6	*	2.9	7.3	6.1		-1.6
1190003M12Rik	3.4	2.1	*	-3.7	2.3	3.9	*	2.9
1190007F08Rik	7.4	9.5	*	2.5	3.9	4.0		-0.0
1500005I02Rik	15.9	19.3	*	2.4	4.8	6.3		1.8
1500011K16Rik	153.2	168.5		1.5	40.5	63.9	*	5.0
1700003M07Rik	6.9	5.4	*	-2.6	4.8	5.0		0.0
1700009P17Rik	2.0	1.8			3.7	2.6	*	-2.4
1700019N12Rik	6.7	6.1		-1.1	2.0	3.1	*	2.1
1700084C01Rik	11.6	10.0	*	-2.0	8.3	8.3		-0.2
1700094D03Rik	5.1	3.7	*	-3.0	5.9	7.2		1.4
1810006K21Rik	32.0	37.4	*	2.2	23.3	24.7		0.4
1810030N24Rik	9.9	10.0		-0.1	11.9	9.5	*	-2.3
1810037I17Rik	23.8	28.3	*	2.4	11.2	12.5		0.8
1810059G22Rik	5.9	4.8	*	-2.0	5.4	5.3		-0.4
1810063B05Rik	22.5	27.2	*	2.5	13.3	12.7		-0.6
1810073G14Rik	10.4	8.8	*	-2.1	11.6	13.0		0.9
2010007H12Rik	10.1	12.3	*	2.2	4.8	6.0		1.4

Differentially expressed genes

	Forebrain				Hippocampus			
Gene	Wt (RPKM)	Ko (RPKM)	z>2	z	Wt (RPKM)	Ko (RPKM)	z>2	z
2010100O12Rik	83.2	88.1		0.7	37.6	48.1	*	2.6
2010107E04Rik	216.5	236.9		1.4	158.3	133.9	*	-2.6
2010204K13Rik	16.4	17.7		0.9	12.8	18.0	*	3.2
2210015D19Rik	6.1	5.8		-0.6	7.4	4.4	*	-4.4
2210415I11Rik	4.4	5.7	*	2.1	2.6	3.7		2.0
2310009B15Rik	3.2	5.5	*	4.0	4.7	5.2		0.7
2310036O22Rik	63.5	63.9		-0.2	42.2	53.9	*	2.6
2310047M15Rik	14.7	15.2		0.3	8.6	12.7	*	3.3
2310061F22Rik	9.2	9.4		0.1	3.9	5.8	*	2.5
2610005M20Rik	4.9	6.5	*	2.4	2.6	2.8		
2610204M08Rik	44.0	44.1		-0.2	20.1	24.8	*	2.0
2610524H06Rik	8.9	10.2		1.4	7.6	5.2	*	-3.3
2610529C04Rik	3.8	2.9	*	-2.4	5.5	5.0		-0.9
2810428I15Rik	71.8	79.2		1.4	22.2	30.1	*	3.0
2810432D09Rik	17.3	18.2		0.5	8.8	11.3	*	2.1
2900042B11Rik	8.3	7.6		-1.1	8.2	6.5	*	-2.1
2900052N01Rik	15.9	17.9		1.4	26.2	17.9	*	-4.3
2900075B16Rik	18.9	19.2		0.0	22.0	17.6	*	-2.5
2900097C17Rik	14.6	19.0	*	3.3	22.6	20.3		-1.3
3110040N11Rik	5.2	5.7		0.7	5.2	3.8	*	-2.5
3110056K07Rik	3.7	2.9	*	-2.2	4.2	3.9		-0.8
4632415L05Rik	8.2	11.4	*	3.4	4.9	5.0		-0.1
4833420G17Rik	10.3	9.0		-1.7	7.6	11.3	*	3.2
4930404N11Rik	14.2	17.1	*	2.2	9.8	12.3		1.9
4930413G21Rik	4.1	5.4	*	2.2	1.5	1.4		
4930568B11Rik	4.9	7.3	*	3.4	1.7	2.3		
5033425G24Rik	8.5	10.7	*	2.4	1.3	1.9		
5330410G16Rik	165.6	162.7		-0.7	117.9	103.1	*	-2.1
5530601H04Rik	6.4	4.6	*	-3.3	4.8	4.5		-0.7
5730437N04Rik	40.1	46.1	*	2.0	24.3	27.3		1.1
5730442P18Rik	2.5	3.4	*	2.1	1.0	0.8		
5730449L18Rik	4.9	6.3	*	2.1	4.0	4.5		0.6
6230427J02Rik	3.6	2.2	*	-3.9	3.4	3.5		0.0
6330514A18Rik	10.3	10.0		-0.5	5.0	7.5	*	2.7
6720456H20Rik	2.7	2.5			4.9	3.2	*	-3.3
9030607L17Rik	10.0	12.1	*	2.0	9.3	11.2		1.5
9130221H12Rik	22.5	24.2		0.8	20.2	15.6	*	-2.9
9130404D14Rik	13.0	13.6		0.4	8.2	10.8	*	2.2
A130090K04Rik	6.1	4.5	*	-3.0	2.2	2.8		
A330104H05Rik	16.9	14.4	*	-2.4	16.1	16.8		0.3

Differentially expressed genes

	Forebrain				Hippocampus			
Gene	Wt (RPKM)	Ko (RPKM)	z>2	z	Wt (RPKM)	Ko (RPKM)	z>2	z
A630047E20Rik	1.3	1.4			4.3	3.2	*	-2.3
A730008L03Rik	23.2	20.3	*	-2.2	17.3	17.0		-0.3
A830018L16Rik	7.7	6.8		-1.4	7.2	5.5	*	-2.4
A830036E02Rik	6.5	9.4	*	3.6	1.9	2.1		
A930028N01Rik	6.4	5.5		-1.7	11.8	7.6	*	-4.3
A930034L06Rik	78.6	67.8	*	-2.9	146.8	139.9		-1.0
Abcg2	5.0	3.7	*	-2.8	6.2	6.0		-0.4
Abhd8	190.0	205.7		1.2	71.5	87.3	*	2.1
Abi2	19.1	17.8		-1.2	40.0	33.8	*	-2.1
Acaa1a	20.5	20.6		-0.1	9.0	11.8	*	2.2
Acn9	12.6	13.2		0.5	7.8	6.3	*	-2.1
Acp1	2.8	3.6		1.8	4.4	2.5	*	-4.1
Acta2	10.2	8.4	*	-2.6	8.6	12.5	*	3.2
Adi1	17.7	13.9	*	-3.5	15.8	22.2	*	3.3
Agpat4	15.9	15.3		-0.7	18.7	25.4	*	3.0
Agxt2l1	8.0	7.8		-0.3	7.6	4.6	*	-4.5
AI314180	13.3	11.5	*	-2.0	16.6	16.2		-0.4
Akap11	24.5	23.3		-0.9	44.9	38.0	*	-2.2
Akt1s1	24.7	28.9	*	2.1	14.2	16.9		1.6
Aldh1a2	3.7	4.9	*	2.1	4.7	4.8		-0.1
Aldh7a1	23.9	17.4	*	-5.0	20.9	16.4	*	-2.7
Amn	3.1	5.5	*	4.2	1.8	2.3		
Amotl1	8.8	8.6		-0.3	3.8	5.4	*	2.2
Amy1	8.9	7.3	*	-2.4	9.6	8.1		-1.7
Ankrd13b	25.0	25.3		-0.0	15.8	20.4	*	2.4
Anxa3	4.7	4.8		0.0	3.7	5.6	*	2.6
Anxa5	42.5	51.7	*	2.9	24.0	30.2	*	2.3
Apoe	1550.7	1865.1	*	3.9	826.5	943.0		1.5
Appbp1	13.7	13.9		0.0	13.1	10.8	*	-2.1
Arbp	48.6	45.2		-1.5	26.4	34.0	*	2.6
Arc	86.8	79.9		-1.8	25.7	42.6	*	5.3
Arhgap27	4.9	6.4	*	2.2	3.6	3.8		0.1
Arl15	7.2	6.5		-1.2	13.0	10.5	*	-2.2
Arl4d	18.2	20.7		1.6	10.1	13.5	*	2.5
As3mt	6.3	8.1	*	2.3	4.9	5.3		0.3
Astn1	40.9	36.6	*	-2.1	46.2	42.0		-1.4
Atf5	16.1	19.4	*	2.3	10.0	10.2		0.0
Atp5c1	116.8	117.9		-0.1	99.2	86.3	*	-2.1
Atp5d	298.2	323.8		1.3	132.5	162.8	*	2.3
Avp	25.7	38.0	*	5.6	0.3	0.8		2.4

Differentially expressed genes

	Forebrain				Hippocampus			
Gene	Wt (RPKM)	Ko (RPKM)	z>2	z	Wt (RPKM)	Ko (RPKM)	z>2	z
Avpi1	21.9	22.9		0.4	7.7	10.3	*	2.4
B3galt2	10.8	11.1		0.1	12.3	9.8	*	-2.3
Bai1	86.0	91.7		0.8	47.0	57.5	*	2.1
Basp1	263.5	304.9	*	2.6	110.3	126.4		1.4
BB146404	3.0	2.2	*	-2.4	4.4	4.5		-0.0
BC002163	9.1	12.0	*	3.0	5.3	3.1	*	-4.3
BC003324	9.0	11.9	*	2.9	7.2	8.3		1.0
BC004044	23.5	27.9	*	2.3	9.6	11.1		1.2
BC010787	27.4	25.6		-1.3	13.8	17.3	*	2.1
BC025575	41.2	44.7		1.1	18.6	23.4	*	2.2
BC028663	14.4	17.2	*	2.2	5.9	7.4		1.5
BC030500	6.1	7.9	*	2.4	5.5	5.4		-0.2
BC038167	3.4	2.8		-1.6	3.4	1.8	*	-4.0
BC055107	71.7	88.8	*	3.5	137.2	133.1		-0.8
BC072620	20.3	21.2		0.4	13.1	16.4	*	2.0
Bcas1	54.3	52.4		-0.9	47.1	61.0	*	2.8
Bfsp2	3.7	2.3	*	-3.8	1.5	1.2		
Bid	4.6	6.5	*	2.9	4.4	4.1		-0.5
Blvrb	12.0	15.7	*	3.3	4.5	6.2		2.0
Bmyc	63.1	72.6	*	2.1	35.7	38.4		0.6
Bnip3	12.3	11.5		-1.0	8.1	6.3	*	-2.4
Bola1	17.3	21.5	*	2.8	9.3	7.8		-1.7
Brp44l	21.2	27.3	*	3.4	5.1	5.7		0.6
C030002E08Rik	1.6	3.3	*	4.4	2.1	2.3		
C1qb	51.9	52.3		-0.1	24.1	30.8	*	2.4
C1qc	43.6	46.7		0.8	18.9	23.4	*	2.1
C1qtnf4	195.4	231.8	*	3.0	56.0	62.9		1.1
Cacng3	45.1	40.0	*	-2.3	27.8	28.3		0.0
Cacng4	15.2	15.6		0.1	5.3	7.8	*	2.7
Calb2	46.7	57.7	*	3.3	24.0	22.5		-0.8
Calml4	3.1	3.2		0.3	10.9	8.5	*	-2.5
Calr	226.1	199.1	*	-2.9	205.7	227.5		1.0
Camk2a	483.7	533.2		1.7	612.2	726.9	*	2.1
Camk4	16.4	18.2		1.2	11.7	14.7	*	2.1
Cap2	65.6	58.8	*	-2.2	60.1	62.0		0.1
Capza2	86.6	80.2		-1.7	123.1	103.9	*	-2.5
Car14	8.2	6.6	*	-2.5	9.9	11.6		1.3
Car7	7.0	8.7	*	2.1	5.1	5.3		0.1
Cartpt	15.3	18.3	*	2.2	2.3	2.7		
Casp2	3.5	2.6	*	-2.3	3.3	3.2		-0.3

Differentially expressed genes

	Forebrain				Hippocampus			
Gene	Wt (RPKM)	Ko (RPKM)	z>2	z	Wt (RPKM)	Ko (RPKM)	z>2	z
Casp6	3.0	2.0	*	-3.3	2.4	2.0		
Cbln2	15.6	16.2		0.3	4.9	3.7	*	-2.2
Cbr4	8.1	8.8		0.7	8.8	6.7	*	-2.6
Cbx5	14.5	14.3		-0.4	30.5	25.6	*	-2.1
Ccbe1	1.0	0.8			4.6	3.1	*	-2.9
Ccdc12	12.9	13.0		-0.1	8.2	6.5	*	-2.2
Ccdc23	6.9	8.6	*	2.2	5.7	6.0		0.2
Ccdc28b	16.5	17.9		0.9	12.9	16.1	*	2.0
Ccdc5	3.6	3.8		0.5	3.7	2.7	*	-2.3
Ccdc56	101.6	112.6		1.6	53.6	65.2	*	2.1
Ccdc72	9.3	6.9	*	-3.6	7.6	7.7		-0.1
Ccdc73	1.2	1.4			4.2	2.9	*	-2.8
Ccdc85b	87.3	96.4		1.5	44.7	54.9	*	2.1
Ccdc90a	4.8	4.4		-0.7	5.8	4.2	*	-2.7
Ccdc94	4.9	6.3	*	2.3	2.9	3.2		0.4
Cck	495.3	517.1		0.5	291.0	351.7	*	2.2
Ccl27	13.3	15.9	*	2.2	6.2	9.1	*	2.8
Ccna2	2.6	2.2			3.9	2.8	*	-2.5
Ccnd1	15.1	12.9	*	-2.4	10.4	13.8	*	2.5
Cd53	4.3	3.2	*	-2.7	3.6	3.7		0.1
Cd59a	2.8	5.5	*	4.8	6.8	5.6		-1.7
Cd63	17.9	21.4	*	2.2	17.1	20.3		1.6
Cd74	5.7	4.9		-1.5	3.6	5.9	*	3.0
Cdk2ap2	19.4	16.0	*	-2.9	8.9	10.5		1.3
Cdk5r2	201.8	219.0		1.3	68.9	88.7	*	2.8
Cdk5rap1	5.5	4.0	*	-3.0	4.4	5.0		0.7
Cdkn1a	13.3	16.8	*	2.8	6.7	9.7	*	2.8
Cdkn1c	6.4	8.5	*	2.7	6.7	6.5		-0.4
Chchd7	21.3	24.9	*	2.0	11.6	11.8		0.0
Chchd8	4.5	6.3	*	2.9	3.2	4.2		1.4
Chga	96.1	109.7	*	2.1	47.5	54.0		1.2
Chl1	15.3	14.9		-0.5	30.6	24.6	*	-2.6
Cirbp	30.7	36.8	*	2.6	29.5	23.3	*	-2.8
Cldn5	41.6	48.0	*	2.1	12.4	16.1	*	2.4
Clec3b	1.6	4.3	*	6.1	2.0	3.0	*	2.1
Cmbl	9.9	10.6		0.6	10.2	7.9	*	-2.5
Cmtm5	43.5	44.2		-0.0	30.7	37.6	*	2.0
Cnksr2	22.7	22.5		-0.3	51.8	43.5	*	-2.3
Cno	12.0	14.4	*	2.1	8.3	7.3		-1.3
Cnp1	179.3	173.7		-1.0	94.1	117.1	*	2.4

Differentially expressed genes

	Forebrain				Hippocampus			
Gene	Wt (RPKM)	Ko (RPKM)	z>2	z	Wt (RPKM)	Ko (RPKM)	z>2	z
Cobl	19.7	16.2	*	-3.0	7.6	7.3		-0.5
Cox18	8.4	7.4		-1.5	7.7	6.0	*	-2.3
Cox7a1	4.6	3.5	*	-2.3	3.4	3.9		0.7
Cox7c	33.3	40.7	*	2.9	13.9	12.2		-1.5
Crabp2	3.3	4.0		1.4	2.0	3.3	*	2.4
Crh	4.8	7.4	*	3.8	1.5	1.8		
Crhbp	12.2	12.9		0.5	10.8	14.1	*	2.3
Crip1	10.2	10.2		-0.2	7.0	9.7	*	2.6
Cryab	86.8	67.7	*	-4.8	47.3	74.5	*	5.0
Crybb1	5.1	6.0		1.4	2.2	3.6	*	2.6
Cul4b	6.6	6.5		-0.2	13.8	10.8	*	-2.5
Cyb5r1	7.9	8.1		0.1	11.5	8.9	*	-2.6
Cyb5r4	8.2	6.7	*	-2.4	4.6	6.0		1.7
Cyba	8.1	9.8	*	2.0	4.3	4.2		-0.3
Cyfip2	146.8	134.1	*	-2.1	163.1	158.7		-0.7
D0H4S114	31.8	34.3		1.0	33.2	27.5	*	-2.3
D10Ertd322e	27.0	32.1	*	2.4	26.5	24.9		-0.9
D19Ertd737e	5.0	7.1	*	3.1	5.0	4.2		-1.4
D630014A15Rik	3.7	4.0		0.5	10.3	8.1	*	-2.3
D8Ertd738e	95.3	101.1		0.8	45.9	56.2	*	2.1
D8Ertd82e	7.1	7.7		0.7	6.6	9.3	*	2.7
Dapk3	39.2	45.5	*	2.2	16.3	19.1		1.5
Dbi	111.8	126.9	*	2.0	123.8	123.1		-0.4
Dbndd2	37.5	37.5		-0.3	26.0	32.1	*	2.1
Dcn	10.9	10.8		-0.2	37.2	29.8	*	-2.7
Dctn5	40.8	36.1	*	-2.3	36.0	36.6		-0.0
Ddit4	32.9	38.7	*	2.3	34.5	43.3	*	2.3
Ddit4l	7.3	6.9		-0.6	3.6	2.6	*	-2.2
Deadc1	3.9	5.6	*	3.0	4.6	5.1		0.7
Dear1	14.4	13.9		-0.6	14.8	11.9	*	-2.3
Dgat1	7.4	9.1	*	2.1	6.7	6.8		-0.0
Dgkz	110.7	107.5		-0.9	74.5	92.2	*	2.3
Diras1	61.7	67.5		1.3	33.1	40.5	*	2.0
Dlgap3	86.1	91.5		0.8	45.0	55.7	*	2.2
Dlk1	8.4	10.8	*	2.6	3.8	3.3		-1.2
Dlx2	3.3	4.4	*	2.0	1.4	1.3		
Dnajb5	52.1	53.6		0.2	43.6	54.3	*	2.3
Doc2g	22.9	36.0	*	6.5	1.7	1.9		
Dpm3	45.3	50.0		1.4	18.7	26.5	*	3.5
Dtx1	29.4	32.3		1.2	17.1	21.6	*	2.2

Differentially expressed genes

	Forebrain				Hippocampus			
Gene	Wt (RPKM)	Ko (RPKM)	z>2	z	Wt (RPKM)	Ko (RPKM)	z>2	z
Dtymk	24.9	26.6		0.8	15.3	12.5	*	-2.2
Dus3l	26.4	30.7	*	2.1	16.7	20.1		1.7
Dusp1	36.4	35.2		-0.8	10.2	14.0	*	2.8
Dusp12	6.6	8.4	*	2.2	7.9	7.4		-0.8
Dusp14	29.9	30.3		-0.0	11.2	14.7	*	2.4
Dusp15	4.8	7.0	*	3.2	3.8	3.0		-1.7
E030003E18Rik	4.9	6.3	*	2.1	6.3	6.7		0.3
E330009J07Rik	7.1	5.8	*	-2.2	5.8	6.5		0.7
E530011F12Rik	1.6	3.6	*	5.1	0.0	0.0		
Ecm1	2.8	3.8	*	2.1	2.3	3.8	*	2.7
Edf1	102.8	123.0	*	3.0	47.4	56.0		1.7
Eef1a1-ps1	3.6	2.6	*	-2.5	4.2	4.4		0.1
Eef1d	18.5	18.6		-0.1	11.5	14.6	*	2.1
Efcab1	3.2	3.6		0.8	5.3	3.9	*	-2.5
EG382844	3.6	1.4	*	-7.7	1.3	0.9		
EG384885	4.2	6.9	*	4.1	2.0	1.8		
EG433273	3.0	2.2	*	-2.5	1.7	1.8		
EG434402	6.9	8.8	*	2.5	3.3	3.2		-0.3
EG434860	4.3	3.2	*	-2.6	3.2	4.6	*	2.1
EG435996	5.5	3.2	*	-5.2	1.6	3.2	*	3.4
EG545989	4.0	3.7		-0.7	5.5	3.9	*	-2.8
EG546663	28.2	38.6	*	4.6	9.8	9.9		-0.1
EG622178	6.4	3.9	*	-5.0	2.2	4.3	*	3.7
EG624124	6.0	4.4	*	-3.2	2.6	5.1	*	3.7
EG625054	3.8	2.7	*	-2.9	4.5	4.1		-0.9
EG627415	5.8	7.2	*	2.0	0.6	0.4		
EG629383	2.3	3.5	*	3.0	1.0	1.0		
EG629389	3.3	2.6	*	-2.0	1.2	1.0		
EG629397	8.3	11.0	*	2.9	5.2	6.5		1.5
EG631990	12.6	9.9	*	-3.2	23.7	23.1		-0.5
EG633736	0.8	1.1			1.4	4.4	*	5.6
EG638833	3.1	2.3	*	-2.3	1.4	1.2		
EG664868	2.8	3.7		1.8	2.3	4.1	*	3.1
EG665733	1.3	1.0			3.6	0.8	*	-9.7
EG666071	16.3	19.0		1.8	7.5	10.5	*	2.7
EG666856	10.8	14.1	*	3.0	6.7	7.8		1.0
EG667587	3.0	1.6	*	-4.9	1.6	1.9		
EG668144	0.9	16.3	*	15.3	5.9	12.4	*	5.5
Egr1	83.1	79.3		-1.1	33.9	42.0	*	2.2
Eif2b2	29.3	29.9		0.1	14.3	17.9	*	2.0

Differentially expressed genes

	Forebrain				Hippocampus			
Gene	Wt (RPKM)	Ko (RPKM)	z>2	z	Wt (RPKM)	Ko (RPKM)	z>2	z
Eif4ebp3	4.2	3.4		-2.0	3.2	4.6	*	2.2
Eme1	4.1	4.0		-0.4	2.2	3.2	*	2.1
Enc1	169.1	154.3	*	-2.1	241.8	243.2		-0.3
Enpp2	142.0	128.9	*	-2.2	415.1	391.6		-1.3
Entpd4	31.0	39.2	*	3.4	28.7	24.2	*	-2.1
Eomes	1.9	3.1	*	3.2	0.6	0.4		
Epm2a	9.6	8.9		-1.0	9.9	8.0	*	-2.2
Eppb9	15.7	13.4	*	-2.3	13.2	10.0	*	-2.8
Esd	13.0	15.5	*	2.1	14.1	11.0	*	-2.6
Esrra	28.6	31.4		1.2	13.1	17.1	*	2.5
Evi2a	14.0	11.6	*	-2.6	11.4	11.9		0.2
Exosc9	12.8	10.7	*	-2.4	17.1	12.3	*	-3.5
F630110N24Rik	13.4	16.0	*	2.1	9.4	10.8		1.0
Fabp5	10.7	9.8		-1.2	13.8	8.9	*	-4.4
Fabp7	61.4	79.1	*	4.1	20.2	22.1		0.8
Fads6	7.1	8.8	*	2.1	3.8	4.6		1.0
Fcf1	7.6	6.2	*	-2.3	8.3	7.9		-0.6
Fcho1	25.7	25.8		-0.1	10.2	13.4	*	2.3
Fdx1	10.8	13.8	*	2.8	8.8	7.6		-1.5
Fhit	4.2	3.1	*	-2.7	2.0	2.7		
Filip1	3.9	4.8		1.6	4.2	2.6	*	-3.6
Fjx1	33.4	38.8	*	2.1	14.3	16.3		1.2
Fos	25.0	24.6		-0.5	4.3	7.9	*	4.1
Fosb	5.2	6.7	*	2.2	3.3	4.5		1.7
Foxj1	4.6	6.0	*	2.2	4.3	4.8		0.6
Foxo6	7.2	8.1		1.0	6.4	8.5	*	2.1
Ftl1	34.0	33.5		-0.5	20.0	25.1	*	2.2
Fundc2	12.5	13.2		0.5	13.7	11.3	*	-2.1
Fvt1	10.3	8.4	*	-2.7	11.2	10.6		-0.6
Fxyd2	6.8	9.4	*	3.2	4.1	3.8		-0.7
Fxyd5	7.7	10.1	*	2.8	5.9	5.8		-0.3
G0s2	7.4	10.4	*	3.5	4.9	5.7		0.9
Gabpb1	4.2	3.3	*	-2.1	4.4	4.1		-0.7
Gabra2	11.7	10.6		-1.4	56.5	40.9	*	-4.1
Gabra5	31.5	27.5	*	-2.4	63.3	59.8		-0.9
Gabrb1	8.4	8.1		-0.6	26.9	21.8	*	-2.4
Gadd45b	12.8	13.9		0.9	6.0	8.2	*	2.2
Gadd45g	17.8	20.1		1.5	10.2	13.1	*	2.2
Galk1	9.0	10.9	*	2.0	4.4	5.4		1.2
Galk2	7.6	8.9		1.6	7.4	5.7	*	-2.4

Differentially expressed genes

	Forebrain				Hippocampus			
Gene	Wt (RPKM)	Ko (RPKM)	z>2	z	Wt (RPKM)	Ko (RPKM)	z>2	z
Gda	20.3	17.7	*	-2.2	45.7	41.7		-1.3
Gdpd3	0.5	3.3	*	8.7	1.6	3.2	*	3.4
Gemin5	4.8	3.8	*	-2.1	4.9	5.1		0.2
Gfap	62.9	74.5	*	2.6	96.2	109.9		1.4
Gfra2	11.9	14.2	*	2.0	9.9	9.1		-0.9
Glo1	27.7	29.5		0.7	23.2	29.5	*	2.4
Glra2	4.2	3.6		-1.5	3.3	2.5	*	-2.1
Glt8d2	4.7	4.0		-1.6	5.6	4.3	*	-2.3
Gm1673	54.3	66.0	*	3.0	16.5	20.1		1.8
Gm1693	2.8	2.7			2.2	3.3	*	2.2
Gm323	37.1	39.5		0.7	28.9	36.0	*	2.2
Gm71	9.2	11.4	*	2.4	6.9	6.5		-0.7
Gm88	26.4	31.1	*	2.3	14.4	16.8		1.3
Gna12	40.7	40.5		-0.4	27.2	34.3	*	2.3
Gng10	36.1	32.2	*	-2.1	33.1	31.6		-0.7
Gng2	28.9	28.2		-0.6	61.9	52.9	*	-2.1
Gng4	27.3	32.9	*	2.6	9.9	10.2		0.1
Gpr22	9.4	8.8		-0.9	24.6	18.8	*	-3.1
Gpsm1	19.0	22.4	*	2.1	8.1	8.8		0.6
Gramd3	7.1	5.7	*	-2.5	5.4	4.8		-1.1
Gsg1l	30.2	26.5	*	-2.3	9.8	10.5		0.5
Gsk3a	70.5	81.8	*	2.3	51.5	37.9	*	-3.9
Gstt2	2.1	3.3	*	3.0	2.2	2.2		
Gtdc1	10.4	10.0		-0.7	13.3	11.0	*	-2.0
Gtf2h2	6.7	6.4		-0.5	7.0	5.5	*	-2.1
Gtpbp6	29.1	31.2		0.8	11.4	14.9	*	2.4
Gtrgeo22	62.1	73.6	*	2.6	22.5	25.6		1.2
H1f0	46.3	54.6	*	2.5	38.6	38.7		-0.2
H2-K1	12.6	15.1	*	2.1	8.0	10.5	*	2.1
H2afj	27.3	36.7	*	4.3	13.6	12.1		-1.2
H3f3a	6.0	7.9	*	2.5	3.5	3.8		0.3
H3f3b	51.9	59.6	*	2.1	36.3	37.2		0.1
Hapln4	39.1	41.8		0.8	24.7	32.7	*	2.8
Hba-a1	47.0	41.3	*	-2.5	5.7	6.3		0.7
Hbb-b1	49.3	45.7		-1.6	10.3	7.0	*	-3.7
Hddc3	13.1	23.6	*	7.4	15.4	7.8	*	-7.0
Hdhd2	21.6	18.2	*	-2.7	17.2	17.3		-0.1
Hdhd3	4.3	5.5	*	2.0	3.7	4.0		0.4
Hes5	8.7	10.8	*	2.3	3.7	3.4		-0.7
Hhatl	8.2	7.6		-1.0	3.2	4.7	*	2.3

Differentially expressed genes

	Forebrain				Hippocampus			
Gene	Wt (RPKM)	Ko (RPKM)	z>2	z	Wt (RPKM)	Ko (RPKM)	z>2	z
Hint3	4.9	6.8	*	2.8	10.4	7.7	*	-2.9
Hipk4	24.1	21.4	*	-2.0	14.0	15.3		0.7
Hist1h1c	14.8	18.1	*	2.5	10.1	9.0		-1.2
Hist1h4h	2.3	4.1	*	3.9	0.9	1.5		
Hist1h4i	1.8	3.4	*	4.1	1.7	1.6		
Hmox1	2.8	2.7			2.1	3.2	*	2.0
Hnrpa0	57.5	67.8	*	2.5	44.1	42.5		-0.7
Hr	9.4	9.7		0.2	2.3	3.4	*	2.1
Hsd11b1	8.1	6.7	*	-2.2	11.3	11.7		0.2
Hsf4	9.0	11.0	*	2.1	3.6	3.7		-0.1
Hspa5	148.3	118.9	*	-4.5	119.6	132.5		1.0
Hspa8	132.3	141.2		0.9	54.7	75.1	*	3.5
Htr3a	2.9	2.8			3.7	5.2	*	2.1
Id2	82.7	83.5		-0.1	43.0	36.4	*	-2.2
Idh2	20.1	24.8	*	2.8	20.3	20.9		0.1
Ier3ip1	21.6	25.3	*	2.0	21.2	21.7		0.1
Ifitm3	17.1	17.6		0.2	12.2	17.5	*	3.3
Ift52	13.6	12.6		-1.2	13.0	10.6	*	-2.1
Igf2	18.2	20.5		1.5	42.0	52.8	*	2.4
Igfbp2	52.5	63.5	*	2.9	38.5	47.1	*	2.1
Igfbp7	23.0	26.8	*	2.0	13.4	15.4		1.2
Igh-1b	1.6	1.3			0.1	4.2	*	10.5
Igk-C	1.0	2.5			0.8	18.0	*	13.4
Il17d	14.2	16.8	*	2.1	4.4	4.8		0.4
Iqcb1	6.0	5.8		-0.5	8.6	7.0	*	-2.0
Irf1	3.5	2.5	*	-2.5	2.4	2.0		
Islr	13.4	15.9	*	2.1	8.2	10.2		1.8
Itfg3	7.6	7.8		0.1	5.8	7.8	*	2.0
Itpa	10.4	9.7		-0.9	9.8	6.8	*	-3.4
Iws1	5.5	5.6		-0.0	5.9	7.8	*	2.0
Josd2	43.6	41.9		-0.9	18.8	24.0	*	2.4
Jtv1	28.1	28.3		-0.2	17.0	21.7	*	2.3
Junb	59.9	64.6		1.0	16.1	20.9	*	2.5
Jund1	116.1	136.1	*	2.6	49.4	54.6		0.9
Jundm2	22.7	23.9		0.5	10.1	12.8	*	2.0
Kcnab3	29.1	33.8	*	2.1	9.6	10.1		0.4
Kcne1l	4.4	5.7	*	2.1	2.4	2.6		
Kcnj10	48.3	41.6	*	-2.8	39.5	47.1		1.8
Kcnj12	6.0	7.5	*	2.0	2.6	3.3		1.3
Kctd1	20.0	17.4	*	-2.2	15.1	15.2		-0.1

Differentially expressed genes

	Forebrain				Hippocampus			
Gene	Wt (RPKM)	Ko (RPKM)	z>2	z	Wt (RPKM)	Ko (RPKM)	z>2	z
Khdrbs2	3.4	5.0	*	2.9	2.9	2.8		
Klf13	21.5	24.8		1.8	19.1	23.9	*	2.2
Kptn	11.7	14.5	*	2.5	7.1	6.7		-0.6
Larp7	5.8	4.5	*	-2.6	5.7	4.8		-1.5
Lars2	150.4	126.3	*	-3.7	72.3	64.6		-1.7
Leng4	40.7	36.5	*	-2.1	29.6	29.6		-0.2
Lfng	10.5	12.3		1.7	6.9	9.1	*	2.0
Lnpep	2.3	2.4			7.2	5.6	*	-2.3
LOC100038822	9.0	7.6	*	-2.1	7.2	6.4		-1.2
LOC100038842	18.4	20.9		1.5	10.4	13.2	*	2.1
LOC100038852	69.2	84.5	*	3.2	22.4	28.7	*	2.5
LOC100038945	3.1	4.2	*	2.1	3.5	3.6		-0.0
LOC100038991	6.5	6.7		0.1	3.0	5.4	*	3.4
LOC100039316	18.6	22.6	*	2.5	7.2	9.3		1.9
LOC100039317	2.5	4.0	*	3.2	1.2	1.4		
LOC100039341	96.8	94.8		-0.7	18.2	24.7	*	3.0
LOC100039636	3.0	16.3	*	12.6	9.6	9.2		-0.6
LOC100039759	15.8	13.4	*	-2.4	29.1	28.5		-0.4
LOC100039826	5.4	2.2	*	-8.4	5.3	3.7	*	-2.9
LOC100039831	16.2	28.0	*	7.2	2.8	3.0		
LOC100039888	14.5	10.5	*	-4.5	3.5	3.5		-0.3
LOC100039915	20.4	17.9	*	-2.1	21.4	19.6		-1.1
LOC100039928	3.5	2.5	*	-2.7	0.9	1.4		
LOC100040066	7.5	4.1	*	-6.5	1.8	2.1		
LOC100040068	21.4	27.6	*	3.5	5.8	6.4		0.6
LOC100040128	20.3	21.4		0.5	43.1	36.5	*	-2.1
LOC100040207	6.1	8.3	*	2.8	3.0	3.1		0.0
LOC100040294	2.5	4.5	*	4.1	1.0	1.9		
LOC100040305	2.9	4.8	*	3.6	3.4	3.3		-0.3
LOC100040310	3.9	5.7	*	2.9	2.5	1.9		
LOC100040331	4.1	3.1	*	-2.5	2.4	1.8		
LOC100040332	3.3	1.6	*	-5.8	1.2	1.4		
LOC100040532	3.2	2.4	*	-2.3	2.2	1.3		
LOC100040551	7.0	5.9		-1.9	7.3	2.4	*	-9.3
LOC100040561	1.0	0.9			3.2	2.0	*	-3.2
LOC100040577	30.9	27.3	*	-2.2	61.7	60.0		-0.6
LOC100040724	7.9	9.1		1.4	5.7	7.7	*	2.1
LOC100040728	10.3	13.3	*	2.9	3.0	3.1		-0.1
LOC100040931	5.2	5.6		0.5	3.8	2.0	*	-4.2
LOC100041192	3.5	2.7	*	-2.1	3.5	2.5	*	-2.3

Differentially expressed genes

	Forebrain				Hippocampus			
Gene	Wt (RPKM)	Ko (RPKM)	z>2	z	Wt (RPKM)	Ko (RPKM)	z>2	z
LOC100041277	41.9	50.8	*	2.9	7.3	8.8		1.5
LOC100041503	15.1	19.6	*	3.3	5.0	8.3	*	3.6
LOC100041581	8.8	8.6		-0.4	15.3	11.7	*	-2.8
LOC100041613	6.4	9.1	*	3.4	3.0	3.6		0.9
LOC100041707	0.8	1.1			2.2	3.9	*	2.9
LOC100041788	5.3	5.6		0.4	3.7	2.1	*	-4.0
LOC100041799	2.6	2.6			1.7	3.8	*	4.0
LOC100041901	4.6	3.6	*	-2.4	3.5	1.9	*	-4.3
LOC100042028	8.4	7.8		-0.9	6.6	11.0	*	4.0
LOC100042194	3.3	3.1		-0.7	1.5	3.1	*	3.5
LOC100042364	3.9	5.3	*	2.5	1.4	1.9		
LOC100042378	5.9	8.3	*	3.1	2.6	4.5	*	3.1
LOC100042459	0.6	0.7			3.2	1.4	*	-5.4
LOC100042496	14.1	12.3		-1.9	22.2	18.4	*	-2.2
LOC100042553	7.9	9.4		1.8	2.5	3.7	*	2.2
LOC100042616	6.5	6.5		-0.1	5.5	7.4	*	2.1
LOC100042638	3.5	5.0	*	2.7	0.7	1.6		
LOC100042884	4.1	2.7	*	-3.5	2.0	2.2		
LOC100042972	11.7	9.9	*	-2.3	11.3	10.3		-1.0
LOC100042978	22.7	26.0		1.8	10.4	13.4	*	2.2
LOC100043003	20.1	24.5	*	2.6	11.1	12.9		1.3
LOC100043036	56.7	70.2	*	3.4	8.9	8.4		-0.7
LOC100043062	2.4	3.5	*	2.5	5.3	4.7		-1.0
LOC100043072	7.0	6.5		-0.9	8.2	6.2	*	-2.5
LOC100043141	2.2	2.3			3.0	2.1	*	-2.5
LOC100043157	3.3	2.4	*	-2.3	2.8	1.8		
LOC100043179	15.9	17.0		0.7	8.8	12.0	*	2.5
LOC100043272	9.5	11.7	*	2.3	4.0	4.3		0.3
LOC100043357	85.0	90.6		0.8	47.5	58.9	*	2.2
LOC100043392	7.9	6.0	*	-3.1	6.0	5.7		-0.5
LOC100043425	7.3	8.5		1.5	10.9	8.8	*	-2.2
LOC100043496	11.0	13.2	*	2.1	12.7	12.5		-0.3
LOC100043601	4.6	4.4		-0.5	10.9	8.7	*	-2.3
LOC100043612	4.2	5.6	*	2.2	3.4	3.6		0.0
LOC100043621	11.1	13.4	*	2.1	6.1	6.2		-0.0
LOC100043651	13.2	16.5	*	2.6	20.3	16.9	*	-2.1
LOC100043681	10.2	13.0	*	2.7	1.9	1.6		
LOC100043703	2.7	3.6	*	2.0	3.6	2.2	*	-3.3
LOC100043715	17.1	24.9	*	4.9	29.4	31.2		0.4
LOC100043912	6.9	5.4	*	-2.6	1.1	2.5		

Differentially expressed genes

	Forebrain				Hippocampus			
Gene	Wt (RPKM)	Ko (RPKM)	z>2	z	Wt (RPKM)	Ko (RPKM)	z>2	z
LOC100043950	4.5	6.3	*	2.9	2.6	3.0		
LOC194197	3.5	3.7		0.3	6.6	1.9	*	-10.4
LOC238091	3.3	2.4	*	-2.5	1.6	2.5		
LOC240160	6.4	4.7	*	-3.2	4.1	4.6		0.5
LOC384091	2.8	5.7	*	5.1	0.6	0.4		
LOC384379	11.1	7.8	*	-4.5	0.6	0.8		
LOC434047	4.4	2.9	*	-3.7	4.6	4.4		-0.4
LOC435145	6.4	9.6	*	3.9	0.5	0.7		
LOC545267	1.1	1.1			4.4	1.1	*	-9.6
LOC545536	3.3	2.1	*	-3.4	0.5	1.6		
LOC620695	28.7	35.0	*	2.8	13.0	14.9		1.2
LOC620787	12.1	10.6		-1.8	15.7	11.4	*	-3.3
LOC623094	4.0	2.9	*	-2.9	4.4	3.4		-2.0
LOC625174	8.8	11.1	*	2.5	7.9	6.0	*	-2.5
LOC626061	1.8	1.5			3.1	2.1	*	-2.5
LOC627110	3.0	2.2	*	-2.3	2.0	2.2		
LOC627695	472.3	511.5		1.3	159.0	209.1	*	3.3
LOC632000	5.5	3.7	*	-3.9	11.4	11.0		-0.5
LOC636070	4.2	3.2	*	-2.4	2.4	3.0		1.0
LOC665181	4.2	4.8		1.0	2.1	3.7	*	2.9
LOC665231	2.8	4.2	*	2.8	1.4	1.9		
LOC665298	38.0	64.0	*	8.2	41.5	2.2	*	-34.1
LOC665532	8.2	10.6	*	2.6	5.0	6.4		1.7
LOC665672	3.9	2.8	*	-2.7	3.0	3.2		0.1
LOC665931	4.1	5.3	*	2.2	3.5	4.5		1.6
LOC666244	4.1	4.5		0.6	3.3	2.1	*	-3.1
LOC666508	3.4	2.0	*	-4.2	2.3	2.5		
LOC666793	19.7	19.9		-0.0	7.1	11.0	*	3.4
LOC666835	7.8	4.8	*	-5.3	3.6	3.1		-1.1
LOC666841	7.4	9.3	*	2.2	8.8	9.2		0.2
LOC667107	4.0	3.0	*	-2.5	1.0	0.9		
LOC667296	2.6	4.1	*	3.2	0.8	1.5		
LOC667755	6.0	3.7	*	-4.7	2.6	3.2		1.0
LOC668010	3.3	2.4	*	-2.5	1.3	1.2		
LOC668406	4.5	5.7	*	2.1	1.8	2.1		
LOC669429	10.7	13.3	*	2.4	5.8	5.7		-0.4
LOC672857	1173.6	1042.7	*	-3.2	256.1	275.8		0.6
LOC675514	4.7	3.5	*	-2.7	1.3	2.1		
LOC677375	3.7	5.1	*	2.5	3.8	3.2		-1.4
LOC727711	24.7	15.0	*	-7.6	19.9	20.8		0.3

Differentially expressed genes

	Forebrain				Hippocampus			
Gene	Wt (RPKM)	Ko (RPKM)	z>2	z	Wt (RPKM)	Ko (RPKM)	z>2	z
Lpl	1.8	2.1			8.6	12.2	*	2.9
Lrfn1	17.9	21.1	*	2.1	12.1	12.8		0.4
Lrrc24	28.4	33.4	*	2.2	9.0	10.2		1.0
Lrrn3	20.2	19.5		-0.7	28.5	23.8	*	-2.1
Lsm2	8.3	5.5	*	-4.7	4.5	5.2		0.8
Lsm3	21.9	18.8	*	-2.4	16.0	17.6		0.8
Ly6g6e	3.0	4.5	*	3.1	2.2	2.3		
Ly86	8.8	6.8	*	-3.0	3.7	4.3		0.8
Lyar	4.5	5.8	*	2.2	5.3	4.6		-1.2
Lyplal1	5.1	4.3		-1.6	6.6	5.1	*	-2.3
Lzts2	17.9	18.2		0.1	10.8	14.1	*	2.3
M6prbp1	9.7	10.6		0.9	7.7	10.0	*	2.1
Manba	3.1	3.0		-0.3	3.5	2.4	*	-2.5
Mapk1	80.4	74.1		-1.8	117.3	99.3	*	-2.5
March7	10.1	9.8		-0.6	13.9	11.0	*	-2.4
Mbp	395.9	359.2	*	-2.4	241.0	279.6		1.6
Mcts2	11.4	9.6	*	-2.2	9.2	7.4	*	-2.0
Me3	8.1	11.6	*	3.8	9.2	7.9		-1.4
Megf9	23.6	23.1		-0.5	34.3	28.3	*	-2.4
Mettl1	5.5	8.3	*	3.6	4.8	4.5		-0.6
Mettl8	5.3	3.9	*	-2.9	3.9	4.4		0.7
Mgp	32.2	46.8	*	5.6	43.3	53.6	*	2.2
Mgst1	10.4	8.8	*	-2.1	6.8	7.9		1.1
Mobkl1a	1.4	1.5			4.3	3.3	*	-2.0
Mobp	61.2	57.8		-1.3	45.3	58.0	*	2.6
Mrpl12	49.9	53.4		0.9	23.6	31.0	*	2.7
Mrpl53	46.5	52.7		1.8	27.1	35.6	*	2.8
Msr2	9.8	6.9	*	-4.3	5.7	5.2		-0.9
Mt1	750.7	949.3	*	4.8	563.4	611.1		0.7
Mt2	141.9	203.0	*	6.5	205.6	204.2		-0.5
Mt3	888.2	951.2		1.1	543.8	737.1	*	4.1
Myg1	16.2	19.9	*	2.6	10.6	11.3		0.4
Myh11	1.6	1.6			2.4	3.6	*	2.1
Myl4	9.8	14.3	*	4.3	0.7	1.5		
Myl6	24.2	21.1	*	-2.3	15.5	17.9		1.3
Myo5b	7.2	7.1		-0.3	16.5	13.7	*	-2.0
Myoc	4.9	8.6	*	5.0	6.7	7.2		0.5
Nab2	13.1	15.6	*	2.1	10.0	12.8	*	2.2
Naglu	4.4	5.8	*	2.2	3.1	3.1		-0.1
Nat12	5.7	5.8		0.0	8.6	6.9	*	-2.1

Differentially expressed genes

	Forebrain				Hippocampus			
Gene	Wt (RPKM)	Ko (RPKM)	z>2	z	Wt (RPKM)	Ko (RPKM)	z>2	z
Nat5	22.0	23.9		1.0	13.5	10.1	*	-3.0
Nat9	9.1	11.1	*	2.1	5.9	6.0		-0.1
Nde1	11.0	9.3	*	-2.2	11.4	12.4		0.7
Ndg2	173.0	189.6		1.4	71.5	86.4	*	2.0
Ndufa13	127.2	134.7		0.7	55.9	68.1	*	2.1
Ndufa2	214.9	226.1		0.6	83.9	105.7	*	2.6
Ndufb6	134.1	154.1	*	2.3	64.9	74.0		1.3
Ndufc1	93.0	107.3	*	2.3	64.6	67.5		0.3
Ndufs5	10.2	9.7		-0.7	6.6	11.5	*	4.4
Ndufs7	155.8	174.5		1.8	55.7	71.3	*	2.7
Neo1	15.1	15.6		0.3	19.9	16.0	*	-2.4
Neurl2	5.0	6.5	*	2.3	2.3	3.3		2.0
Neurod2	17.1	18.3		0.7	35.1	43.6	*	2.2
Nexn	3.1	2.4	*	-2.0	0.4	0.6		
Nfkbia	14.8	17.8	*	2.2	16.8	21.4	*	2.3
Nkx6-2	18.1	18.9		0.4	5.2	7.3	*	2.3
Nlgn1	11.7	11.6		-0.4	17.4	14.2	*	-2.2
Nmb	6.5	8.9	*	3.0	2.6	3.1		0.8
Nme2	23.7	24.0		-0.0	11.1	15.2	*	2.8
Nmral1	15.2	12.2	*	-3.0	8.4	9.7		1.1
Nov	40.8	42.6		0.4	53.7	45.5	*	-2.2
Npas4	9.1	6.8	*	-3.5	2.2	3.1		1.8
Nptx2	36.8	41.7		1.7	12.2	16.9	*	3.0
Npy2r	4.2	4.0		-0.3	16.1	12.9	*	-2.4
Nr2f6	22.6	26.4	*	2.0	9.4	10.7		1.0
Nr4a1	48.4	52.6		1.1	18.4	23.1	*	2.2
Nrbp2	22.9	20.0	*	-2.1	32.1	33.4		0.2
Nrp	17.0	22.1	*	3.4	8.4	11.0	*	2.3
Nrtn	4.9	7.6	*	3.7	1.2	1.3		
Nsmce1	13.7	11.2	*	-2.8	7.0	6.4		-0.8
Nts	8.7	8.2		-0.8	6.9	5.3	*	-2.2
Ntsr2	100.1	97.9		-0.7	58.3	73.6	*	2.5
Nudt16	8.8	10.6	*	2.0	6.6	6.4		-0.4
Nudt8	7.0	9.1	*	2.5	3.5	4.0		0.7
Nupl1	12.6	13.0		0.3	15.0	12.3	*	-2.1
Nupr1	8.7	8.9		0.2	4.1	5.7	*	2.2
Nxt1	6.0	7.7	*	2.3	5.1	5.4		0.2
Nxt2	13.3	11.2	*	-2.3	12.3	11.8		-0.5
Ocel1	3.1	5.3	*	4.0	1.9	4.6	*	4.6
Ogn	3.1	3.1		-0.1	7.6	6.1	*	-2.0

Differentially expressed genes

	Forebrain				Hippocampus			
Gene	Wt (RPKM)	Ko (RPKM)	z>2	z	Wt (RPKM)	Ko (RPKM)	z>2	z
Olfml3	13.8	10.7	*	-3.4	9.9	9.9		-0.1
Omg	80.2	76.2		-1.2	63.4	53.8	*	-2.3
Omp	4.8	6.9	*	3.1	0.1	0.1		
Opcml	20.3	18.6		-1.5	44.4	37.7	*	-2.1
Orc5l	8.0	8.8		0.9	9.7	7.9	*	-2.0
ORF5	4.7	4.8		0.1	5.0	3.9	*	-2.1
Ormdl3	22.9	23.0		-0.1	15.7	19.8	*	2.2
Osgepl1	5.2	5.2		-0.1	4.3	3.1	*	-2.5
OTTMUSG00000104461	7.1	6.0		-1.9	7.0	5.1	*	-2.8
Pafah1b3	14.2	17.4	*	2.5	5.2	6.0		0.8
Paqr9	9.1	11.5	*	2.6	13.5	13.0		-0.5
Pcdh21	11.4	14.4	*	2.7	2.6	2.7		
Pcdhb7	2.1	2.7			2.2	3.6	*	2.7
Pcdhb9	3.9	3.9		-0.1	4.5	2.5	*	-4.2
Pcna	12.7	15.0	*	2.0	7.8	7.1		-0.9
Pcnp	8.8	7.1	*	-2.4	10.7	9.6		-1.1
Pcsk1n	772.1	933.6	*	3.8	259.8	337.9	*	3.2
Pde10a	38.9	34.3	*	-2.3	11.3	10.9		-0.5
Pde11a	0.7	0.8			3.2	2.4	*	-2.0
Pde1a	33.4	29.9	*	-2.0	59.0	53.8		-1.4
Pde1b	114.0	104.0	*	-2.0	30.4	30.8		-0.0
Pdia4	16.5	13.6	*	-2.9	20.6	21.8		0.4
Pdia6	56.2	48.9	*	-2.7	41.1	47.1		1.3
Pdk4	2.5	2.4			3.2	5.2	*	2.9
Penk1	185.3	195.5		0.7	14.5	18.9	*	2.5
Pex6	25.4	28.7		1.6	14.3	18.5	*	2.4
Pfdn2	111.1	131.0	*	2.7	75.6	86.2		1.3
Pglyrp1	8.8	6.7	*	-3.2	7.8	9.8		1.7
Pgrmc1	164.7	171.0		0.4	156.9	138.4	*	-2.0
Phka1	3.6	3.5		-0.5	5.6	4.4	*	-2.0
Phlda3	24.4	27.3		1.4	7.4	9.8	*	2.2
Phldb1	23.1	23.6		0.1	14.1	18.1	*	2.3
Pib5pa	27.7	33.1	*	2.4	18.9	21.9		1.3
Pja2	134.1	120.8	*	-2.3	172.4	153.6		-1.9
Pkig	34.6	37.3		0.9	19.5	24.5	*	2.2
Pkm2	250.8	249.8		-0.4	140.3	174.7	*	2.5
Plvap	5.3	6.9	*	2.3	3.0	4.9	*	2.7
Pmvk	30.8	28.2		-1.7	15.9	21.5	*	2.9
Pnck	45.1	44.8		-0.4	41.9	32.3	*	-3.2
Pofut2	13.0	15.7	*	2.2	7.9	9.2		1.2

Differentially expressed genes

	Forebrain				Hippocampus			
Gene	Wt (RPKM)	Ko (RPKM)	z>2	z	Wt (RPKM)	Ko (RPKM)	z>2	z
Pold2	13.8	17.3	*	2.8	5.7	6.9		1.3
Pold4	11.2	10.0		-1.5	4.6	6.3	*	2.1
Pole3	15.1	18.8	*	2.7	14.4	14.3		-0.2
Polr2i	34.3	40.4	*	2.3	18.8	19.8		0.4
Polr3gl	7.5	7.5		-0.2	7.9	10.4	*	2.2
Pon3	1.0	1.1			3.1	2.2	*	-2.2
Pop4	14.2	11.8	*	-2.6	16.2	16.2		-0.1
Pou6f1	21.6	25.7	*	2.3	18.1	18.6		0.1
Ppcs	3.8	3.0	*	-2.1	1.6	1.8		
Ppm1k	6.8	6.5		-0.6	11.7	9.5	*	-2.1
Ppp1r14a	31.1	34.3		1.3	12.8	16.6	*	2.4
Ppp1r1a	51.4	52.5		0.1	30.9	37.8	*	2.0
Ppp1r1b	209.1	192.0	*	-2.0	27.8	29.3		0.4
Ppp3r1	234.0	217.0		-1.9	332.4	289.1	*	-2.5
Prkcb1	98.4	88.7	*	-2.2	132.1	126.7		-0.9
Prkcd	31.2	34.6		1.3	8.9	13.5	*	3.6
Psma4	26.5	23.0	*	-2.4	26.2	24.5		-0.9
Psmb5	27.5	24.7		-1.9	19.1	14.8	*	-2.8
Pstk	9.7	12.0	*	2.4	7.9	8.4		0.4
Ptgds	871.8	981.2	*	2.3	741.0	904.9	*	2.6
Ptgs1	5.6	4.6	*	-2.0	3.8	3.6		-0.4
Ptk2	27.3	24.1	*	-2.1	25.1	24.6		-0.4
Ptma	4.5	6.7	*	3.3	4.8	6.2		1.6
Pttg1	14.1	8.4	*	-6.9	6.9	6.6		-0.6
Pus3	5.3	4.8		-1.0	6.4	4.9	*	-2.2
Rab7-ps1	3.4	4.6	*	2.4	1.9	2.5		
Ramp3	19.7	19.6		-0.3	2.8	4.7	*	3.0
Rasd1	9.5	10.1		0.6	21.7	26.7	*	2.0
Rbm22	11.6	10.8		-1.0	14.6	11.9	*	-2.2
Rcn3	4.6	5.9	*	2.0	4.2	6.1	*	2.4
Rdh13	7.8	9.9	*	2.4	6.6	6.9		0.2
Rem2	7.1	7.5		0.6	6.7	9.2	*	2.4
Rgs16	10.6	11.9		1.3	3.1	4.8	*	2.6
Rims3	37.1	42.6		1.9	7.4	11.3	*	3.4
Rit2	46.0	40.7	*	-2.3	38.6	37.4		-0.6
Rmnd1	3.1	2.4	*	-2.0	2.2	2.7		
Rmrp	23.5	14.9	*	-6.9	4.3	3.5		-1.6
Rnf141	14.5	12.4	*	-2.2	16.6	14.8		-1.3
Rnf144	6.2	5.0	*	-2.3	4.5	4.7		0.1
Rnu15-b	7.5	4.8	*	-4.8	1.6	1.8		

Differentially expressed genes

	Forebrain				Hippocampus			
Gene	Wt (RPKM)	Ko (RPKM)	z>2	z	Wt (RPKM)	Ko (RPKM)	z>2	z
Rnu32	29.9	18.0	*	-8.1	2.9	0.6		
Rnu33	8.2	5.8	*	-4.0	1.6	2.2		
Rnu35a	7.7	5.4	*	-3.9	1.8	0.3		
Rnu35b	6.7	5.3	*	-2.5	3.7	2.8	*	-2.0
RP23-25C1.8	12.6	15.7	*	2.6	8.1	9.0		0.7
Rpl13	14.2	12.2	*	-2.2	18.7	16.9		-1.2
Rpl15	16.7	16.1		-0.7	20.2	16.8	*	-2.1
Rpl18	16.0	17.6		1.1	10.7	7.8	*	-3.0
Rpl26	84.1	76.1	*	-2.1	46.4	57.5	*	2.3
Rpl3	9.1	8.9		-0.4	0.7	3.1	*	6.1
Rpl30	29.5	27.0		-1.7	4.5	8.5	*	4.2
Rpl35a	13.1	9.1	*	-5.0	29.7	27.7		-1.0
Rpl39	49.3	60.3	*	3.1	58.2	53.4		-1.3
Rpl41	12.3	15.2	*	2.5	6.2	9.4	*	3.0
Rpl7	23.8	22.6		-1.0	20.8	16.6	*	-2.5
Rplp1	350.4	418.2	*	3.3	115.0	158.4	*	3.8
Rpp21	23.8	25.6		0.8	11.9	14.9	*	2.0
Rpp25	14.5	14.5		-0.2	5.2	7.8	*	2.8
Rpph1	10.9	6.7	*	-6.1	1.3	1.4		
Rps14	184.3	182.4		-0.5	130.7	114.9	*	-2.0
Rps15a	10.0	8.3	*	-2.4	10.7	9.6		-1.1
Rps16	32.6	33.8		0.3	12.7	16.4	*	2.3
Rps2	22.0	21.2		-0.7	15.7	20.5	*	2.6
Rps21	201.5	241.1	*	3.2	104.7	137.4	*	3.1
Rps24	4.2	5.7	*	2.4	3.6	3.7		-0.1
Rps3a	16.2	10.8	*	-5.6	17.2	8.8	*	-7.1
Rps4x	21.9	19.0	*	-2.2	17.3	14.8		-1.8
Rrs1	7.6	10.0	*	2.8	5.3	7.1		2.0
Rtn4rl2	21.9	26.8	*	2.7	21.1	22.5		0.5
S100a1	84.9	90.7		0.9	54.6	67.7	*	2.3
S100a16	55.0	55.1		-0.3	26.5	32.6	*	2.1
S100a8	1.3	4.1	*	6.7	0.9	0.2		
S100a9	2.0	5.5	*	6.6	0.9	0.5		
Sacm1l	21.7	18.2	*	-2.7	22.7	22.8		-0.1
Safb2	13.7	14.6		0.7	12.2	15.9	*	2.4
Sat2	5.7	4.5	*	-2.3	5.4	4.7		-1.2
Scfd1	10.4	10.4		-0.1	13.1	10.8	*	-2.0
Scp2-ps2	3.9	2.5	*	-3.6	1.9	2.4		
Scrt1	44.6	50.5		1.8	19.3	26.1	*	3.0

Differentially expressed genes

	Forebrain				Hippocampus			
Gene	Wt (RPKM)	Ko (RPKM)	z>2	z	Wt (RPKM)	Ko (RPKM)	z>2	z
Scx	2.3	3.4	*	2.7	0.8	0.5		
Sdf2l1	18.0	15.3	*	-2.5	7.9	10.4	*	2.3
Sdsl	2.2	3.6	*	3.3	1.6	1.9		
Sec61b	14.8	12.1	*	-2.8	7.1	6.9		-0.5
Sec61g	2.6	3.8	*	2.7	0.8	1.9		
Selm	81.9	96.5	*	2.6	34.5	40.4		1.5
Sfmbt1	4.8	3.8	*	-2.2	5.8	6.2		0.3
Sgk	22.9	31.3	*	4.4	52.9	57.6		0.7
Sh3bgrl	11.7	10.1	*	-2.0	31.3	26.4	*	-2.1
Shank1	32.6	35.1		0.9	46.5	56.5	*	2.0
Shank3	36.8	36.0		-0.6	23.6	29.3	*	2.1
Shd	14.2	17.7	*	2.8	5.9	6.6		0.7
Shfm1	112.1	114.7		0.1	78.4	103.8	*	3.2
Skp1a	157.7	166.4		0.7	171.0	149.8	*	-2.1
Slc25a18	36.4	37.8		0.3	18.5	22.8	*	2.0
Slc25a29	9.0	9.0		-0.1	6.2	8.2	*	2.1
Slc27a1	27.4	31.8	*	2.0	20.9	23.4		1.0
Slc2a1	44.7	46.4		0.4	43.5	53.9	*	2.2
Slc39a10	40.0	34.7	*	-2.6	28.7	27.8		-0.6
Slc5a5	6.0	5.8		-0.4	4.7	3.3	*	-2.7
Slc6a15	11.9	12.4		0.4	19.5	16.2	*	-2.1
Slc8a1	9.4	8.9		-0.7	22.6	18.6	*	-2.3
Slc9a3r1	24.7	28.0		1.6	14.7	19.0	*	2.4
Slc9a3r2	19.8	23.4	*	2.2	12.0	13.7		1.1
Slco1a4	8.8	8.6		-0.5	11.8	9.4	*	-2.4
Slitrk2	5.5	5.1		-0.8	7.9	6.4	*	-2.0
Slitrk4	5.4	5.2		-0.5	9.6	7.7	*	-2.1
Snora64	3.0	3.6		1.4	2.5	4.6	*	3.4
Snord61	2.0	3.0	*	2.7	0.0	0.0		
Snrpa1	15.4	18.9	*	2.5	11.9	14.3		1.6
Snrpd2	29.7	32.7		1.2	13.5	20.3	*	3.8
Snx10	29.7	30.4		0.1	37.9	32.2	*	-2.1
Snx12	16.0	14.0	*	-2.0	17.9	16.9		-0.7
Sostdc1	2.8	2.8			12.8	10.2	*	-2.3
Sox21	2.4	3.2	*	2.1	1.9	2.1		
Sp9	7.1	9.2	*	2.6	1.9	2.2		
Spa17	3.1	2.6		-1.4	3.9	2.8	*	-2.5
Sparc	199.0	210.8		0.8	128.3	157.9	*	2.3
Spink8	5.2	4.1	*	-2.2	22.8	21.5		-0.8
Ssbp4	62.8	71.8	*	2.0	29.1	35.6	*	2.0

Differentially expressed genes

	Forebrain				Hippocampus			
Gene	Wt (RPKM)	Ko (RPKM)	z>2	z	Wt (RPKM)	Ko (RPKM)	z>2	z
Ssr4	44.1	51.4	*	2.3	25.4	28.4		1.0
Sssca1	30.5	37.7	*	3.1	16.7	17.2		0.2
Sst	421.3	461.5		1.5	214.9	264.5	*	2.4
Sstr4	11.5	9.8	*	-2.2	15.4	16.4		0.5
Stac2	26.7	32.3	*	2.6	18.8	21.0		1.0
Stard10	60.4	74.1	*	3.2	12.0	14.5		1.7
Stxbp5l	5.6	4.8		-1.7	12.8	9.9	*	-2.6
Supt3h	5.9	6.0		-0.0	6.3	4.6	*	-2.6
Surb7	25.6	22.6	*	-2.1	19.9	20.5		0.1
Sv2b	85.8	77.1	*	-2.2	101.7	90.3		-1.8
Syce2	1.5	2.0			4.2	2.1	*	-4.9
Syngr2	6.0	7.6	*	2.2	4.6	4.9		0.3
Taf10	15.1	18.7	*	2.7	8.3	7.9		-0.6
Tagap1	3.6	2.8	*	-2.0	2.3	2.3		
Tagln	6.9	6.2		-1.2	6.8	8.8	*	2.0
Tbca	25.3	29.7	*	2.2	24.9	25.7		0.1
Tbrg4	12.1	14.4	*	2.1	8.8	10.0		1.0
Tceb1	37.5	37.6		-0.2	43.5	37.0	*	-2.1
Tcfe2a	7.9	8.1		0.2	4.1	5.7	*	2.0
Tesc	54.8	47.3	*	-2.8	29.6	31.5		0.5
Tfrc	19.8	21.1		0.7	22.1	17.6	*	-2.6
Tgfb2	2.5	2.6			13.2	10.7	*	-2.2
Th	11.9	17.4	*	4.6	0.3	0.2		
Thap7	17.6	19.4		1.2	8.9	11.4	*	2.1
Thrb	5.5	4.4	*	-2.2	5.3	5.0		-0.6
Tipin	7.9	7.4		-1.0	7.3	5.6	*	-2.4
Tjap1	5.1	4.8		-0.7	4.2	6.1	*	2.4
Tlk1	19.8	19.1		-0.7	21.1	17.5	*	-2.2
Tmem11	25.0	28.2		1.6	13.7	17.6	*	2.3
Tmem149	2.7	3.0			2.9	4.6	*	2.6
Tmem160	47.3	57.0	*	2.8	20.5	21.4		0.3
Tmem74	3.9	3.0	*	-2.3	8.6	7.3		-1.6
Tmub1	15.7	18.8	*	2.2	8.3	8.2		-0.2
Tnfrsf25	1.0	1.1			3.0	4.7	*	2.6
Tnnt1	6.0	3.8	*	-4.5	0.8	2.3		
Tomm7	115.5	136.8	*	2.8	81.9	91.2		1.0
Top1mt	6.6	8.3	*	2.2	6.3	5.8		-0.8
Tpsg1	1.7	1.6			3.0	4.4	*	2.3
Tpt1	69.2	84.5	*	3.2	22.4	28.7	*	2.5
Trappc6a	8.1	11.0	*	3.2	4.2	4.6		0.4

Differentially expressed genes

	Forebrain				Hippocampus			
Gene	Wt (RPKM)	Ko (RPKM)	z>2	z	Wt (RPKM)	Ko (RPKM)	z>2	z
Trh	9.8	12.1	*	2.4	1.3	1.4		-1.3
Trip6	2.6	2.6			2.0	3.2	*	2.2
Tspo	7.3	9.1	*	2.2	4.4	5.7		1.7
Tuba8	11.3	14.6	*	2.9	5.5	5.4		-0.3
Tubg1	23.3	23.0		-0.4	11.7	15.6	*	2.6
Tyrobp	15.9	15.2		-0.8	8.7	11.4	*	2.2
Uap1l1	10.2	12.8	*	2.6	6.3	6.7		0.3
Uba52	5.0	5.6		0.9	4.0	2.8	*	-2.5
Ubc	44.2	35.1	*	-4.1	29.3	37.1	*	2.4
Ugt8a	16.2	12.7	*	-3.5	12.2	13.7		1.0
Usmg5	81.1	94.6	*	2.4	34.2	31.8		-1.0
Usp53	3.3	2.5	*	-2.4	5.0	4.9		-0.4
Utp18	6.6	6.4		-0.4	7.6	5.9	*	-2.2
Vgf	174.0	193.4		1.7	79.8	107.5	*	3.4
Vps37b	16.3	19.4	*	2.1	10.4	10.9		0.2
Vps72	15.6	18.4	*	2.1	9.5	9.7		0.0
Vwf	3.6	3.7		0.1	3.6	5.5	*	2.5
Wdfy1	6.3	7.6		1.8	1.9	3.8	*	3.6
Wdr17	6.3	6.5		0.2	6.0	4.6	*	-2.1
Wwox	10.6	17.6	*	6.0	6.8	8.3		1.4
Xbp1	46.6	39.0	*	-3.3	31.0	30.9		-0.2
Xpa	6.6	8.4	*	2.2	6.2	6.6		0.3
Xrn2	10.2	10.4		0.2	15.0	12.4	*	-2.0
Xtrp3s1	5.7	9.0	*	4.2	8.5	7.1		-1.7
Yipf4	13.7	13.4		-0.5	15.9	13.2	*	-2.0
Zc3h6	4.1	3.8		-0.6	5.5	4.1	*	-2.4
Zcchc9	3.0	3.1		0.2	4.1	5.7	*	2.1
Zcd2	13.6	14.1		0.3	15.7	12.1	*	-2.8
Zdhhc2	12.2	12.5		0.1	14.7	11.5	*	-2.5
Zdhhc24	7.4	6.5		-1.4	5.5	7.4	*	2.1
Zfp180	15.3	12.8	*	-2.6	14.6	16.1		0.8
Zfp236	4.8	3.5	*	-2.9	5.0	4.3		-1.3
Zfp291	6.5	6.1		-0.7	8.3	6.5	*	-2.3
Zfp367	5.2	5.1		-0.4	5.1	3.7	*	-2.6
Zfp511	13.2	12.8		-0.6	9.0	7.3	*	-2.1
Zfp593	5.7	5.7		-0.1	2.1	3.2	*	2.0
Zfp810	4.6	4.3		-0.8	6.1	4.8	*	-2.0
Zfpm1	11.4	11.4		-0.1	6.6	8.7	*	2.0
Znhit1	42.8	45.3		0.7	17.6	21.8	*	2.0

Chapter 7

Appendix B

7.1 Comparison of expression in the wild-type forebrain and hippocampus

We compared transcription in the hippocampus of wild-type mice to that in the cortex (Figure 7.1). Of all genes measured, seventy percent are expressed at lower levels in the hippocampus than in the forebrain. This trend persists in genes differentially expressed between forebrain and hippocampus; sixty percent are lower in the hippocampus. Although genes are typically highly expressed in the hippocampus, it is a simpler structure than the forebrain as a whole, and many gene products are unnecessary for its function.

Nine genes identified as PSD proteins in a proteomic study by (Cheng et al., 2006) were differentially expressed in the densin knockout mouse: cofilin 1, CHCHD3 (coiled-coil-helix-coiled-coil-helix domain containing 3), citron (rho-interacting, serine/threonine kinase 21), FXYD5 (FXYD domain containing ion transport regulator 5), PPP1CC (protein phosphatase 1, catalytic subunit, gamma isoform), PTPRZ1

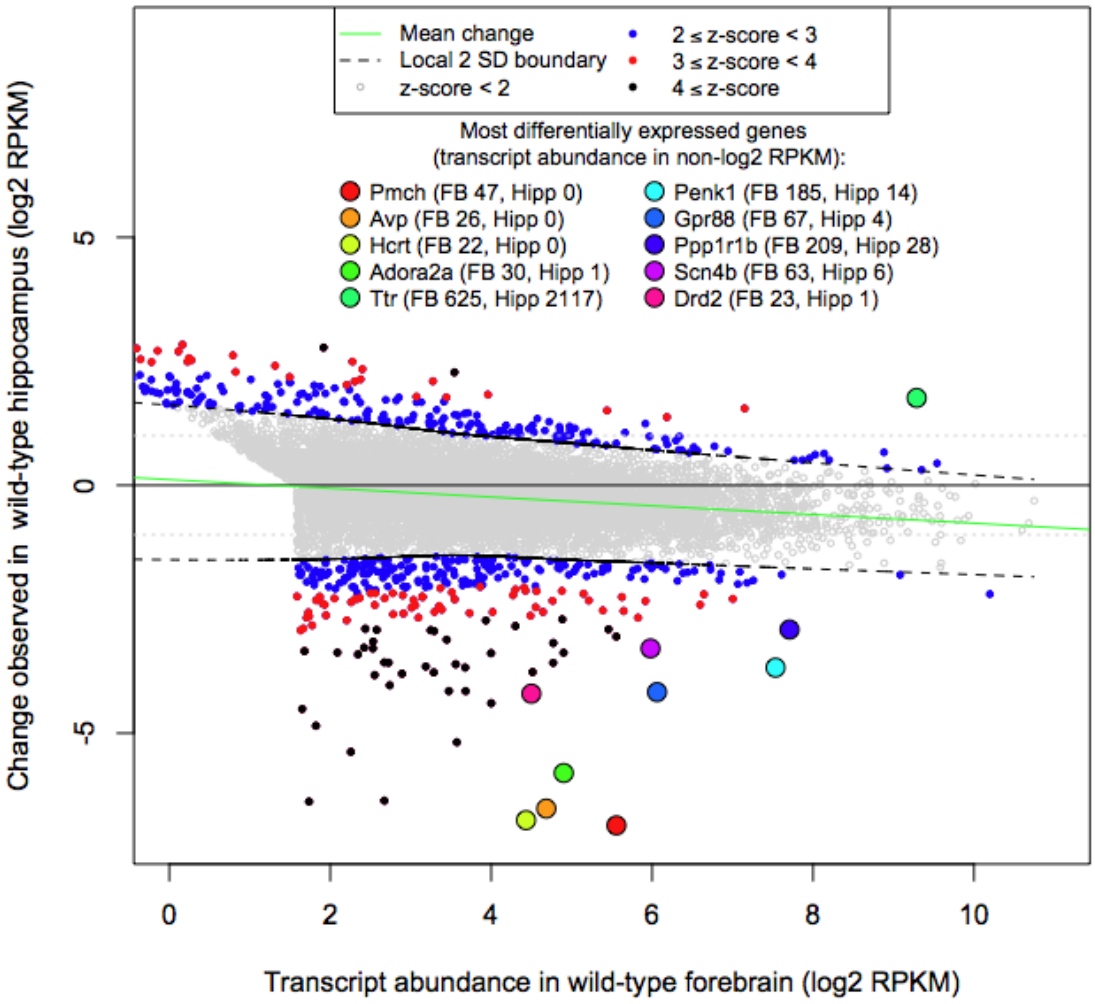

Figure 7.1: Measurements from wild-type mice indicate that many genes are expressed at lower levels in the hippocampus than in the forebrain. Differences in hippocampal gene expression were plotted against the control condition: expression in the forebrain. Unlike the two previous comparisons which examine the effect of genotype on gene expression, here we see larger changes (note the changed scale of the ordinate) and a clear trend toward lower expression. Key to named genes: Adora2a (adenosine A2a receptor), Avp (arginine vasopressin), Drd2 (dopamine receptor 2), Gpr88 (G-protein coupled receptor 88), Hcrt (hypocretin), Penk1 (preproenkephalin 1), Pmch (pro-melanin-concentrating hormone), Ppp1r1b (protein phosphatase 1, regulatory (inhibitor) subunit 1B), Scn4b (sodium channel, type IV, beta), Ttr (transthyretin).

(protein tyrosine phosphatase, receptor-type, Z polypeptide 1) RPL23 (ribosomal protein L23), SynGAP (synaptic Ras GTPase activating protein), and TUFM (Tu translation elongation factor, mitochondrial).

References

Cheng D, Hoogenraad CC, Rush J, Ramm E, Schlager MA, Duong DM, Xu P, Wijayawardana SR, Hanfelt J, Nakagawa T, Sheng M, Peng J (2006) Relative and Absolute Quantification of Postsynaptic Density Proteome Isolated from Rat Forebrain and Cerebellum. Molecular Cellular Proteomics 5:1158–1170.